The University Of Sheffield.

Using STORMForce for the investigation of bacterial peptidoglycan structure

By:

Raveen Kaur George Tank

A thesis submitted in partial fulfilment of the requirements for the degree of Doctor of Philosophy

The University of Sheffield

Faculty of Science

School of Physics and Astronomy

July 2019

Declaration

The work presented and described in this thesis was undertaken at the University of Sheffield between July 2014 and July 2019 under the supervision of Prof Jamie K Hobbs, Prof Simon J Foster and Dr Ashely Cadby. Unless stated otherwise it is the work of the author and has not been submitted, in whole or in part, for any other degree at this or any other institute.

Signed

Raveen Kaur George Tank

July 2019

Acknowledgements

I would firstly like to thank the EPSRC for funding this work and my supervisors Professor Jamie Hobbs, Professor Simon Foster and Dr Ashely Cadby, for their advice and guidance throughout my PhD. I am especially grateful to my primary supervisor Prof Jamie Hobbs, you have been incredibly supportive during my PhD and have always been available to give your time and help. Thank you for giving me the opportunity to be apart of an amazing research group. I would particularly like to thank Dr Bob Turner, Dr Victoria Lund, Dr Sandip Kumar and Dr Nic Mullin who have been an endless fountain of knowledge for all my microbiology and AFM questions. Thank you to all of the Foster and Hobbs group for making the more stressful PhD times a lot easier by making the environment fun and friendly. Sharing an office with Dr Jonathan Burns, Dr David Owen, Spyros Sovatzoglou, Vinny Verma and Laia Pasquina has made the experience that much better. I have made life long friends and I thank you all for making this an amazing experience.

I would finally like to thank my family, especially my husband William and my Son Daya. William, you have been a source of unwavering support for me during this time, especially through this final year. Your faith in me has seen me through and for that I'll always be grateful. The last experiments were done whilst I was pregnant with my son Daya. Alone in the microscope room his little kicks made me feel like I was unstoppable. Writing a thesis and becoming a new mum has been by far the most challenging thing I have ever done. Daya, your gorgeous smiles are the only motivation I'll ever need to be the best possible version of myself. This one is for you.

Abstract

STORMForce is the combination of Stochastic Optical Reconstruction Microscopy (STORM) and Atomic Force Microscopy (AFM) imaging techniques. The integration method of STORMForce and application on biological samples is presented in this work. The STORM-Force technique was developed to gain a greater understanding of bacterial samples to aid the combat against antibiotic resistance. Here I have studied the cell wall structure of peptidoglycan in *E. coli* and *B. subtilis*. Peptidoglycan is a material that provides the cells with mechanical strength to resist the internal turgor pressure, and is the primary target for many antibiotics. The details of the architecture and the way in which that architecture is formed is still poorly understood.

Firstly a STORMForce image was obtained through imaging on separate equipment, which were then overlayed. A protocol was developed for sample production that is suitable for both AFM and STORM. A STORMForce image was obtained from correlating images on separate instruments. Once this overlay was obtained, STORM components were added to the AFM to allow STORM and AFM (STORMForce) imaging to take place on one instrument. The sample protocol was developed further to allow AFM imaging to take place before or after STORM imaging, depending on the sample. The development of equipment and method used for imaging is presented.

STORMForce was used to identify a difference in the structure of the peptidoglycan of *E. coli* in different areas of the sacculi during the exponential growth phase. A blank band of fluorescence was identified in the STORM images in the middle of the sacculi; AFM

then targeted the same area to identify the architectural difference. Literature suggests the blank stripe was due to the removal of the peptide cross-link by amidase enzyme activity. AFM was used to obtain high resolution images showing a reduced fibre spacing in the area of the blank stripe when compared to the surrounding area. This suggests the spacing is reduced due to the lack of peptide cross-link, although resolution was not achieved to image the molecular difference. An amidase deleted mutant was also imaged; results showed there was no longer a visible blank stripe of fluorescence.

Peptidoglycan insertion within the septum and the main rod body of *B. subtilis* is also investigated via STORMFORCE in this study. Using fluorescently pulse labelled material, STORMForce results showed that although newly inserted peptidoglycan is mostly added to the leading (internal) edge of the septum as it develops, material is also sparsely added through the entire septum. High-resolution AFM images show large holes present within the septum material, suggesting newly inserted material also targets these areas to fill in the large holes to maintain structural integrity. Structured illumination microscopy (SIM) images where also taken of the same pulse labelled material and similar insertion patterns where observed. A quantitative analysis is given for both SIM and STORMForce data.

Peptidoglycan insertion within the main rod body of *B. subtilis* during cell elongation showed a banding insertion in the pulse labelled material. As well as STORMForce, SIMForce was also used; this was achieved by adapting the imaging protocol by using correlative glass grids. To truly understand the periodicity of the banding structure, single layers of peptidoglycan were imaged via SIMForce as well as double layered intact sacculi. The data was then quantitatively analysed, showing that the frequency of the banding is approximately doubled in a double layer of material compared to a single layer. As MreB is thought to be responsible for the banding insertion of the peptidoglycan, a deleted MreB mutant was also imaged. The mutant showed a loss of any banding formation within the peptidoglycan and a loss of rod shape. This confirms the role of MreB in governing cell shape and controlled peptidoglycan insertion within the rod of the cell.

List of Figures

List of Abbreviations

%	Percentage
~	Approximately
°	Degree
°C	Degree Celsius
µg	Microgram
µl	Microliter
µM	Micromolar
µm	Micrometre/microns
2D	Two dimensional
3D	Three dimensional
Å	Angstrom
ADA	3-Azido-D-alanine
AFM	Atomic force microscopy
Ami	Amidase
BHI	Brain Heart Infusion
DMSO	Dimethyl sulphoxide

dSTORM	Direct STORM
FDAAs	Fluorescent D-amino acids
g	Grams
GlcNAc	N-acetyl glucosamine
L	Litre
M	Molar
MEA	Mercaptoethylamine
mg	Milligram
min	Minute
ml	Millilitre
mM	Millimolar
MurNAc	*N-acetyl muramic* acid
mW	Milliwatts
n	Number
NA	Numerical aperture
nm	Nanometres
PALM	Photoactivated localisation microscopy
PBS	Phosphate buffered saline
PSF	Point spread function
rpm	Revolutions per min
S0	Ground state
S1/S2	Excited singlet state
SDS	Sodium dodecyl sulphate
SIM	Structured illumination microscopy

STED	Stimulated emission depleted microscopy
STORM	Stochastic optical reconstruction microscopy
w/v	Weight for volume
WGA	Wheat Germ Agglut*inin*
x	Times
λ	Wavelength

Contents

Chapter 1

Project aims and overview

The integration of Atomic Force Microscopy (AFM) and Stochastic Optical Reconstruction Microscopy (STORM) to produce STORMForce allows an additional level of understanding to be achieved from the sample under investigation. AFM allows samples to be imaged at sub nanometre resolution, whilst measuring forces to study molecular and cellular processes. AFM only probes the surface of the sample and molecule identification is problematic. STORM allows for super-resolution (sub-diffraction limited) optical imaging below the surface of the sample and specific molecules can be fluorescently labelled and investigated, complimenting the information acquired with AFM. In this project the STORMForce technology has been used to investigate the bacterial cell wall structural polymer peptidoglycan, which is a primary target for antibiotics. Antibiotics are used routinely across the world to cure infection and save lives, however bacteria are becoming resistant to antibiotics. By using STORMForce we wish to gain a better understanding of the peptidoglycan structure to potentialy aid in the development of new antimicrobial strategies. The STORM allows for specific labelling of the peptidoglycan, the AFM then focuses on these areas to obtain high resolution structural information. By observing how new material is inserted into the peptidoglycan and how the peptidoglycan structure rearranges during the bacterial life cycle, we develope the potential of understanding how bacteria adapt to become resistant to

antibiotics.

All work presented in this thesis is done by myslef unless stated otherwise.

Chapter 2 explains the development of AFM and the experimental set up, as well as the many modes of imaging. Imaging can be tailored to the sample by using specific cantilevers and imaging environments. AFM imaging can take place in a multitude of conditions, making it an incredibly versatile microscopy tool to image bacteria with. Bacteria are crucial organisms in life on earth, present in soil, effecting crops, infrastructure and of course human life in both positive and negative ways. AFM allows imaging of bacteria in native conditions to get a clear understanding of dynamic processes and unaltered structures. Chapter 2 also highlights areas that are problematic in AFM such as imaging artefacts and ways in which they can be identified and mitigated.

Chapter 3 gives an overview to light microscopy and the developments over more recent years. Due to the diffraction limit in light microscopy resolution of features below 200-250 nm was not achievable until the development of single molecule localisation microscopy techniques. The main factors that effect image resolution and quality are discussed. The definition of resolution is looked into and how knowledge of the point spread function of single molecule localisations can be used to form higher resolution images. The super resolution fluorescence microscopy techniques SIM, STED and STORM are explained. The stimulation of fluorophores used to label samples is discussed, and the difference in stimulated emission and stochastic emission are explained.

Chapter 3 explains the localisation process and the uncertainty involved, the types of cameras used to aquire data in STORM microscopy is also shown. The key important features of high efficiency cameras are discussed and the differences in CCD, EM-CCD and CMOS cameras are explained.

An overall background of bacteria is given in chapter 4. The importance of research on bacterial species is highlighted, and how the topic of antimicrobial resistance is an increasing global issue. The categorisation of bacteria into Gram-negative and Gram-positive

species is explained, highlighting the difference in structures. The peptidoglycan structure is the area of interest in this study. A detailed description is given of the material and literature is reviewed, demonstrating previous structural models. Structural differences of the peptidoglycan in the cell wall of *E. coli* and *B. subtilis* are compared. In both species it is observed that the internal and external peptidoglycan structure is different as well as the structure of new and old material. Literature is shown highlighting peptidoglycan insertion in the species of interest. Cell wall hydrolase activity is explained and literature is presented proposing the role of hydrolase activity in the structural difference between old and new material.

Information on peptidoglycan insertion and septum formation is examined in both species of interest. The mechanisms governing septum formation are shown and the structures previously observed within the septum are discussed. A main focus of the work presented here is the peptidoglycan insertion within the septum during cell division. Studies where fluorescent labelling is used to identify newly inserted peptidoglycan within the septum are discussed, leaving a desire for further investigation via the STORMForce technique developed in this work.

Chapter 4 highlights the fluorescently labelling techniques used to identify peptidoglycan in this study. The mechanisms in which the label is incorporated into the peptidoglycan is explained and other dyes used are also shown. The origin and importance of antibiotics are presented. There is an understanding that antibiotics which target penicillin-binding proteins (PBPs) bind irreversibly to the PBPs resulting in defective cell walls and prevent cell division causing the cell to lyse and die. Highlighting the importance of peptidoglycan, which is the main target for antibiotics and the focus of this study.

Chapter 5 lays out the methods used to produce the samples imaged in this study. The species of interests are first grown in cell culture in precise conditions, allowing for optimal growth. The media and conditions of growth are listed for both species. Once the cells have reached exponential stage of growth, peptidoglycan extraction is performed. The

Gram-negative species *E. coli* has a thin peptidoglycan layer and the extraction process is more complicated involving the use of an ultra centrifuge to separate out the lighter weight peptidoglycan from the rest of the cellular components. The Gram-positive species *B. subtilis* has a thick peptidoglycan layer, the less time consuming peptidoglycan extraction process involves breaking the cells with a French press and using a centrifuge to separate out the peptidoglycan from the rest of the material. Both species are tagged by incorporating a fluorescent D-Amino Acids (FDAA) in to the peptidoglycan structure where a fluorophore is attached prior to imaging.

The method of AFM imaging of biological samples is show in chapter 5. The development of imaging on an AFM and STORM friendly substrate is explained and the use of sample adhesive is presented. The variables in the data acquisition process for STORM imaging are described and the data processing methods are explained.

Chapter 6 focuses on the instrumentation development of the STORMForce equipment. The initial development of a substrate compatible for both AFM and STORM is given and the use of correlative grids and fiducial markers are shown, allowing for AFM and STORM to be taken on separate machines. Difficulties in obtaining high-resolution images on the developed STORMForce samples and correlating areas that have both high quality AFM and STORM are discussed.

The step by step process is given as STORM components are added to the AFM set up. Noise is monitored through the integration and mitigated where possible to retain image quality. The integration of a fluorescent light source for epifluorescence STORM imaging is shown. A laser coupled fibre is used due to the easy attachment to the equipment, easy alignment and space-saving nature. Chapter 6 gives a detailed explanation of the development of an open sample holder that allows for AFM and STORM imaging on the same STORMForce equipment.

To maintain AFM imaging quality, the biological sample, bacteriorhodopsin, was imaged on the STORMForce equipment. Turning off integrated STORM components and

using a number of different cantilevers and imaging modes improved image quality. Allowing for the trimeric structure to be imaged. This process was repeated when imaging biological samples under investigation by STORMForce, which is shown in chapter 7. Methods to increase longevity of STORM imaging acquisition time in the open sample holder developed are shown. The developed sample allows for STORM imaging without the sample being sealed, the conditions in which STORM imaging takes place was therefore tailored for the new imaging parameters.

An investigation of peptidoglycan structure in *E. coli* is given in Chapter 7. The peptidoglycan material was tagged with an azide tag to which a fluorophore was later attached, allowing for STORM imaging of the entire peptidoglycan structure. AFM imaging then allowed for high resolution topographic imaging of the material.

Through STORM imaging a stripe of missing fluorescence was identified in the middle of the sacculi. Literature reviewed suggested this could be due to the action of amidase enzymes removing the peptide cross-link in the peptidoglycan structure prior to septum formation. This area then became the target for STORMForce imaging. AFM imaging was required to identify the structural difference between the area of blank fluorescence and the rest of the peptidoglycan, to confirm the lack of peptide cross-link. A number of imaging modes, cantilevers and buffers were used to obtain molecular resolution. Although this was not achieved, strand like features where observed, which were more closely packed together in the area lacking fluorescence compared to the rest of the peptidoglycan.

Peptidoglycan insertion during septum formation and cell elongation of *B. subtilis* was investigated in chapter 8. Previous work highlights the structure seen within the septum of *B. subtilis* shown as a snail shell like spiral. Work shown in chapter 8 shows the spiral shell is a result of a drying artefact of the multi-layered structure drying to each other. A model is shown to depict where the different structures of the peptidoglycan lie within the sacculi and septum.

Previous studies showing peptidoglycan insertion in comet like patterns is shown via

SIM data. STORMForce was used to identify peptidoglycan insertion within the septum in short time pulses, 15 seconds, 2 minutes and 10 minutes. The data is shown and quantitatively analysed to show insertion patterns during septum formation. The insertion pattern of the pulse labelled material is also investigated with SIM imaging and quantitatively analysed.

The peptidoglycan insertion in the main body of the sacculi is also investigated in chapter 8. STORM and SIM is correlated with high resolution AFM images. Adapted correlative methods using glass grids were used to allow for SIMForce imaging to take place. Data taken shows that peptidoglycan is inserted in stripes along the width of the rod, which is seen in the 15 second and 2 minute data, but at 10 minutes the entire sacculi is fluorescent. To truly understand the periodicity of the banding structure single layers of peptidoglycan are imaged via SIMForce as well as intact sacculi, the data was then quantitatively analysed.

Past literature shows that MreB plays a key role in cell elongation and thought to play a part in the insertion of peptidoglycan. This is investigated further by imaging an MreB deleted mutant using SIMForce. The data was analysed using the same method as the wild type and no periodic banding was visible in either SIM of AFM.

Chapter 9 concludes the work shown in the study. A summary review is given on the investigation of the bacterial species using the STORMForce technology. Future work is also suggested of how STORMForce could continue to be used to gain a greater understanding of a wide range of biological samples. There is a large scope for STORMForce to become an advantageous experimental tool in the world of biophysics.

Chapter 2

Atomic Force Microscopy

2.1 Background

Atomic Force Microscopy (AFM) was invented by Binning *et al* in 1986 [**?**] when working on modification to the scanning tunneling microscope (STM) to overcome problems when imaging non-conducting samples. It is an imaging technique that does not use lenses or sample illumination methods to obtain images. By doing this, the Abe diffraction limit of approximately 250 nm is exceeded and high resolution images are obtained. AFM can achieve spatial resolutions in the few nanometre scale and can even get pushed into the few 100 Angstrom scale in ideal imaging conditions, which compared to conventional light microscopy, where a resolution of approximately 250 nm is typically achievable. AFM has advantages over other high-resolution imaging techniques, such as electron beam imaging techniques, as the sample can be imaged in a native environment without using chemical fixation or under vacuum conditions.

AFM has many biological applications, from force mapping cells in bone [19] to high-resolution images of the bacterial cell wall [14]. The data is obtained in close to native aqueous conditions and can be used to track dynamic behaviour in live specimens at single molecule scales. This chapter explains the basic techniques of AFM and the different modes

with emphasis on the modes of imaging used in the work presented along with difficulties that arose in the form of imaging artefacts.

2.2 AFM configuration

An AFM is based on the principle of STM, where a sharp metal tip scans close to a conducting sample surface, where a voltage bias is applied between the sample and tip. This allows the electon tunneling phenomenon to take place due to the small distance between the tip and sample, enabeling sensitive tip-sample distance measurements to be taken. This set up was modified into the AFM, allowing for the imaging of non-conducting samples. The adaptions made results in a microscope composed of four main components: a cantilever with a tip which is used for probing the sample, an optical deflection system consisting of a laser and photo-detector, a piezoelectric scanner and an electrical feedback system. Cantilevers tend to be made from silicon or silicon nitride with a reflective coating on the backside to allow maximum signal reading of the laser from the deflection of the cantilever whilst moving over the sample. The design of the cantilevers varies to fit different methods of imaging and different microscopes. The cantilever is used to measure the attractive or repulsive forces between the tip and sample by measuring the deflection of the cantilever from the sample. Hooke's law can be used to describe the behaviour of the cantilevers as they can be thought of as acting as springs at typical small deflections. Therefore equation 2.1 can be used to describe the interactions, where $x = -aV$, a is the rms of the vertical motion per volt of the deflection of the cantilever, which is specific to the cantilever used and V is the deflection of the cantilever measured in Volts.

$$F = -kx \tag{2.1}$$

In the original development of the AFM a diamond tip was fastened onto a conductive metal cantilever, an STM probe was then used to measure the deflection of the cantilever

as the tip moved across the sample. Most commercially available AFMs now use an optical deflection system. A laser spot is focused onto the back of the cantilever which reflects onto a position sensitive four quadrant photo-detector, that allows both the vertical and lateral deflection of the cantilever to be measured. Usually the back of the cantilever has a reflective coating to allow for this reflection to be efficient. When the position of the cantilever changes, due to the deflection caused by the interaction between the tip and the sample, the position of the laser spot on the photo detector moves. The sensitivity of the equipment allows deflections as small as 10^{-4} Åto be detected.

A feedback loop works by pre setting a value to keep the deflection of the cantilever constant. During contact mode imaging the deflection of the cantilever is constantly measured, where changes trigger a response which changes the voltage sent to the piezo which changes the height of the tip from the sample, with the aim of keeping deflection constant at the set-point value. A common parameter that is adjusted by the user is the feedback gains. These settings control the speed at which the feedback loop adjusts to a perturbation from the set point value. If the values set for the gain are too low then the feedback loop will not track the surface effectively resulting in a damaged sample and tip due to the tip not climbing over large features. However if the feedback loop gains are too high then noise can be introduced into the system as the cantilever lifts off the surface completely for only small features, resulting in the surface not being tracked well.

There are two main configurations of the AFM, where the AFM head moves and the sample is stationary and where the AFM head is stationary and the sample moves. In the work presented the sample was stationary and the AFM head was mobile. The AFM head is attached to a piezoelectric scanner that allows for precise three-dimensional movement of the tip when imaging the sample. Where the AFM measures tip-sample interactions and the feedback loop regulates them, allowing for soft samples to be imaged where the force applied to the surface of the sample is as low as possible. Figure 2.1 shows the basic setup of an AFM.

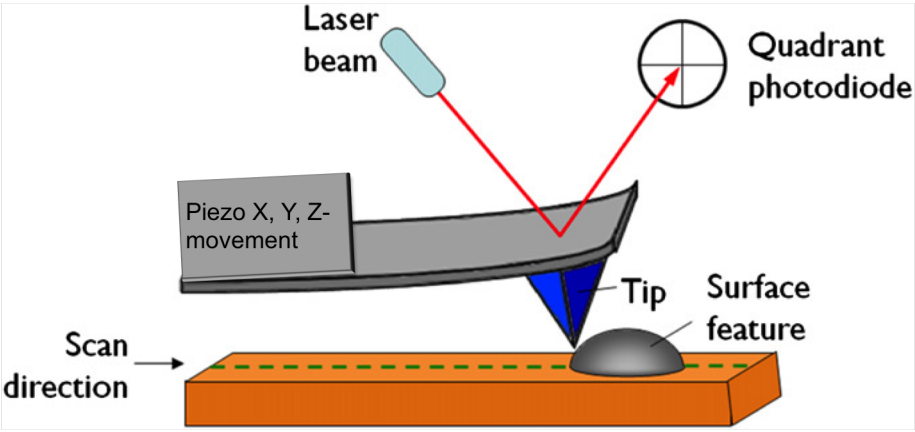

Figure 2.1: Diagram showing basic components of the AFM when the sample is stationary and the tip moves.

2.3 Imaging

There are many different modes of AFM imaging where the common difference is the parameter used to which the feedback loop corrects for. There are different modes which are more suitable for different sample types and conditions, the imaging modes result in different tip sample force interactions show in figure 2.2. The force distance curve demonstrates the balance of attractive and repulsive forces between the tip and sample as the distance between them changes. With a large separation there are no strong forces felt between the tip and sample, which changes as the tip- sample distance changes. At long-range distances the tip will feel a weak attractive forces caused by Van der Waals forces, which increase in strength, as the tip gets closer to the sample. At short-range distances there are repulsive forces due to the tip and sample touching. The repulsive forces are caused by the atoms in the tip and sample repelling each other due to the Pauli exclusion effect, the repulsive force increases as the distance between the sample and tip decrease [**?**].

There are additional forces that interact between the tip and the sample. When imaging in air, a capillary forms between the sample and the tip due to water layers forming around the tip, this can be reduced or removed by imaging in ultra high vacuum (UHV) and imaging in liquid.

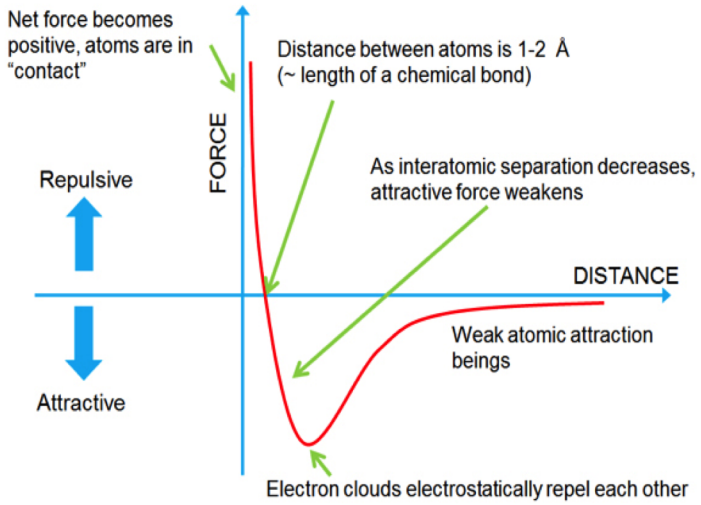

Figure 2.2: A force vs distance curve showing the relationship between the tip sample interaction as the tip sample separation changes.

2.3.1 Contact mode

As AFM can be used in different environments, different modes have been developed to find structural, mechanical, chemical and functional properties. Contact mode is useful in obtaining 3D topographical information on nanostructures and surfaces. The tip and the sample remain in constant contact represented by the repulsive regime of the intermolecular force curve, the part of the curve above the X-axis in figure 2.2. When imaging the height can be kept constant where the feedback loop is not used and the height is set by the user. Alternatively the feedback loop can be used to provide a constant deflection, where the deflection of the cantilever is monitored and the Z piezo adjusted to keep the deflection setpoint constant.

When using contact mode, the surface of the samples must be stiffer that the cantilever or both the sample and the cantilever will become deformed [20]. Most cantilevers have a spring constant of less than 1 Nm^{-1}, which is less than effective spring constant holding the atoms together which is on the order of 1-10 nN/nm[21]. When imaging in ideal conditions and a stiff sample, contact mode can achieve molecular resolution. Problems with contact mode are caused by excessive lateral force applied by the probe to the sample [22]. This

can lead to artefacts and damaged samples. However small lateral forces can be used to provide information on the friction between the tip and the sample, which can show the chemical contrast of the sample. The torsional angle will change in every new zone. If you subtract the trace and retrace you are able to see chemical difference in different regions in the sample [23].

2.3.2 Tapping Mode™

In this mode the tip makes intermitted contact with the surface, fluctuating between the attractive and repulsive regime, shown in figure 2.2. The tips resonant frequency is kept constant and either the reduction of the oscillation amplitude or the shift in the resonant frequency is kept constant. It was originally developed to overcome the problem of frictional lateral force [23]. In many models of AFM the cantilever oscillates due to a piezoelectric oscillator in the cantilever holder, which is oscillated at a range of different drive amplitudes and frequencies to achieve the tapping motion. In some models of AFM, the whole Z piezo oscillates up and down which also achieves the tapping motion. The tip moving over the sample in Tapping Mode™ is shown in figure 2.3

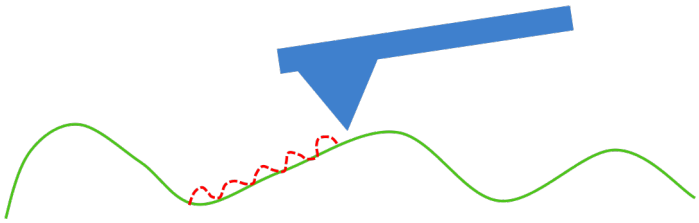

Figure 2.3: Diagram showing the AFM tip oscillating on sample surface, imaging in Tapping Mode™.

All AFM probes have a different a resonance frequency, even probes of the same models. For this reason it is essential that each cantilever used is tuned to oscillate at its resonant frequency before imaging. Recording the RMS amplitude of the cantilever oscillations as the piezo sweeps through a range of drive frequencies does this. Whichever frequency gives the highest amplitude response is chosen as the drive frequency. When using Tapping Mode™ in air stiffer cantilevers are normally used, with a resonant frequency or around 200 - 400kHz

and a spring constant of more than 10 N/m [1]. The stiffer cantilever produces more stable imaging conditions, as they are able to overcome capillary forces between the tip and sample.

Another parameter that is controlled in Tapping Mode^{TM} is the free amplitude, which is the oscillation of the tip above the sample. The amplitude set point controls the amplitude that the AFM maintains the amplitude of this oscillation, which is set by the user. If the amplitude set point is higher than the free amplitude the tip and sample do not touch and the set point must be reduced until the tip and sample can become engaged. As the tip is brought closer to the surface of the sample there are interaction forces between the tip and surface, reducing the amplitude of the oscillations of the cantilever. Once the set point amplitude and the free amplitude are equal, the tip starts to scan the surface.

Because of the small intermediate contact times, the lateral forces are reduced dramatically. Tapping Mode^{TM} is usually preferred to image samples with structures that are weakly bound to the surface or samples that are soft [24]. Different mechanisms in Tapping Mode^{TM} are amplitude imaging, phase imaging and height imaging. In amplitude imaging the feedback loop adjusts the Z-piezo so that the amplitude of the cantilever stays constant. The voltage needs to keep the amplitude constant and can be compiled into an image which can provide high contrast between features on the surface.

In phase imaging the phase difference between the driven oscillation of the cantilever and the measured oscillation can be attributed to the different material properties. The relative amount of phase lag between the freely oscillating cantilever and the detector signal can provide qualitative information about the difference in chemical composition, adhesion, stiffness and frictional properties [24]. A height image is formed by the topography of the sample as the tip scans over the surface, produced by measuring the change in voltages used to keep the set point at the set value.

2.3.2.1 Frequency modulation mode

In this mode of imaging the tip oscillates close to the sample surface without touching it, as shown in figure 2.4. The frequency of the oscillating tip is monitored by the feedback loop. Complications using this mode include the tip jumping into contact with the sample due to capillary forces. Water molecules in the atmosphere when imaging in ambient conditions cause this. For this reason only very stiff cantilever are used, which are not usually suitable for soft biological samples.

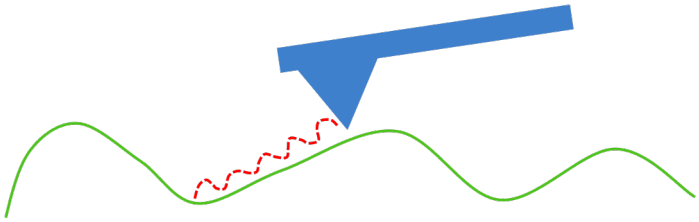

Figure 2.4: Diagram showing the AFM tip oscillating above sample surface.

2.3.2.2 Force modulation mode

Force modulation is where the tip is in full continuous contact with the sample whilst oscillating. Where the force applied on the tip from the sample is used monitored by the feedback loop. The issue related to this technique involve damage to soft samples and contamination of the tip causing tip artefacts. Shown in figure 2.5

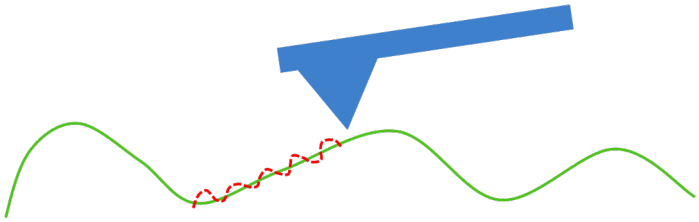

Figure 2.5: Diagram showing the AFM tip oscillating whilst in complete contact sample surface in force modulation mode.

2.3.2.3 Hyper Drive™ mode

HyperDrive™ is a trade marked JPK mode of imaging, developed to obtain high resolution AFM images of flat biological samples in liquid and air. Issues of soft sample damage and

tip contamination are reduced as there is minimal tip sample forces.

HyperDrive^{TM} is a type of phase modulation mode. The change of phase is detected and used as a feedback for obtaining topography information of the sample. During imaging the feedback loop tracks the surface by adjusting the tip-sample distance to keep the phase (rather than the amplitude, like in Tapping Mode^{TM}) constant at the setpoint. There are also Amplitude Gain Controls (AGC) that can also be used (AGC). The AGC feedback loop maintains a constant amplitude during the operation and improves the stability of the phase signal. The cantilever is oscillated in external excitation mode at the cantilevers resonance frequency resulting in more stable imaging. A specifically developed cantilever holder has been developed to oscillate the cantilever [25].

2.4 Force measurements

As well as a high resolution imaging tool an AFM is also capable of force-distance measurements. In this mode the lateral position is set at a fixed point and the Z position of the cantilever is mobile, where the cantilever tip vertically moves towards and away from the surface. The tip pushes against the sample surface where the elastic value can be measured during the indentation. As the tip moves away from the sample there is a delay due to adhesion, which can be measured. A force curve is recorded where the height of the Z piezo is plotted against the vertical deflection of the cantilever. The vertical deflection is caused by the force applied to the spring like cantilever shown by Hooke's law. The tip-sample distance decreases as the tip engages to the surface, it can "snap" into contact due attractive forces. As the tip continues to get pushed down into the sample the cantilever deflects upwards until a trigger deflection is reached, which is a parameter set by the user. This is set as a maximum force by the user to ensure that the tip does not exert over this value on the sample damaging both sample and tip. The tip is then retracts from the sample surface, where the deflection is then reduced until the tip is in its neutral position. The tip then deflects downwards due to the adhesion of the sample acting against the force of the Z piezo

lifting the tip away from the surface. Finally the retracting force becomes greater than that of the adhesive forces of the sample and the tip, the tip is suddenly released from the sample in a "snap" motion. Figure 2.6 shows the force curve produced during this process [1].

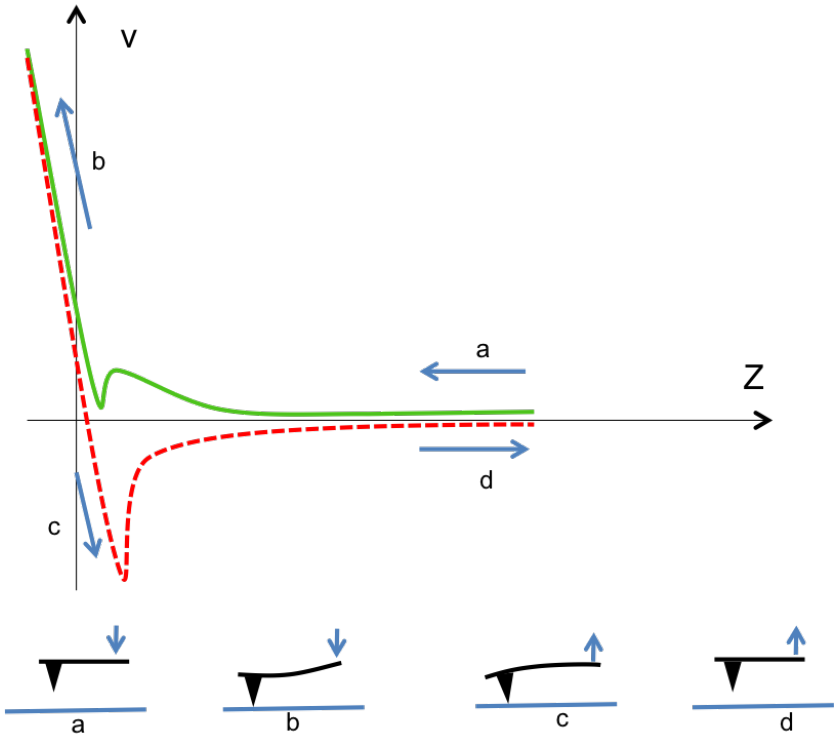

Figure 2.6: Graph showing force curve where areas are highlighted as tip engages and retracts from sample. The green line represents the approach of the probe to the sample and the red line represents the retraction.

2.4.1 Quantative Imaging ™ mode

Quantitive Imaging (QI ™) was developed by AFM manufacturer JPK and is a force curve based imaging mode. A whole force curve is measured at every pixel in the sample region, giving usable force information along with height, adhesion and slope measurements. QI™ mode is faster than force spectroscopy, due to the deceleration procedure it undergoes at the top of the tip's travel as this stops the ringing in the force data that would be caused if normal force spectroscopy were used at this imaging rate. The speed of the imaging is controlled by the ramp speed, which is defined by the user, as is the Z length and the pixel speed, which is the speed when moving the tip to the next pixel location. The ability to

customise these parameters allows the user to optimise imaging for each specific sample. In the work presented this method of imaging was used when investigating *B. subtilis* due to the sample thickness and adhesion properties, the Z length was increased to ensure the sample was not damaged and the tip was not contaminated. Figure 2.7 shows a schematic of how the tip moves in QI mode [1].

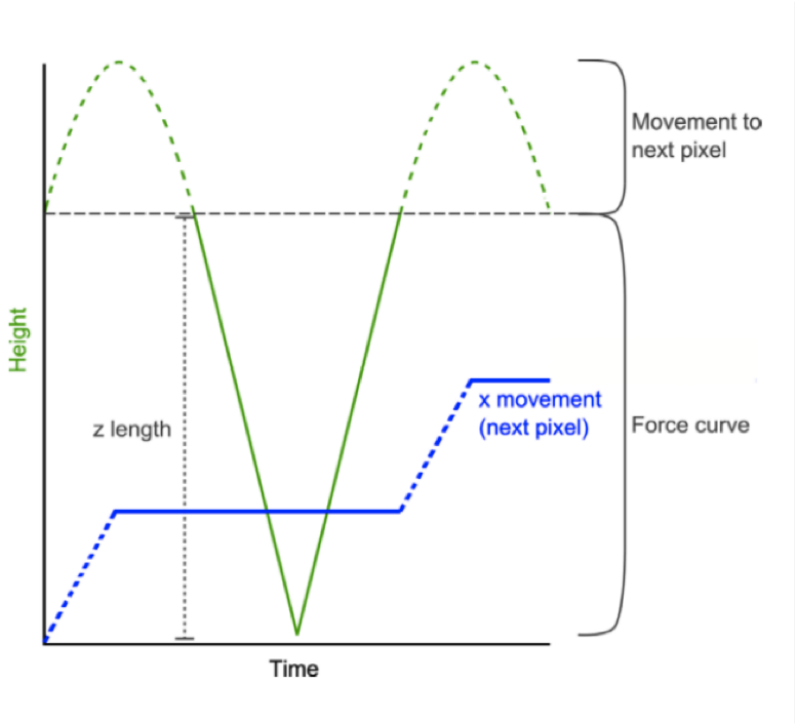

Figure 2.7: A schematic view of the tip movement in QI imaging mode. The green line displays the Z movement of the cantilever and the blue line represents the x movement [1].

2.4.2 Imaging in liquid

It is beneficial to image biological samples in aqueous conditions, not only to mimic the native environment but to also preserve the quality of the fine structures under investigation [26]. It is also possible to obtain high resolution images and force information on living bacteria in media [27], giving information about the formation and development of the cell wall structure. Obtaining more information like this can lead to a better understanding of how bacteria become resistant to antibiotics. To achieve higher resolution in the work presented the biological samples were imaged in liquid. For intermittent contact mode in

liquid, softer cantilevers than those used in air are often used, because when the cantilever and surface are immersed in liquid surface water capillary layers are no longer an issue. So for intermittent contact mode in liquid, often "contact mode" cantilevers are actually used [1].

High-resolution information is carried in the short range forces. To reach these forces the tip must get close enough to the sample without being effected by the repulsive regime. This can be achieved by adding monovalent and divalent salts into the liquid to screen charges to allow the tip to access the forces from the sample. The charged ions in the salt surround both tip and sample screening out the repulsive forces between the sample and the tip, allowing for high-resolution imaging [28]. However this can also lead to tip contamination as loose fragments of sample also get attracted to the tip. This method of imaging can be very successful if used with samples that are well attached to the substrate.

2.4.3 AFM artefacts

Artefacts can occur for a number of reasons when imaging with the AFM. The tip geometry may not be compatible with the sample type, imaging with a damaged tip and tip contamination can all result in artefacts when imaging.

Artefacts are caused due to tip geometry occur when the features that appear on the surface of the sample are sharper than the dimensions of the tip, resulting in the loss of steep ridges and narrow features. This is due to the edge of the tip making contact with the feature of the sample instead of the tip, resulting in an image that looks like a mixture of the tip edge and the feature. Two parameters are commonly used to model tip geometry, the cone angle of the main pyramid that forms the tip and the tip radius [1]. Samples with small sharp features are dominated with artefacts caused by the tip radius and sample with steep edges and larger features are dominated by the cone shape of the tip. These artefacts can be resolved by using cantilevers with long tips, which can be produced by Electron Beam Deposition (EBD). Here AFM tips are modified with another long narrow tip that is

formed on the end of the existing tip. An electron beam is used to deposit a small column of carbon on the tip, leading to a longer tip with a narrow radius and higher aspect ratio.

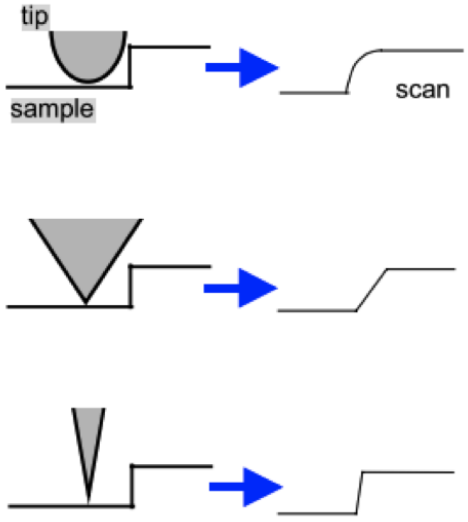

Figure 2.8: Images showing how artefacts are caused by tip geometry [1].

Another common artefact when imaging cells occurs when the height of the cell body is significantly higher than the substrate or other regions of the sample, the cantilever can interact with the these regions before the tip reaches the lower parts of the sample. This is shown in figure 2.9. It can be resolved by using a cantilevers with longer tips.

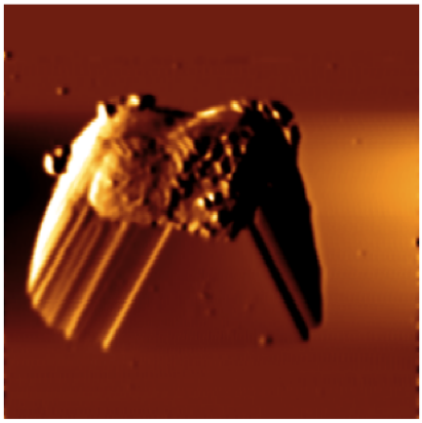

Figure 2.9: Images showing artefact caused by cantilever in contact with high sample features [1].

Using longer tips can lead to artefacts caused by damage to the tip when imaging. Double tips are caused when a tip has been damaged or snapped resulting in two or more end points, both of which contribute to an image. The resulting image has a shadowed edge and smaller features within the sample look doubled which are harder to identify compared to the shadowed edge. Other artefacts can be identified as repeatedly occurring features over the surface, which can be caused by tip contamination and poor tip shape as a result of damage. A damaged tip can also cause a repetitive triangle shaped artefact where the tip has snapped off or become very blunt.

Tip geometry also plays a part in resolution contraints when imaging. When imaging narrow features the tip radius, if larger than the features, can cause broadening artefacts. When scanning the sharp features of the sample interact with the side of the tip instead of the end of the tip. This results in the feedback loop reacting to retract the tip, lifting it higher. The side of the tip may still be in contact with the narrow feature triggering the set point value before the tip is in contact with the feature. This results in a broadened topography for the feature. If multiple narrow features are spaced at a distance smaller than that of the tip radius then both features will not be resolved, again resulting in broadening features. Surface features will only be resolved if the tip can differentiate between features that are placed closely together. When obtaining high-resolution AFM images it is important to try and reduce broadening artefacts. This can be done by selecting tips with appropriate geometry for the sample imaged and using salt screening buffers to allow the tip to get closer to the sample [29]. Figure 2.10 show all the probes used in this studdy and the physical characteristics.

	Cantilever length (µm)	Cantilever width (µm)	Spring constant (N/m)	Resonant frequency (kHz)	Tip radius (µm)
Fast Scan D (USC)	16	4	0.25	110	5
Arrow UHF	35	42	-	2000	<10
TESPA v2	123	40	37	320	7
OLTESPA	240	40	2	70	7
Biolever mini	38	16	0.09	110	8

Figure 2.10: Table showing physical characteristics of all the probes used in this study.

Chapter 3

Light microscopy

3.1 Background

The light microscope was first born as a scientific instrument developed by Robert Hooke in 1665 published in Micrographia. The data were taken of seeds, plants, the eye of a fly and the structure of cork using a compound microscope with a sample stage, light source and three lenses, similar to what is used today. As the times have progressed, the desired information to be obtained from samples has become more complex and the standard light microscopy has become limited in its abilities to provide detailed information. A weakness of light microscopy is the limit of the attainable spatial resolution of only 250 nm known as Abbe's diffraction limit [30], which is well above the resolution necessary to discriminate between different single molecules. Ernst Abbe derived the expression for the resolution power of a lens based optical microscope when the aperture is assumed to be rectangular, shown in equation 3.1 [31].

$$d = \frac{(\lambda)}{(2NA)} \tag{3.1}$$

In recent years many developments have been made to obtain high-resolution images using light microscopy. High-resolution images have been achieved with the development of

single molecule localisation techniques and the ability to highlight specific areas of a sample with fluorescent tags. This enables more detailed data to be taken from with in the cell, helping us to understand more about cell dynamics.

3.1.1 Numerical aperture

The numerical aperture of an objective is a measure of its ability to gather light from a fixed point where the sample imaged sits. The larger the numerical aperture, the higher the potential resolution of the image taken. Equations 3.2 shows the relation for numerical aperture.

$$NA = n \bullet sin(\theta) \tag{3.2}$$

where NA is the numerical aperture, n represents the refractive index of the medium between the objective and the sample and θ is the half of the angular aperture of the objective, as shown in figure 3.1

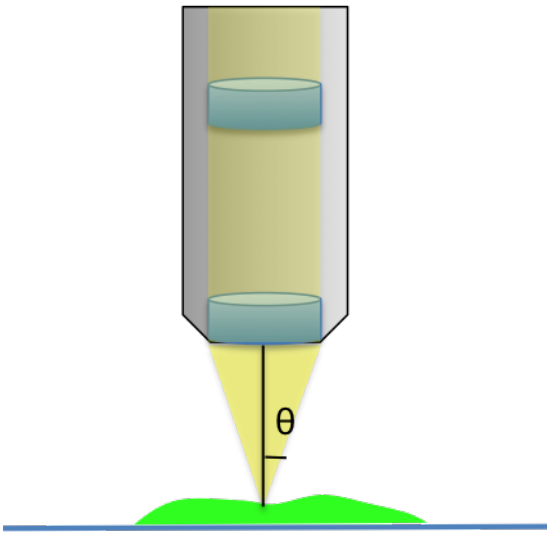

Figure 3.1: Diagram showing objective sample set up, displaying features needed to obtain a value for numerical aperture. A dissection of the objective lens is shown to highlight the lenses within it which are used to collimate light.

The value for θ is determined by the focal length of the objective and the diameter of the lens, the smaller the focal length the higher the value for θ thus resulting in a higher value

for the numerical aperture. When the focal length has been reduced as much as possible and imaging in air has been utilized, the refractive index (n) of the medium between the objective and the substrate can be increased to obtain a higher numerical aperture [32]. Objectives have been developed to image in water and immersion oil mediums, can further increase the numerical aperture to values as high as 1.51.

3.1.2 Resolution

The resolution of an image obtained by an optical microscope is defined by the smallest measurement achievable that is able to differentiate two points. Resolution is arguably the most important feature of an optical system as it allows the examination and study of fine structures within a sample. When light passes through an aperture a diffraction pattern occurs which is shown as airy disks in optical systems. The width of an Airy disk is used to define the theoretical maximum resolution of an optical system. The spot at the centre of an Airy pattern is described as the best focus of light by the objective used in the optical system. The NA has a direct effect on the size of the Airy disk, which affects the resolution, the higher the total NA of a system the higher resolution. The total NA of a system is the summation of the NA of the objective used and any tube condensers used. A three dimensional representations of the Airy disk at the image plane is known as the point spread functions, where the limit of the resolution refers to the ability to distinguish between two point spread functions. Resolution is often assessed by means of an optical unit termed the Rayleigh criterion. The Rayleigh criterion is defined in terms of the minimum resolvable distance between two point sources of light. The two point sources are resolvable if their Airy disk diffraction patterns are further apart than the distance at which the principal maximum of one Airy disk coincides with the first minimum of the second Airy disk shown in Figure 3.2B. The NA effects the radius size of the point spread function and the distance between point spread functions. The larger the NA value the smaller the point spread function, increasing the resolution. The resolution limit is formed at the distance where

the point spread functions are too close together and the individial peaks can no longer be identified as seperate, as shown in 3.2C.

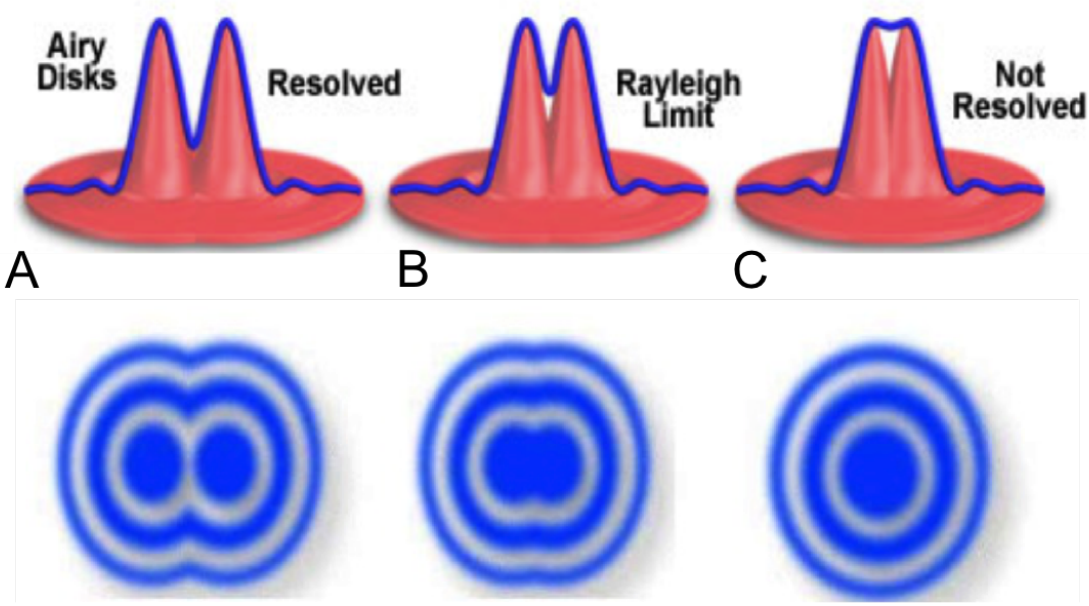

Figure 3.2: A) shows how two point spread functions need to be far enough apart to be resolved as two individual localisations. B) shows the resolution limit in the Rayleigh criterion of the minimum resolvable distance. C) shows two point spread functions that are not resolved due to a small distance between the Airy disks. Adapted from Olympous-lifescience user resources.

The equation for radius is shown in 3.3 which is equal to the Airy radius, where the aperture is assumed to be circular.

$$D = \frac{0.61\lambda}{NA} \tag{3.3}$$

where D is the resolution, and λ is the wavelength of light used.

3.2 SIM

Structured illuminated microscopy (SIM) relies on a laser-based widefield microscopy setup where a movable diffraction grating is placed into the excitation beam path. Zero order and/ or only first order diffracted laser beams pass through the objective. Here the laser

beams interfere with each other at the focal plane of the objective and create an illumination in stripes. This stripe pattern caused by the laser beam is superimposed with the sample and generates a Moiré effect [33]. Under this structured illumination the overlap between the high frequency organization of the objects within the sample and the high frequency of the illumination stripes creates a pattern of lower frequency, which is collected by the objective. The final super resolution image is then reconstructed by collecting several raw images, each acquired at different orientation of the structural illumination grid [34]. A set up showing the SIM principle is shown in figure 3.3. This kind of SIM imaging increases the spatial resolution over traditional widefield microscopy by 2x, achieving spatial resolution of 100-130 nm [35]. Only a small number of raw images are needed to produce a SIM image, for 2D data only 9 raw images are needed and for 3D only 15 due to the different positions of the diffraction grating . There is no need to use photoactivable or photoswithcable fluorophores when using SIM, so cheap and widely available conventional fluorophores are used. However SIM is often prone to image artefacts, the most common of which being the honeycomb shape and stripe pattern, originating from the illumination grating [36].

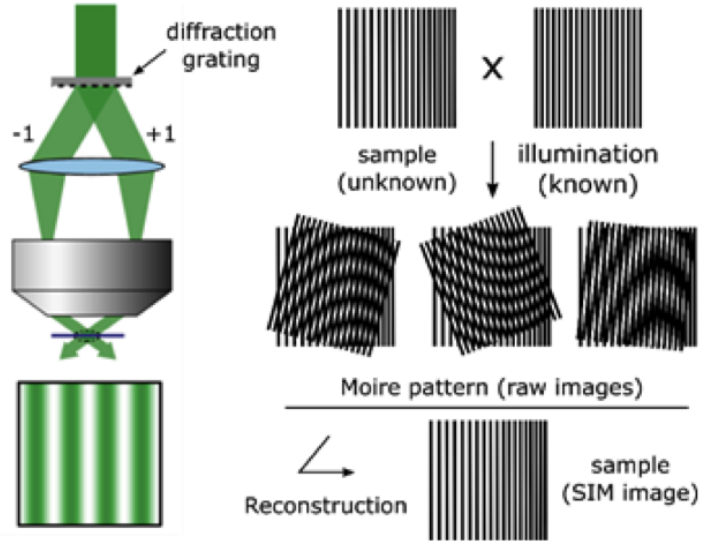

Figure 3.3: Images showing SIM set up where interference patterns are produced by illumination stripes from the diffraction grating, which are superimposed on the high frequency organization of the features within the sample.

3.3 STED

Stimulated emission depletion (STED) microscopy involves switching off the periphery of the fluorescence focus by depleting fluorescence in specific regions with a second beam. The second beam is often donut shaped, allowing fluorescence to occur from the first beam in the hole in the middle of the second beam. Fluorescence occurs when an electron in a fluorophore is excited by a wavelength of light from ground state to an excited electron state. Once the electron relaxes back to ground state a photon is emitted which is seen as fluorescence. However, STED interrupts this process before the photon responsible for the fluorescence is released [37]. The second beam stimulates the excited molecule into a higher energy level than the fluorescence transition would enter, causing the photon released to be red-shifted, as shown in figure 3.4.

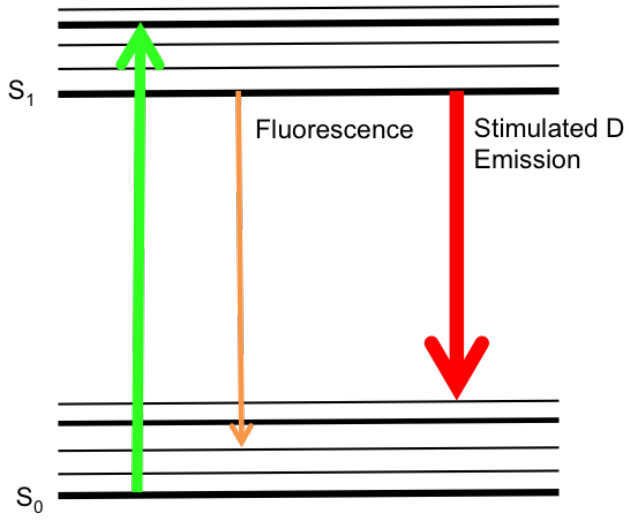

Figure 3.4: *Jablonski* diagram showing energy transfer induced by depleting laser beam on stimulated photon.

The second depleting laser beam inhibits fluorescence emission in the target area making the dye molecules appear dark to the detector. Figure 3.5 shows the resulting area of fluorescence once the second beam depletes fluorescence caused by the first beam [38].

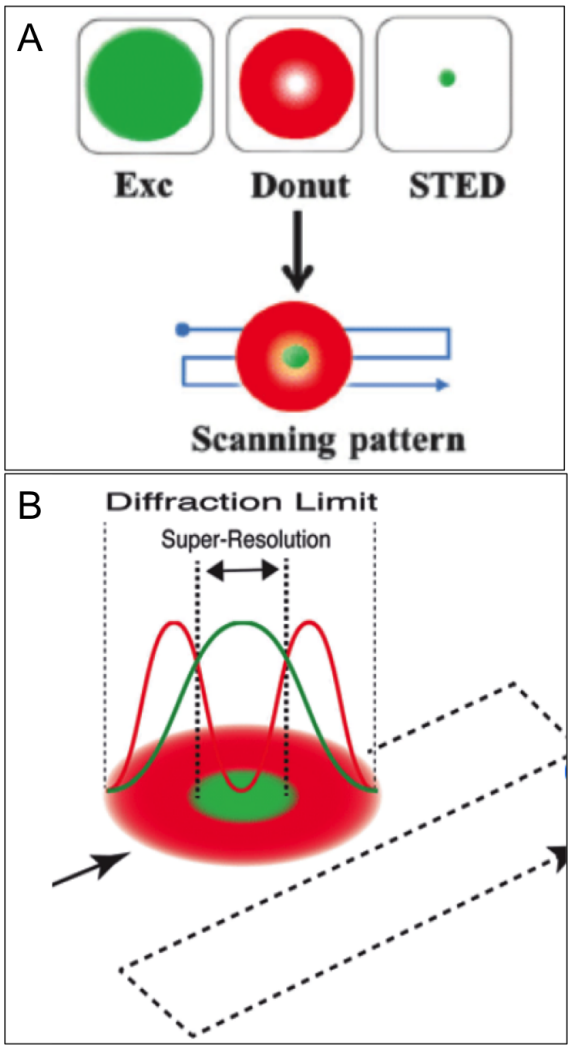

Figure 3.5: A) shows the green excitation laser and the specially designed donut shaped depletion laser. When superimposed, the second beam extinguishes the periphery fluorescence from the first beam leaving the super-resolution STED excitation area. B) Shows how the second donut shaped laser beam reduced the point spread function of the first excitation beam, resulting in super resolution imaging. Reproduced from [2].

To produce high quality STED images the photons of the depleting laser must strike the fluorophores within the sample, where the number of incident photons directly impacts the efficiency of the imaging. A high intensity laser produces a large number of incident photons that supress the fluorescence, but this can also bleach the sample, so a fine balance must be achieved. STED imaging occurs in a raster-scan method unlike brightfield light imaging or STORM where the entire imaging area is exposed to light. This allows the STED technique to be integrated to similar raster scan imaging methods, such as AFM

[37]. Specific buffers are not necessary for STED images, as the fluorophores used do not need specific environments in order to produce fluorescence. The spatial resolution achieved by STED microscopy is 30-80 nm [35]. It is routienly used on biological samples.

3.4 STORM

STORM: Stochastic Optical Reconstructive Microscopy. STORM is another type of super resolution light microscopy, which involves the stochastic switching of single-molecule fluorescence signal. To obtain a high-resolution image a sample must have means for a fluorophore to be incorporated. There are many different types of fluorophore cell labelling which vary from sample to sample. An ADA Snap tag can be added to a cell culture as it grows, this replaces newly formed peptidoglycan and a protein tag protrudes from the surface of the cell, described in chapter 5. The tag forms a highly stable, covalent thioether bond with fluorophore [39]. Once the fluorophore are bound to the tags via a click reaction explained in Chapter 5.4, the sample is exposed to a laser of sufficient intensity.

A complex process in which the sample blinks stochastically begins. The monochromatic laser beam is made up of photons which all have the same wavelength, the fluorophores absorb these photons and the electrons in the fluorophore become excited. The electron has a number of options on what path can be taken; it can go into the singlet state or the relatively long-lived triplet state. The electron drops down from both states releasing a photon, which is the fluorescence seen; however it stays in the triplet state for longer before a photon is released, as shown in 3.6. Resulting in the fluorophore looking darker for longer, it is in its darkened state. Once in the darkened stated, the electron has a longer period of time to form irreversible covalent modification by interacting with other molecules such as oxygen from the atmosphere. This results in the fluorophore becoming photo bleached. The average number of excitation and emissions that occur for a specific fluorophore are dependent on the molecular structure and the local environment (eg the buffer used) [4].

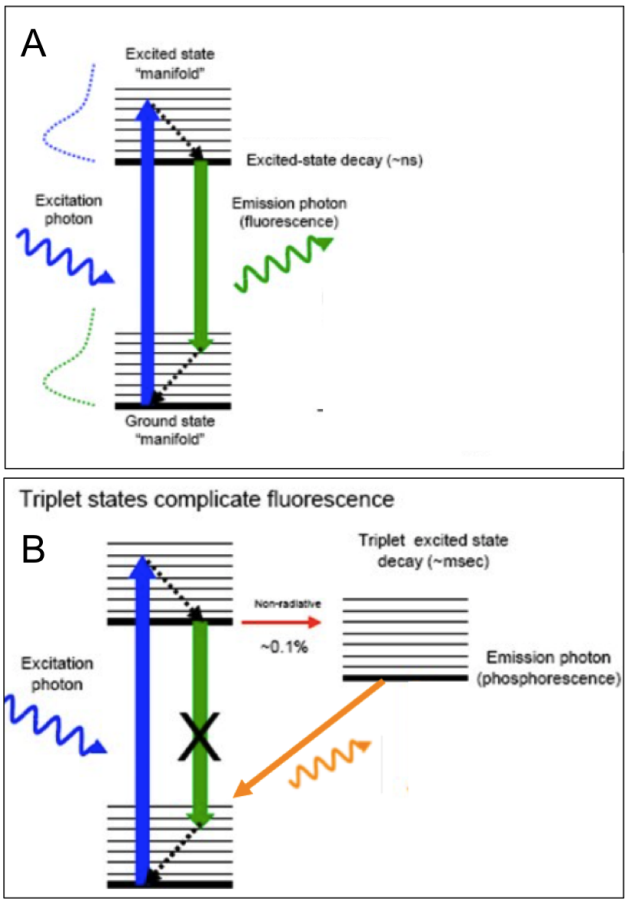

Figure 3.6: A shows a *Jablonski* diagram showing the electron path during fluorophore excitations. B shows diagram of electron path when in the triplet state.

When the fluorophore fluoresces, it is possible to precisely locate the molecule providing that another molecule is not fluorescing in a radius of the diffraction limit of the detection system used. When a single molecule is localized an image can be reconstructed. To generate a STORM image 500-100,000 image frames are needed. Software is used to reconstruct the large amount of images, a simple diagram is shown in 3.7. It can be seen that in coventional fluorescence microscopy each individual fluorophore cannot be identified, just the sum of all the fluorophores together is shown. This results in lost information from the sample under investigation. STORM imaging identifies each individual fluorophore as they are active at diferent times. The summation of all the localisations identified produce a high-resolution image.

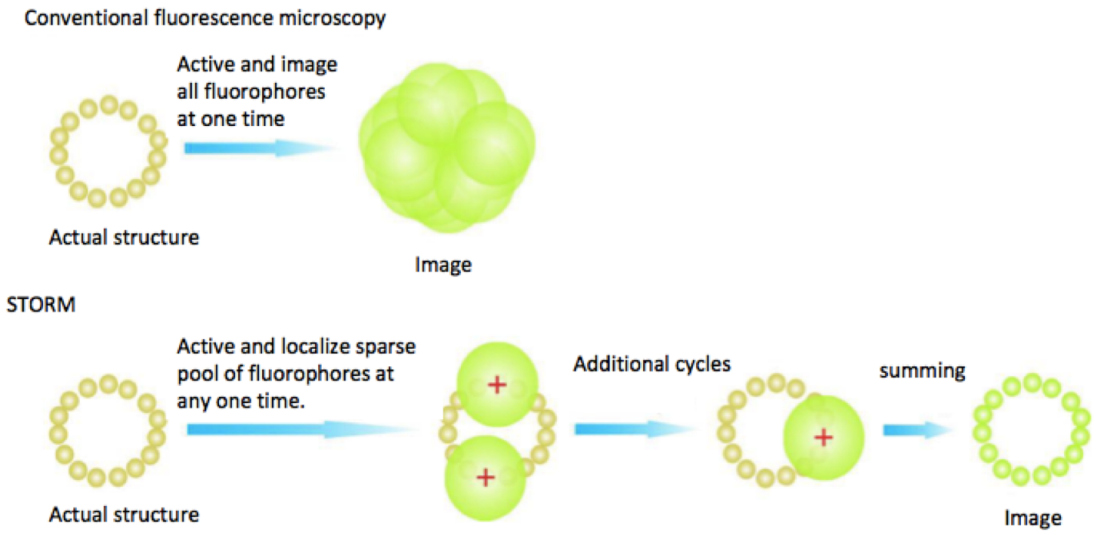

Figure 3.7: Schematic showing how single molecule localisation techniques such as STORM compare to coventional fluorescence microscopy [3].

Software identifies the fluorescent molecules in each image and fits them to a precise location. This is done fitting the point spread function of the fluorescent molecule to a two dimensional Gaussian function, shown in 3.4.

$$I(x,y) = A_0 + I_0 e - (\frac{1}{2}\frac{x0}{a} + \frac{y0}{a}) \tag{3.4}$$

A is the background fluorescence level, I0 is the amplitude of the peak, a) and b) outline the widths of the Gaussian distribution in the x-y direction and x0 and y0 are the coordinates of the centre of the peak. These Gaussian peaks can also be subtracted from eachother, if two molecules are too close to each other a wide Gaussian will be used to fit both molecules as one. However if then one of these molecules becomes photo bleached this larger Gaussian is replaced with a smaller one. If the smaller Gaussian is subtracted from the original Gaussian then the location of both molecules can be accurately deciphered, which is shown in 3.8.

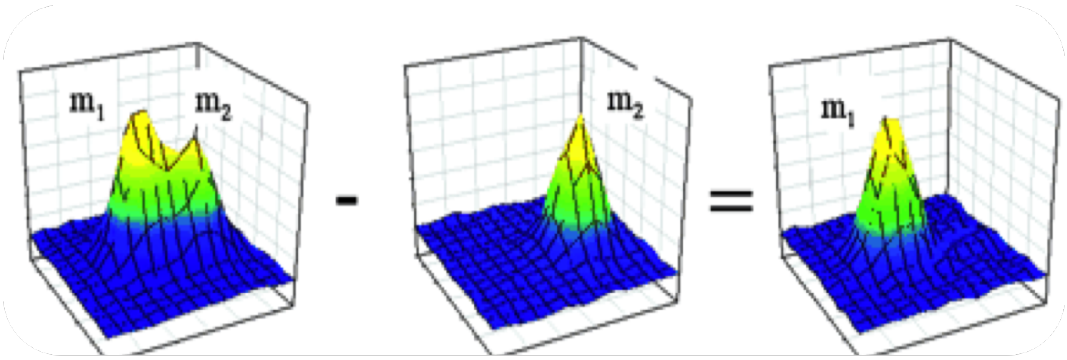

Figure 3.8: Diagram showing how two single localisation can be identified in an area where two fluorophores are turned on. When one fluorophore bleaches that position can be subtracted from the single large position identified initially, revealing both positions. [4].

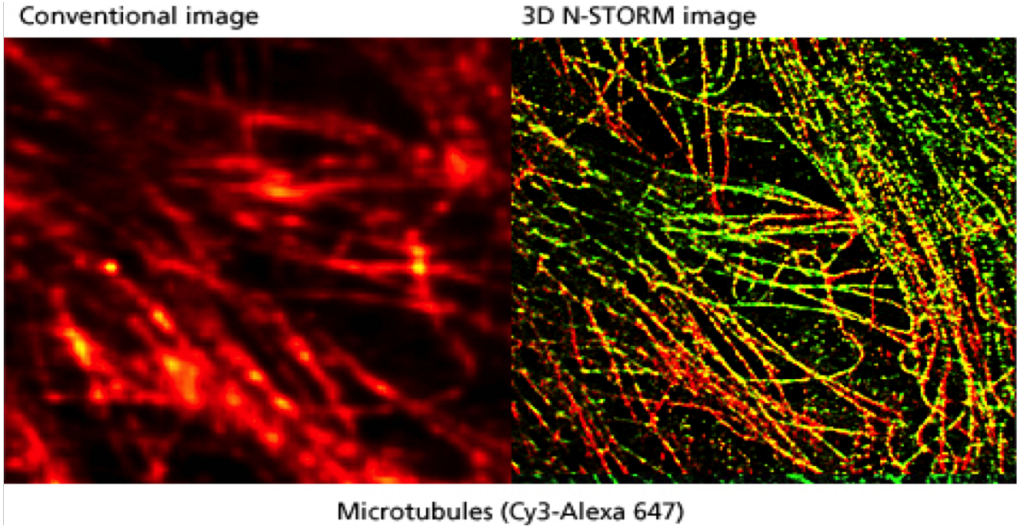

Figure 3.9: Data showing the increased resolution of a STORM image compared to conventional fluorescence microscopy. Taken from Nikon Microscopy U tutorial guide.

The precision of the exact position of the molecule determined can be increased by increasing the provided number of photons captured. Each captured photon is an independent measurement. There is also a level of uncertainty that comes with these measurement [40]. This is shown by the following equation.

$$\sigma = \frac{s}{\sqrt{N}} \tag{3.5}$$

σ the uncertainty s the standard deviation of the Gaussian function approximating the true point spread function of the emitter. N is the number of photons captured from the

fluorophore. The larger the number of photons captured the lower the uncertainty.

The spatial resolution of 20-30 nm is routienly achieved by STORM microscopy. A ten-fold improvement compared to conventional microscopy and the highest resolution achieved compared to the other super-resolution fluorescence mircoscopy techniques [41].

3.4.1 STORM buffers

In order to obtain the ideal conditions for stochastic blinking the local environment in which the sample is imaged must be tailored. Buffers are used to control this environment; they contain a variety of components, which ensure the consistency, and reproducibility of the controlled environment. Reversible blinking is necessary for STORM to be possible, this can be achieved with standard fluorescent dyes by adding chemicals in the imaging buffer which influence the photophysical properties. Chemically-induced blinking is determined by a long-lived non-fluorescent state when the excited electron is in the darkened triplet state. The buffer must provide an environment where the electron excited by the laser in the fluorophore, is able to stay in the triplet state for longer [42]. STORM buffers contain an enzymatic oxygen removing system as oxygen is the main source of photo bleaching [43]. Buffers, which provide this environment, contain glucose and two enzymes, glucose oxidase and catalase (GLOX) and a reducing agent in the form of Mercaptoethilamine (MEA). However the GLOX enzymes lead to buffer acidification due to oxygen exposure, which limits the life span to just a few hours, thus the buffers must be freshly made for each experiment [44]. The development of buffers is essential for the development of super resolution imaging. The quality of the image depends on the quality of blinking from the sample, which depends on the buffer quality.

3.4.2 Cameras used for STORM

In order to capture a large number of photons a camera with high quantum efficiency must be used. The "quantum efficiency" (Q.E.) is the ratio of the number of carriers collected

by the solar cell to the number of photons of a given energy incident on the solar cell. The quantum efficiency may be given either as a function of wavelength or of energy [45]. A pixel is typically composed of a photodiode and a potential well, the photons from the fluorescent molecules incident on the camera pixel surface producing a photoelectron. This generates a charge that is read by electronics and converted into a digital image to visually represent the brightness, size and location of the fluorescent molecules. The quantum efficiency of the camera is dependent on the pixels used. The higher the quantum efficiency of the camera the fewer photons needed to produce a photoelectron and hence to locate a molecule [46]. There are different types of cameras, which have different performance and capabilities, including charge coupled device (CCD), electron multiplying charge coupled device (EMCCD) and complimentary metal oxide semiconductors (CMOS).

3.4.2.1 CCD and EM CCD

The pixels in a CCD camera are made up of light-sensing units comprising of metal oxide semiconductors acting as a photodiode with a potential well, which acts as a collection point for photoelectrons. The photoelectrons accumulate in each collection point linearly proportional to the number of incident photons, until they are full and are emptied and read out. Each collection point gives the information about the spatial distribution of the photon signal on the pixel. The charge is gathered pixel by pixel in series into a container at the end of the relay, where the photoelectrons are converted into a voltage which is then processed into an images at the cameras circuit board.

EM CCD has a slightly different arrangement, where there is an addition of an electron multiplication register. This multiplies the photoelectron signal before the sensors are read out, increasing the sensitivity of the camera. This process does, however, introduce a source of noise (noise factor) which reduces the QE by up to 50% [47].

3.4.2.2 CMOS

The pixels in a CMOS camera consist of a photodiode-amplifier pair and as before photons that hit pixels are converted into photoelectrons. However instead of the photoelectrons building up in collection points before being emptied and converted into a voltage, the photoelectrons are converted into a voltage by each pixel's photodiode amplifier. This method results in much faster data acquisition in comparison with CCD cameras, however in the past this has been connected to low QE. Through the optimization of pixel architecture the QE have been improved reaching up to 95% in some models [48].

Chapter 4

Background information on bacterial samples

4.1 Introduction

Bacteria are prokaryotic, single celled organisms that come in a variety of shapes and sizes, in the few microns scale. Bacteria are most commonly known as the cause of disease, however they also play an important role in maintaining human gut flora and the development of medicine, amongst many other things. In recent years the issue of antimicrobial resistance has become a pressing matter, not only in healthcare but also in agriculture. Antibiotics are less effective when treating bacterial infections than they were in the past. This has resulted in increased mortality due to minor infection and increased risk when undergoing previously routine surgical procedures.

Although bacteria are small in size they form large colonies and biofilms. Biofilms are problematic in many areas of healthcare, such as dentistry, joint replacement and medical devices like catheters. The formation of biofilms can result in hard to treat chronic infections, even more so in this current antimicrobial resistance era [49] [50]. Biofilms also cause problems in infrastructure, coating internal surfaces in water lines, increasing friction which

reduces efficiency and invading cracks in concrete structures.

This chapter highlights the basic structures of Gram negative and Gram positive bacteria, focusing primarily on the cell wall material, peptidoglycan, as this is the main target for many antibiotics and thus the focus of this study. The species of interest are *Escherichia coli* (*E. coli*) and *Bacillus subtilis* (*B. subtilis*) where the growth and division process are outlined and discussed.

4.2 The external structures of bacteria

The classification of bacteria largely depends on the structure of the external cell envelope, with the two major categories of Gram-positive and Gram-negative bacteria. Typically Gram-positive bacteria have a much thicker cell wall compared to Gram-negative cells as shown in figure 4.1, a simple Gram stain assay is used to differentiate between the two. The gram stain involves staining the cells with Crystal Violet, which bind to the peptidoglycan of the bacteria by the addition of iodine, the cells are then washed with acetone to which removed loosely bound stain. Gram-positive bacteria are stained a deep purple colour as more stain is absorbed into the thick peptidoglycan layer, where as in Gram negative bacteria the acetone washes the stain from the much thinner peptidoglycan layer resulting in a pink colour [51].

4.2.1 Gram-negative cell envelope

Gram-negative bacteria have an outer membrane layer consisting of lipopolysaccharides (LPS), phospholipids bilayer and porins, including protein channels that allow ions and small molecules to pass in and out of the cell. Next a thin single layered peptidoglycan layer sits where there is only partial peptide cross-linkage. This results in a thin cell wall, ranging from 7-12 nm in thickness [52]. Lipoproteins are present within the peptidoglycan structure, and also protrude out from the surface. After the peptidoglycan layer there is

a region of periplasmic space, which is a gel-like matrix between the inner cytoplasmic membrane and the outer membranes. The periplasm of Gram-negative bacteria provides a unique environment for protein folding and stabilization, which also experiences challenges due to being highly exposed to fluctuations in the external environment. There is also a lack of energy source causing hurdles for processes that need energy, like biosynthesis reactions at the outer membrane. Gram-negative organisms such as *E. coli* overcome these obstacles, a number of mechanisms are used for protein folding and transportation of specific substrates. The cytoplasmic membrane (also known as the inner or plasma membrane) sits beneath the periplasmic space, where it is composed of a phospholipid bilayer where the regulation of passage of substances into and out of the cell occurs. The cytoplasmic membrane is responsible for a variety of processes including energy generation and biosynthesis [53].

Due to the presents of lipopolysaccharides (LPS) in the outer membrane, Gram-negative bacteria have the ability to produce endotoxins which are which are formed from the LPS structural component of the cell envelope. When the cells lysis or die the LPS formed endotoxins are released from the cell envelope, effecting the host in a number of ways causing a number of illness as such as, generic fever caused by infection, urinary track infection, typhoid fever, sepsis and meningococcemia. [54].

4.2.2 Gram-positive cell envelope

Gram-positive bacteria lack the outer membrane layer that Gram-negative bacteria have, but have the same inner membrane. To compensate for the lack of protective outer membrane layer a significantly thicker peptidoglycan layer is present, measuring 15-30 nm [55]. Wall techoic acids (WTA) are covalently linked to the outside of the peptidoglycan layer and are a group of glycopolymers, composed of polyol phosphate polymers bearing a strong negative charge. WTA are highly abundant comprising up to 60% of the cell wall and are thought to have many functions within Gram positive bacteria such as; the regulation of cell morphology and division, regulation of ion homeostasis, protection from host defences

and antibiotics and effects on adhesions and colonization which result in biofilm formations [56]. Beneath the thick peptidoglycan structure a thin layer is present where it is thought to be a thin periplasmic space, where a hypothetic model of peptidoglycan polymerization is aided by peptidoglycan precursors from the cytoplasm to the thin periplasmic space[57]. Like Gram-negative bacteria there is also a cytoplasmic membrane that sits beneath the periplasmic space, responsible for energy generation and biosynthesis.

Unlike Gram-negative bacteria, Gram positive bacteria do not produce endotoxins due to their lack of LPS. Instead they produce exotoxins, which are proteins, which are synthesized in the cytoplasmic space within the cell. Exotoxins are secreted by the bacteria and released outside the cell and are responsible for diseases such as, scarlet fever, diptheria, tetanus and botulism disease [58].

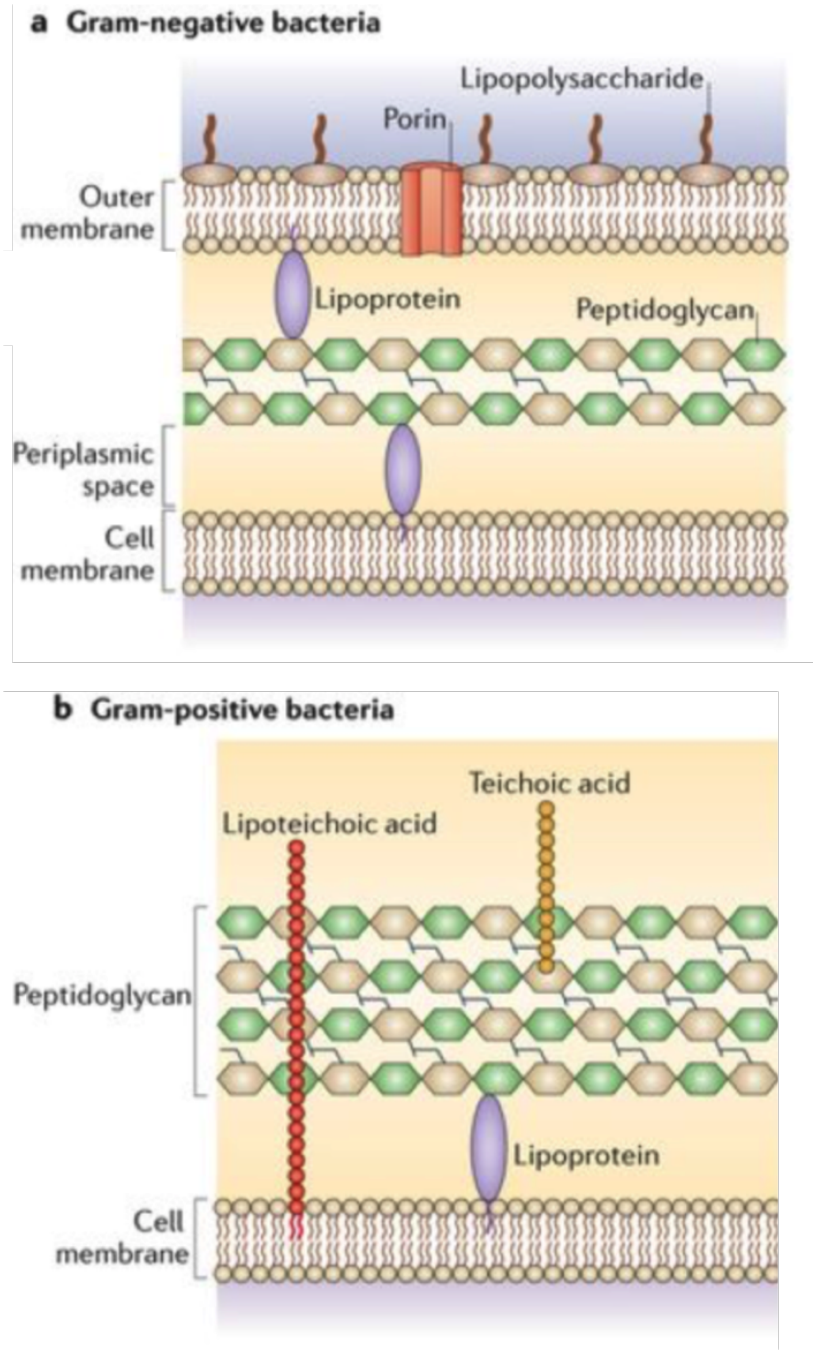

Figure 4.1: Diagram showing the bacterial cell wall, adapted from [5]. Section a) shows the struture of a typical Gram-negative cell evelope and b) shows the structure of a typical Gram-positive cell envelope

4.2.2.1 Flagella and pili

Flagella and pili are appendages that extend from the surface of the cell, both provide mobility for the cells, while also having a number of other functions. Flagella are long whip like structures that are attached to the bacteria via the cell membrane and have a helical form made out of protein, measuring 5-20 µm in length. Although primarily used for mobility, the flagella also sense the surrounding area for environmental information, such as temperature, pH and chemical variations. The movement resembles a propeller like motion and tend to be located at the poles of the bacteria.

Pili resemble small hairs with a hollow glycoprotein structure measuring 0.3-1 µm in length, which are attached to the cell wall. As well as contributing to the mobility via a twitching motion, pili are also responsible for cell attachment and bacterial conjugation for DNA transfer. Pili are located homogeneously on the surface of the cell wall to allow for these processes [59]

4.3 Internal structures

The internal structures all sit within the cytoplasm, which consists of water like fluid called cytosol and organelles. Cytosol is the carrier for all of the life essential components of which are needed for vital synthesis and processes, allowing a stable environment [60]. As bacteria are prokaryotes they do not have a membrane bound nucleus or any other membrane bound organelles. Instead DNA and other cellular content are located within the cytoplasm. Most bacterial DNA form compact circular chromosomes concentrated but not restricted to an area of the cytoplasm called the nucleoid, with the addition of small independent pieces of DNA called plasmids. Plasmids typically encode for advantageous traits but are not essential to the hosts, they can be transferred between bacteria through horizontal gene transfer. The most abundant intracellular structure found in bacteria is the ribosome, which are predominantly composed from RNA and protein with the prime purpose

of protein synthesis. Specialised photosynthetic bacteria, such as *Rhodospirillum rubrum*, contain chromatophores. They sit in the cytoplasm after they are formed via an invagination process of the cytoplasmic membrane. These complexes contain light-harvesting proteins, which allow the bacteria to undergo photosynthesis to produce energy [61].

The cytoplasm can be thought of as a container of relatively homogeneous liquid which is bound by the cellular envelope applying turgor pressure to the external structures such as the peptidoglycan. The turgor pressure cannot exert pressure over the surface tensions of the peptidoglycan or the cell will burst.

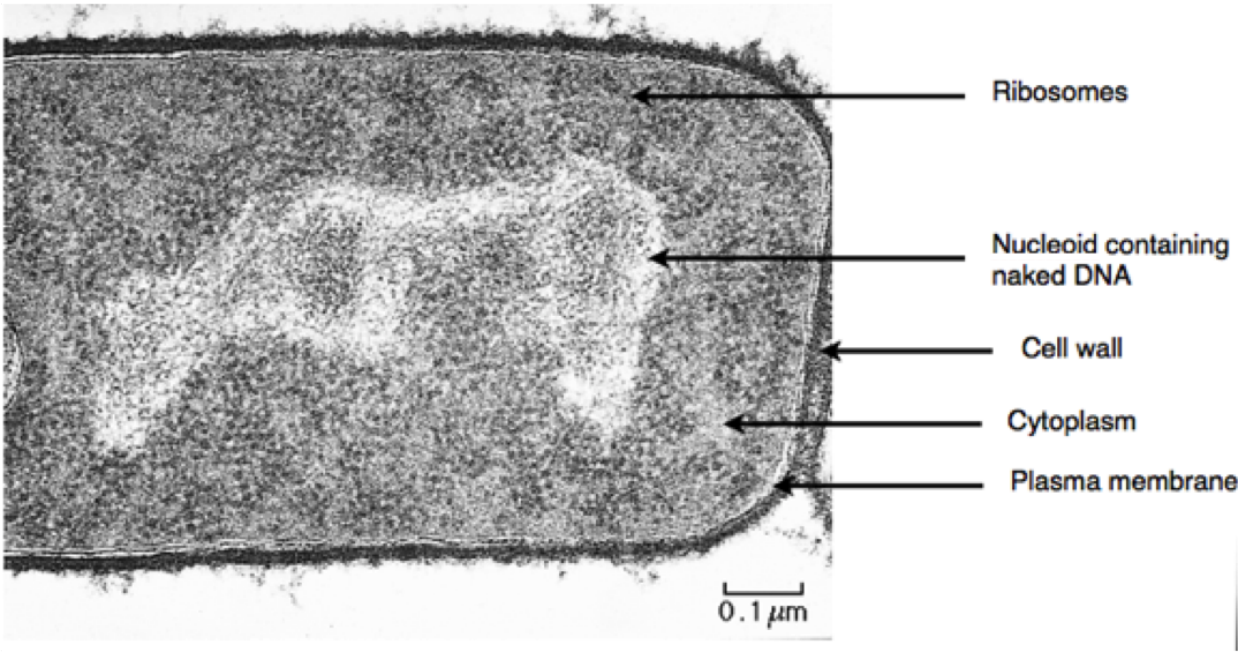

Figure 4.2: A thin slice EM image of an *E. coli* cell highlighting the thin cell envelope, nucleoid, cytoplasm and ribosomes [6].

4.4 Peptidoglycan

Peptidoglycan is the dominant cell wall structure in both Gram negative and Gram positive bacteria, which governs the cell shape and provides the cell with mechanical protection from the turgor pressure exerted by the cytoplasm[62]. The peptidoglycan structure is unique to prokaryotic cells, consisting of a glycan backbone and peptide side chains that cross

link glycan chains. The degree of cross-linking depends on the type of bacteria, Gram-positive bacteria (e.g *B. subtilis*) are highly cross-linked and Gram- negative bacteria (e.g *E. coli*) are partially cross-linked [52]. The glycan strands are made up of alternating *N*-acetylglycosamine (GlcNAc) and *N*-acetylmuramic acid (MurNAc) components, cross-linked at the carboxyl group (position 4) and amino group (position 3) either directly or through a short peptide chain [63] which is shown in figure 4.3. Glycan chain length varies within species of bacteria, and does not depend on thickness of the peptidoglycan layer. *S. aureus* and *B. subtilis* are both Gram positive bacteria with thick peptidoglycan layers, but *S. aureus* has an average chain length of 3-10 disaccharides and *B. subtilis* has an average chain length of 50-250 disaccharides, with some chains reaching 5 µm in length corresponding to 5,000 disaccharides [9].

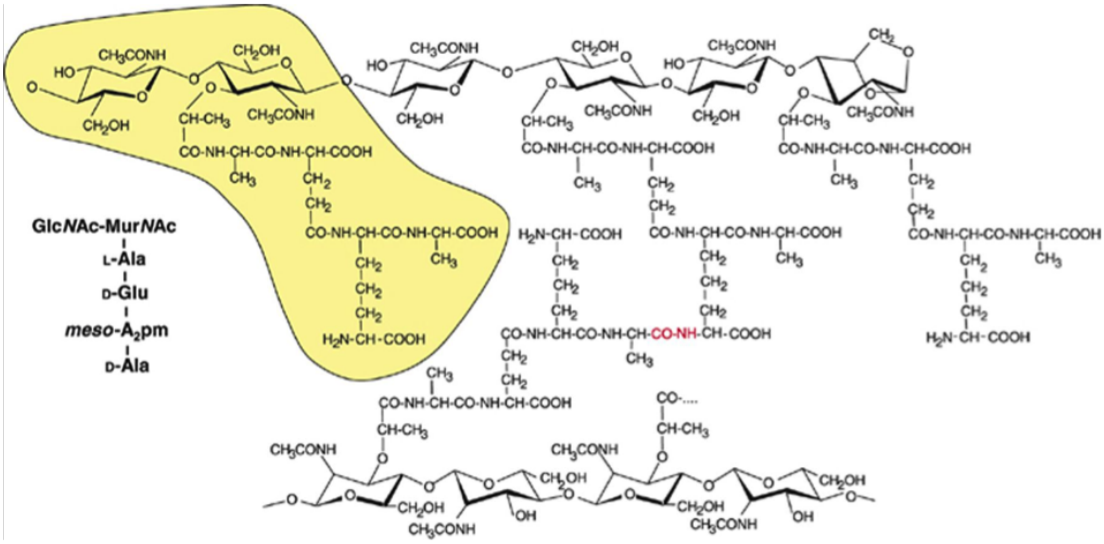

Figure 4.3: The structure of peptidoglycan. The yellow area highlights the basic sub unit and the middle area shows the peptide cross-linkage of the two glycan backbones. The red is the amide group connecting both peptide stems. Adapted from [7]

There have been a number of models for peptidoglycan. Initially it was thought that peptidoglycan formed uniform monolayers. The model is based on electron microscopy data of the *E. coli* cell wall where the glycan strands run parallel to each other in the same plane and are joined via T shaped cross-link bonds [64] shown in figure 4.4.

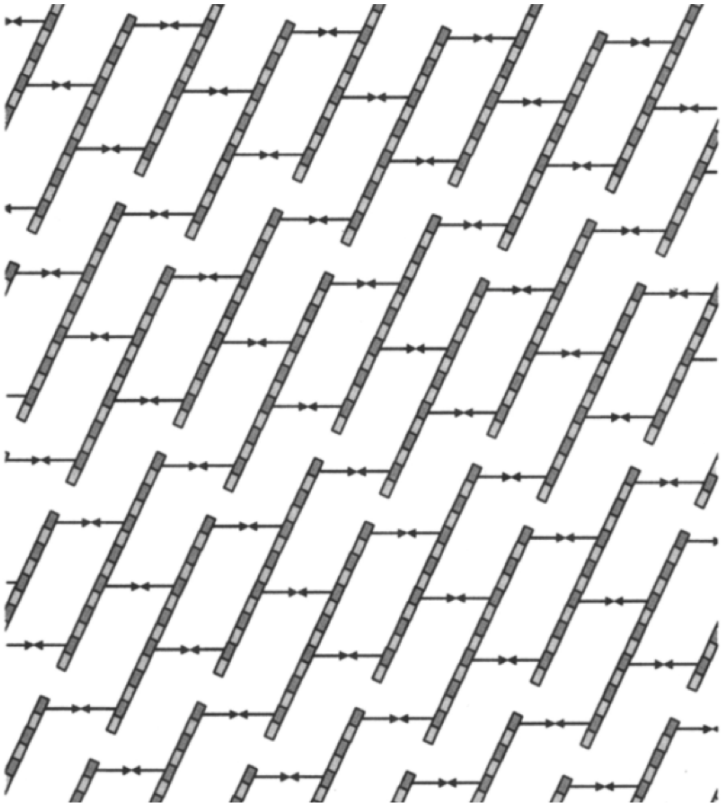

Figure 4.4: A schematic showing the monolayer model where dark grey bars show MurNAc units and light grey bars GlcNAc. The arrows show the peptide cross-links and the T shaped link that attaches monolayers together would sit perpendicular above or below are not shown. Image adapted from "Vollmer, W (2004) The Architecture of the Murein" [8].

Further developments led to the proposal of the scaffold model, where the glycans are oriented perpendicular to the plasma membrane and the peptide cross bridges form in zig zag conformations joining the glycans [65] [10] as shown in figure 4.5.

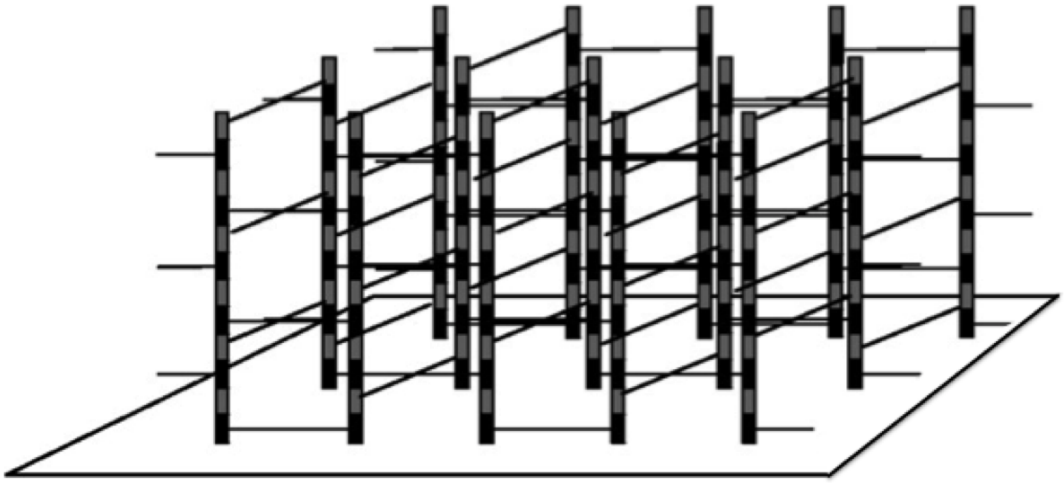

Figure 4.5: A schematic showing the scaffolding model, where the glycans are arranged perpendicular to the plasma membrane. Where dark grey bars show MurNAc units and light grey bars GlcNAc and the thin arrows show the peptide cross-links [8].

Studies on *B. subtilis* showed glycan chains orienting circumferentially around the cell in rope like macro structures called the "coiled coil" model, which became the standard model of peptidoglycan structure around the cell wall [16] shown in figure 4.6. The cables have been recorded to measure around 50 nm wide across the short axes with a helical structure. The smooth ordered cable structure is only present internally, the external cell wall has a more disordered structure. This is due to partial hydrolysis of the cables, giving the outer cell wall surface a rougher, more porous appearance. The contrast of internal and external structure suggest that the cell wall is made up of a multilayer peptidoglycan structure, where newly laid material is inserted internally.[9].

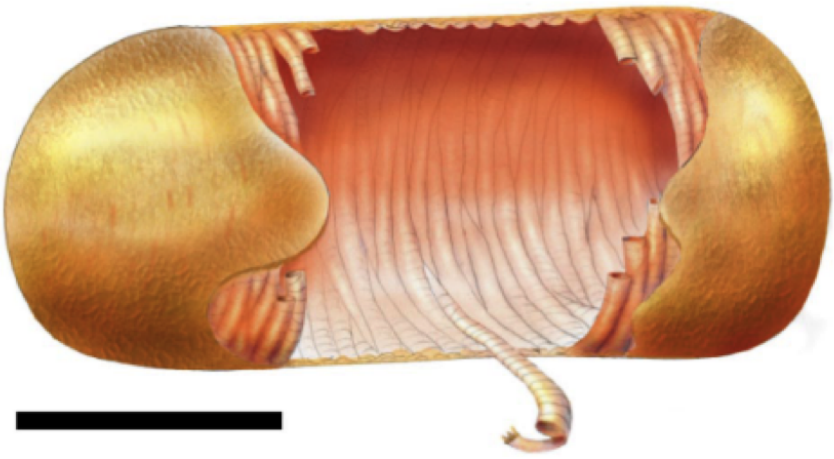

Figure 4.6: A model of *B.subtilis* macro peptidoglycan architecture. A cable like structure is oriented circumferentially around the cell with a coiled substructure. Scale bar 1 µm [9].

Studies have shown that newly laid peptidoglycan material forms a different macro structure to older peptidoglycan [66]. Newly formed material placed at the division planes of the *S. aureus* and *B. subtilis* form ordered concentric rings, as the material ages and the ring structures are lost and a rough disordered structure is adopted.

4.4.1 Growth and division

Bacteria divide via the process of binary fission, where the DNA is copied before being pulled to opposite ends of the cell. A septum composing of peptidoglycan laying a new cell wall is inserted in the middle of the cell separating the two halves before finally separating into two identical daughter cells. The way in which the septum is inserted varies from species to species. This process involves both synthesis of new peptidoglycan material and breaking bonds within the peptidoglycan by hydrolysis. This must be a carefully balanced process to ensure that the cell does not succumb to the cytoplasmic turgor pressure, resulting in lysis of the cell.

4.4.1.1 Cell wall synthesis

Peptidoglycan synthesis can be determined by using fluorescence imaging, where tagging the bacteria whilst in exponential phase highlights where newly formed material is inserted. This is the method used in this study. The insertion of peptidoglycan involves a number of different machineries that differs from the main body of the cell wall to the insertion on the septum as well as different species of bacteria. For coccoid bacteria such as *S. aureus* cell wall synthesis occurs mostly at the division site and is directed by filamentous temperature sensitive protein Z (FtsZ). FtsZ is a protein that forms a concentric ring structure, known as the Z ring, at the division site, which is used as a scaffold for a number of Penicillin-Binding proteins (PBPs 1-4) responsible for peptidoglycan synthesis. The deletion of FtsZ results in the delocalisation of peptidoglycan insertion during synthesis due to the lack of Z ring [67]. The septum synthesis occurs in a spiral ring pattern starting from the outside working inwardly, until the septum is complete forming a new layer of cell wall separating daughter cells. As peptidoglycan synthesis occurs mostly at the division site in *S.aureus* it was previously thought that the cells do not enlarge during the cell cycle and that the conversion of flat division septum into on hemisphere in each daughter cell accounted for the doubling in volume. However more recent studies have shown that during cell division the cells elongate and during the second generation the new cell wall material laid down on the septum constitutes for around 33% of the new cell wall material. Indicating that other mechanisms are involved in cell elongations and peptidoglycan remodelling through synthesis and autolysis of old peptidoglycan structure. This is supported by the change in structure of new material, which is seen at the division plane as concentric rings, and older material, which is seen more as a mesh like structure [10] shown in figure 4.7

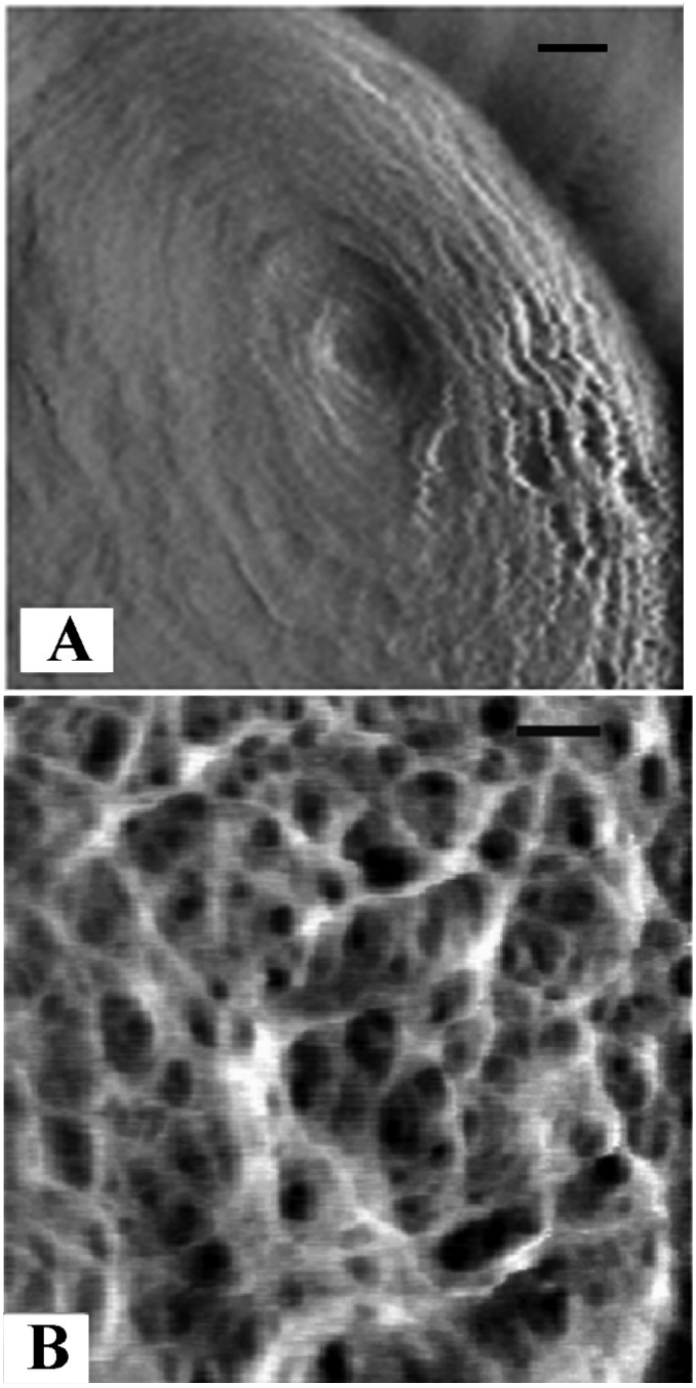

Figure 4.7: A) an amplitude AFM image showing the concentric ring structure of newly formed peptidoglycan at the division plane of model of *S. aureus*, scale bar 50nm. B) a high-resolution height image of the older region of cell wall with a mesh like structure, scale bar 50 nm. Adapted from [10].

Rod shaped bacteria has a more complicated cell wall synthesis process due to extensive cell elongation and septum formation. The protein MreB is required for the maintenance of

rod shaped cells and is localised in spiral formations along the longitudinal axis in *B. subtilis* and *E. coli*. The spiral structures band around the entire cell during cell elongation and become localised to the mid cell region when during septation. The localisation of MreB during septation is dependant on the prescence of FtsZ, which provides the same function of forming a Z ring and providing a scaffold for PBP for peptidoglycan synthesis [68]. Rod shaped bacteria need a lot more PBP for cell elongation and division compared to coccid bacteria, with 12 for *E. coli* and 16 for *B. subtilis* which are localised both at the septum and at the lateral wall [11]. Figure 4.8 show a model of peptidoglycan insertion in rod shaped bacteria, where synthesis occurs along the length of the bacteria in a spiral fashion governed by the localisation of MreB leading to cell elongation and also in the mid cell area during septation governed by the location of FtsZ [11].

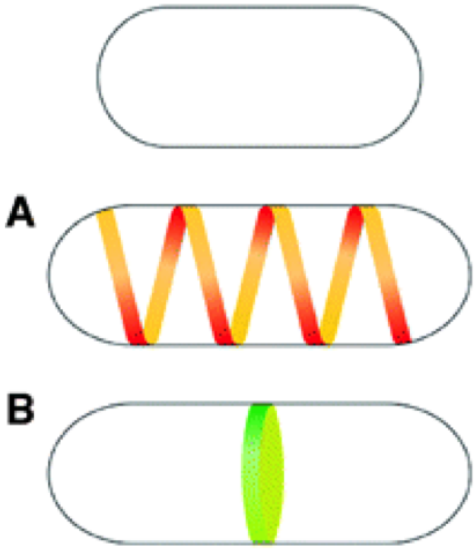

Figure 4.8: A) shows the incorporation of new cell wall in a helical path throughout the length of rod shaped bacteria, governed by the position of MreB. B) shows the insertions at he mid cell during septation. Adapted from [11].

4.4.1.2 Cell wall hydrolases

Cell wall hydrolases are enzymes used by the cell during growth and division. Hydrolases are linked to the degrading of cell wall, however they are tightly regulated by the cell to

aid the growth and division process when daughter cell separates [69]. It has been proposed that hydrolysis of existing bonds under strict cell regulation allows for cell growth whilst maintaining cell wall integrity to withstanding the internal turgor pressure applied by the cytoplasm. For growth and cell elongation a three-for-one model was developed, where three new peptidoglycan strands are cross-linked together, forming a peptidoglycan triplet. The triplet is cross-linked to a single stress-bearing strand of peptidoglycan where the triplet is not bearing any stress. The single strand is then removed by hydrolase activity resulting in the insertion of three new peptidoglycan strands, which are stress bearing, resulting in growth [12].

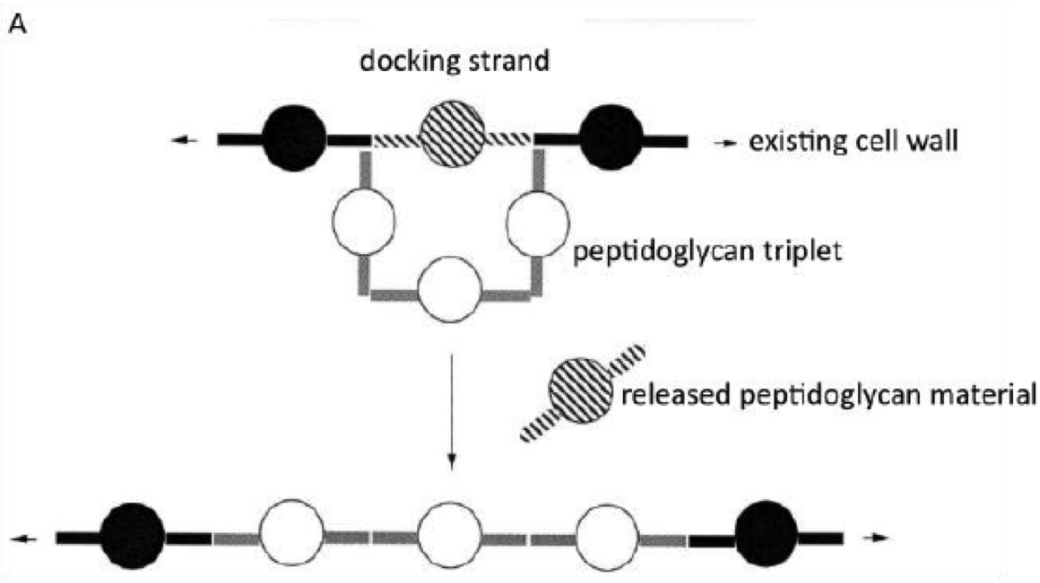

Figure 4.9: a schematic showing the insertion of peptidoglycan triplet around a single stress bearing peptidoglycan strand, the single strand is then hydrolysed and the triplet takes is place as stress bearing material, resulting in growth. Adapted from [12]

4.5 Bacterial species investigated

In the work presented, an investigation of the cell wall material, peptidoglycan, is shown in both *E. coli* and *B. subtilis*. The insertion of peptidoglycan was studied and the development of new material into old material was investigated by imaging the bacteria with STORM

microscopy and AFM. The peptidoglycan material was harvested whilst the bacteria where in exponential phase, where the bacteria are in a rapid growth and division stage.

4.5.1 *Escherichia coli*

E. coli is a rod shaped, Gram negative, anaerobic bacterium. It is most commonly found in the gastrointestinal tracts of human and animals, as apart of normal healthy gut flora. However through the acquiring of virulence factors through exchanging plasmids (or other mechanisms such as bacteriophages) pathogenic *E. coli* has evolved which causes severe disease, making *E. coli* cell wall a topic of interest. As *E. coli* is a Gram negative species the cell wall is very thin consisting of mostly single layers of peptidoglycan, although in some regions this is increased to up to three layers thick [70]. The cell wall also presents thin bands of more dense material, which lay mostly perpendicular to the long axis of the cell, running circumferentially. Through imaging with AFM the circumferential bands were imaged and were too long to account for individual glycan strands, instead high-resolution images showed that the less dense bands contain pores and form a mesh like structure. Through hydrolase digestion of the banding features on the sacculi it became apparent that the glycans that make up the oriented band structure have little to no orientation. These bands were proposed to define regions more or less available for the insertion of new peptidoglycan material, which is governed by PBPs in the inner membrane [13].

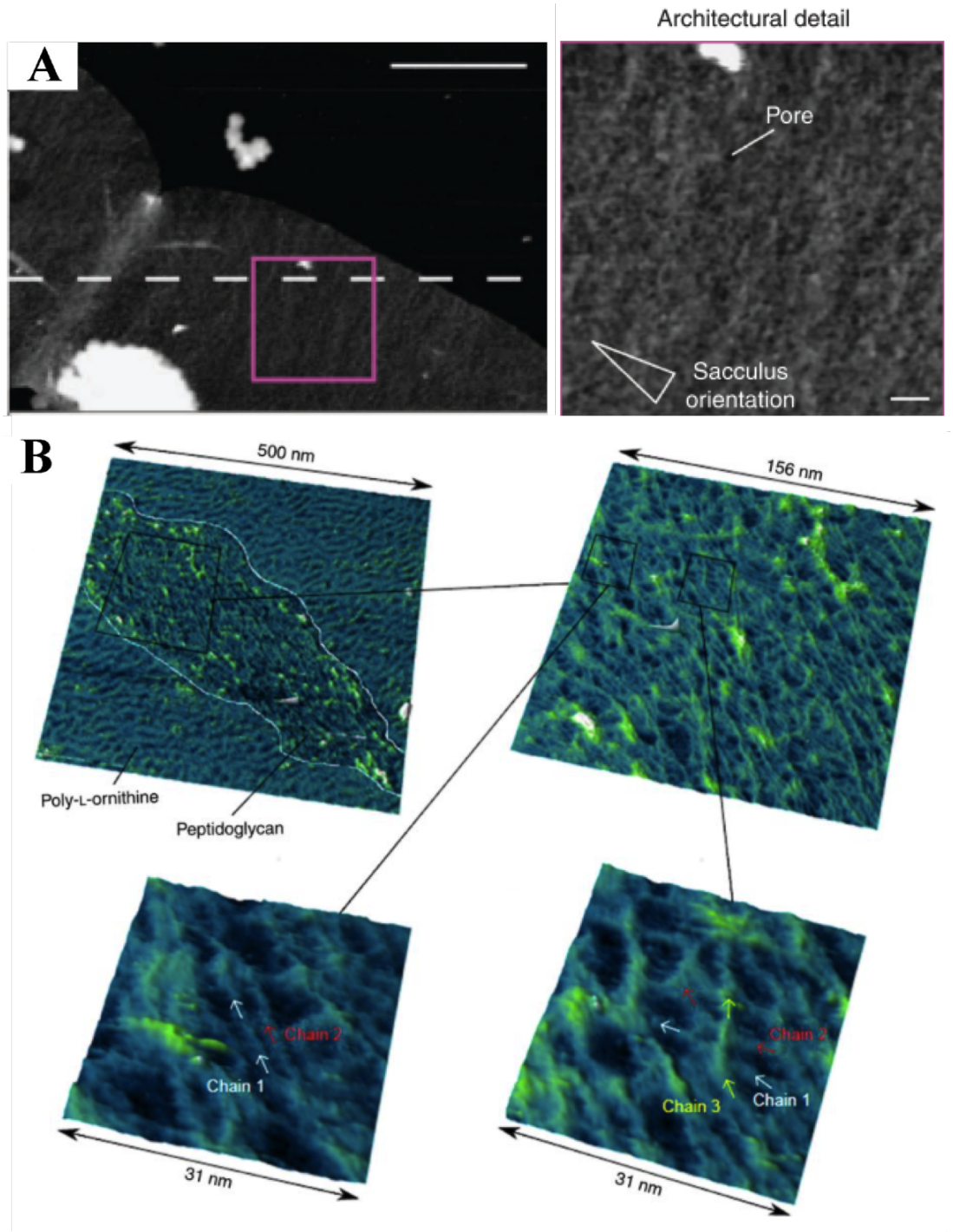

Figure 4.10: A) AFM images showing a section of sacculi imaged from an intact *E. coli* sacculi where the banding structure can be observed with respect to the orientation of the cell. Scale bar 50 nm. B) High resolution AFM images of *E. coli* sacculi showing the lack of orientation of individual glycan strands. Adapted from [13], [14].

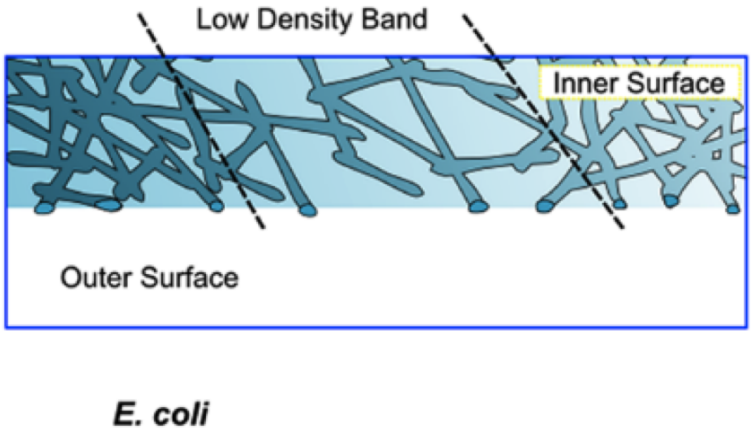

Figure 4.11: a schematic showing a model of the cell wall structure in *E. coli*. The low banding is represented by low and high density banding, where it is suggested that newly formed peptidoglycan would be inserted in low-density areas during cell elongation. The directions of the glycans have no orientation within the bands [13].

To investigate peptidoglycan insertion in *E. coli*, the cells were broken and sacculi purified to exclude any potential non-specific binding to cytoplasmic materials. Using STORM to obtain high resolution imaging, it was observed that peptidoglycan insertion in *E. coli* occurs in multiple distinct foci spreading over the cylindrical area of the cell wall. Where is it thought that new peptidoglycan is placed in low densities areas highlighted in figure 4.11. As before the insertion of newly formed peptidoglycan is governed by MreB complexes as in *B.subtilis* [13] [14].

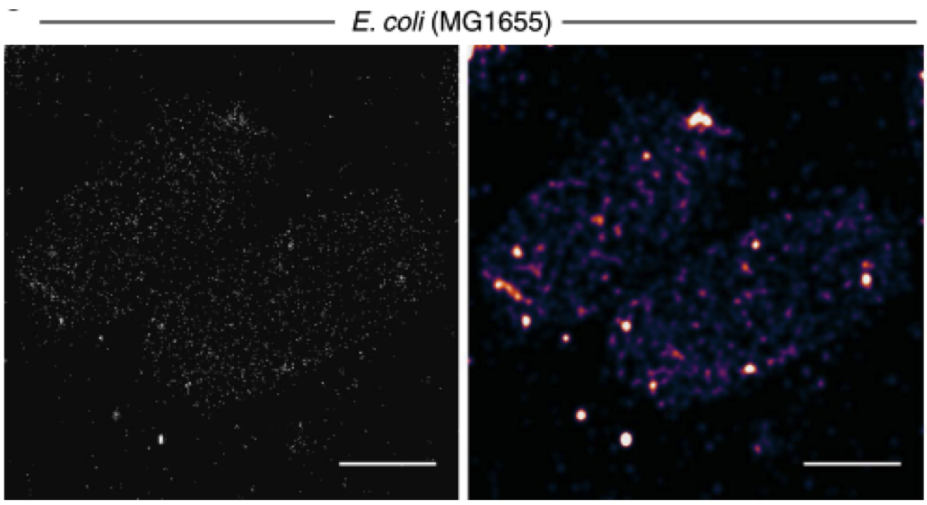

Figure 4.12: STORM images showing peptidoglycan insertion in *E. coli* with no visible pattern, but multiple distinct foci spreading over the cylindrical cell body. Scale bar is 1 µm long [13].

4.5.1.1 Division and septum formation

During cell division *E. coli* the cell constricts due to simultaneous synthesis and cleavage of the septal peptidoglycan before forming two fully formed poles and hence two daughter cells, shown in figure 4.13. During cell elongation hydrolysis occurs via transglycosylase and endopeptidases, degrading older material to make room for new peptidoglycan insertion. During septation it has been reported that three amidase enzymes named AmiA, B and C in *E. coli* are involved in splitting the cell once septation occurs. This is done by removing the peptide cross-link in the peptidoglycan structure, which is investigated further in chapter 7. When AmiA, B and C was deleted the *E. coli* grow into long chains of un-separated cells, with rings of thickened peptidoglycan appearing at the site of blocked septations and separation [71].

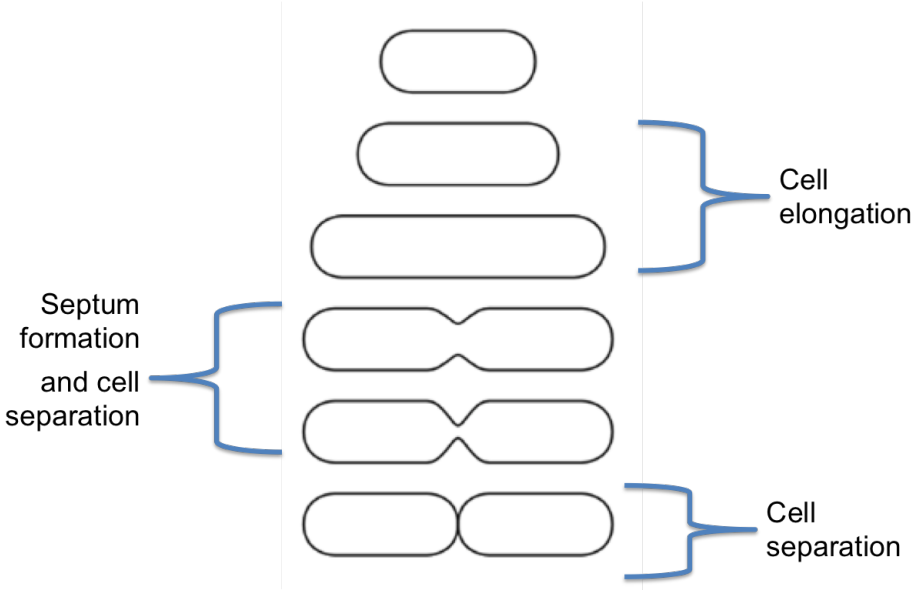

Figure 4.13: a schematic showing a model of the cell division process in *E. coli*[13].

4.5.2 *Bacillus subtilis*

B. subtilis is a harmless Gram positive rod shaped bacteria found in large quantities in soil and a part of the human gut flora. The cells are motile with flagella located at its poles and has the ability to sporalate when grown in unfavourable conditions producing endospores. Endospores are an insurance safe guard for the bacteria to ensure the survival in varied extreme condition, once ideal conditions resume the endospores are able to germinate and the bacteria can once again thrive.

The work presented here focuses on the septum formation of *B. subtilis* and the peptidoglycan insertion in the rod of the cell wall as the cell elongates. *B. subtilis* grows by elongation of the main rod of the cell followed by septation. New peptidoglycan is inserted in the main rod in a helical pattern during cell elongation, which is governed by MreB, MreC and MreD, as stated above. This is demonstrated by using fluorescently labelled vancomycin derivative to visualize the insertion of nascent peptidoglycan in live *B. subtilis* [11]. Observations suggested that peptidoglycan insertion occurs in discrete bands along the cylindrical part of the cell, which has been described as reminiscent of the helical pattern in which the MreB complex moves through the cell [72] [15]. This is shown in figure 4.14. When MreB complexes are removed the shape of the cells are drastically changed, however the septum is still present. Instead of having long the rod shaped morphology, the cells are uniformly spherical and the banding structure is no longer present [73].

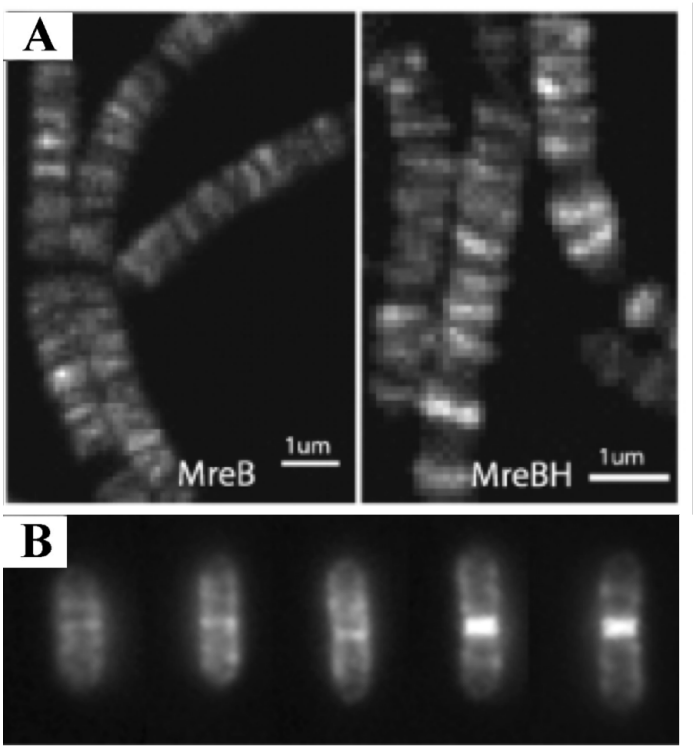

Figure 4.14: A) GFP labelled MreB complexes in *B. subtilis* highlighting the axial motion of the complex. B) vancomycin-stained peptidoglycan in nascent *B. subtilis* during various stages in the cell cycle, highlighting the banding insertion pattern. Adapted from [11], [15].

Peptidoglycan organisation has been proposed to take form in layers of material where peptidoglycan is bundled into thick rope that are parallel to the membrane and run circumferentially relative to the cell. Observations have shown that the inner structure of the cell wall have these wide thick rope like structures, and the outer cell wall structure does not contain the thick rope like features and instead has a disordered mesh structure [9].

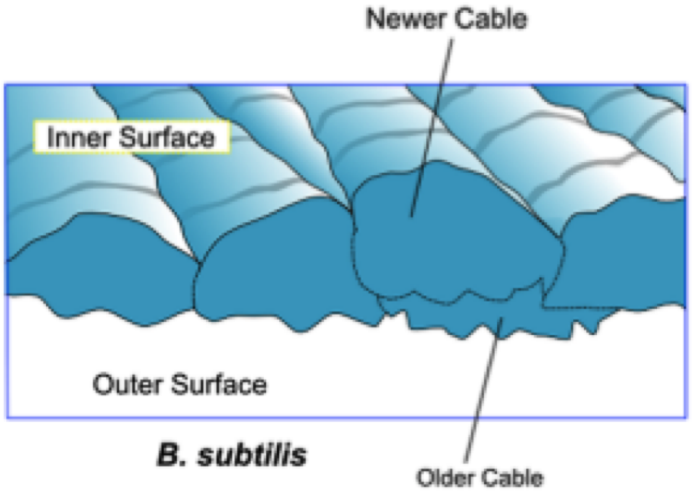

Figure 4.15: A diagram of *B. subtilis* cell wall showing the cable structure on the inside and the mesh, disordered outer surface [16].

When imaged by AFM in air the septum structure consists of a thick outer band surrounding a spiral snail shell structure on the septal disk [16][9]. However when imaged in liquid this spiral structure is no longer visible, instead one side of the septum (the side facing outward resulting in the external pole) has a concentric ring structure similar to the division plane in *S. aureus* and the other side (facing inward into the cell) has a dense, smooth mesh like structure. This is shown in this study in chapter 8, which is also presented in [**?**].

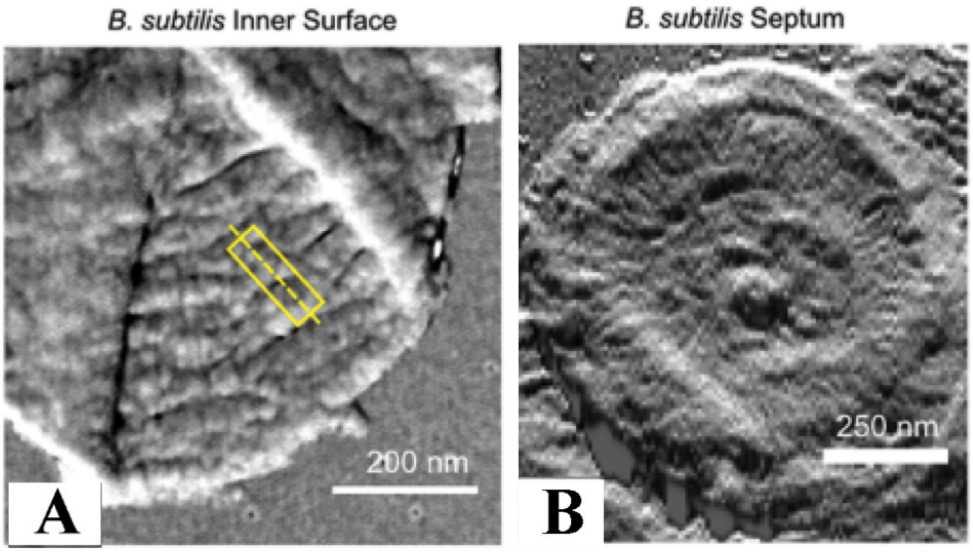

Figure 4.16: AFM images taken in air of *B. subtilis* sacculi, A) shows the internal rope structure and B) shows the snail shell spiral feature in the septal disk [16].

4.5.2.1 Division and septum formation

During the cell division process *B. subtilis* the cell elongates and then a septal disk is produced, once complete the two daughter cells separate via hydrolysis resulting two cells. The material at the division plane matures to form a cell pole. Figure 4.17 shows a simple diagram of how cell division occurs in *B. subtilis*, note how there is no cell separation until the septum is completely formed.

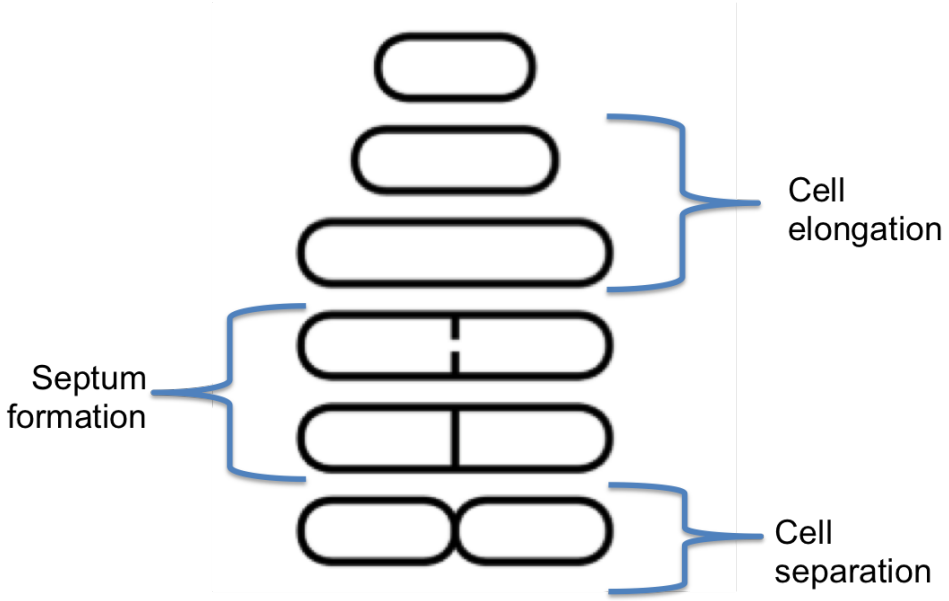

Figure 4.17: A diagram showing cell division in *B. subtilis*, where the cell elongates, septation occurs and followed by cell separation. Adapted from [16].

The way in which peptidoglycan in inserted within the septum is investigated in this work. Previous studies suggest that the septum is formed by the addition of newly formed peptidoglycan at the leading edge of the septum [17]. Here SIM microscopy was used with Fluorescent D-Amino Acids (FDAA) to pulse label the live *B. subtilis* for 60 minutes, 5 minutes and 30 seconds, where sub sequential labelling in a different colour was used after to highlight how peptidoglycan insertion occurs over time. Labelling also occurred for very short periods of time (15 seconds) with the aim of highlighting if newly formed material is

placed only at the leading edge of the septum. This is shown in figure 4.18 where software is used to rotate SIM images taken of septums in whole *B. subtilis*. In the study presented here a similar pulse labelling method was used, however the peptidoglycan was then extracted and purified and imaged using STORM and AFM, as well as SIM.

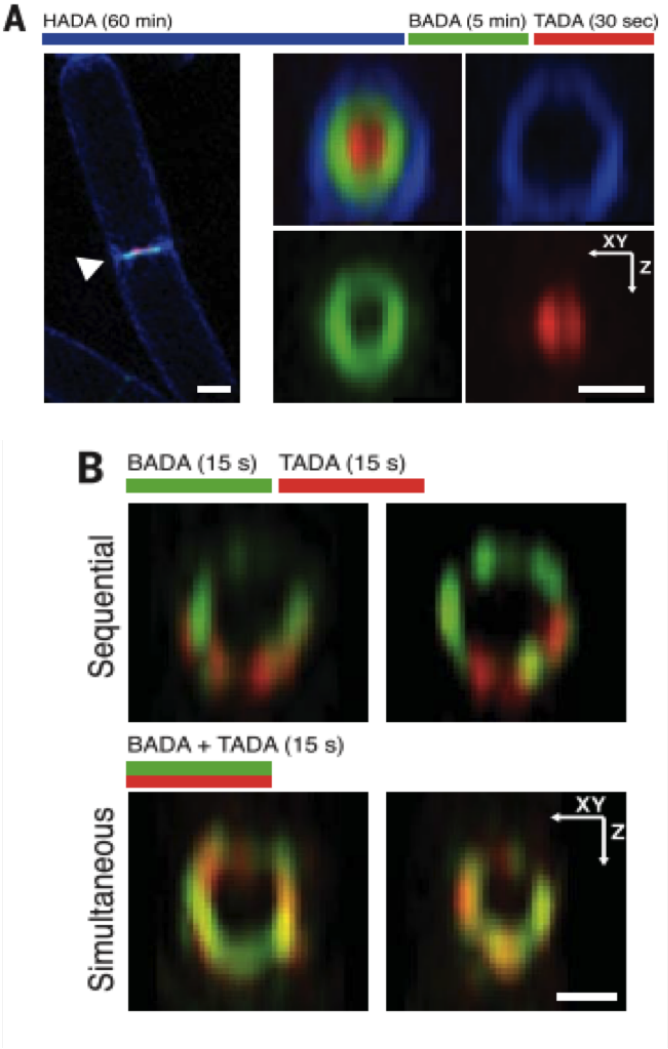

Figure 4.18: A) sequential FDAA labelling in different colours in whole cells, indicating that within 5 mins peptidoglycan insertion only occurs within the septal plate. B) Peptidoglycan insertion occurs within small time frames (15 seconds) where sequential labelling show the site of peptidoglycan synthesis moves around the septum as it is formed. Scale bars 500 nm. Adapted from [17].

4.6 Fluorescently labelling peptidoglycan

There are a number or ways in which peptidoglycan can be fluorescently labelled by either tag or stained. In the work presented here Florescent D-Amino Acids (FDAA) are used to tag the peptidoglycan structure, where a fluorophore can be attached. During cell wall synthesis disaccharide pentapeptide monomers are linked together at corresponding sugars, producing a peptide stem, which is cross-linked via transpeptidation. This pentapeptide chain is assembled sequentially by a series of ligases that incorporated L- and D amino acids, which are both unique to bacteria. During the growth process of the bacteria if an abundance of FDAA is available the ligases that incorporated L- and D amino acids take the FDDA up instead, providing a tag which the fluorophore can later be attached to. This process is reliant on the tolerance of the peptidoglycan machinery to accept D-amino acid analogues [74]. Fluorescent vancomycin can also be used to label peptidoglycan as it also targets the L- and D amino acids [13]. Another stain which can be used is N-Hydroxysuccinmide (NHS) ester. Which is an amine-reactive reagent that binds to protiens, peptides and other amine containg groups, ideal for labelling peptidoglycan.

4.7 Antibiotics

Peptidoglycan is a structure unique to bacteria and is the target of many important antibiotics used. Antibiotics are crucial in modern day medicine to prevent and treat dangerous bacterial infection. Alexander Fleming developed the 1st antibiotic in the 1920s by filtering penicillin from mould fungus, which led to the development of clinical penicillin, which was widely used in the 1940s to save the lives of infected soldiers in World War II [75]. However at the time Fleming stated that the bacteria would soon become resistant to penicillin, which is a trend that has followed with more resent developments of antibiotics. Resulting in the birth of the antimicrobial resistance (AMR) era, where bacteria have become resistant

to a multitude of antibiotics producing 'super bug' infections such as MRSA.

A number of antibiotics target the penicillin binding proteins (PBPs) on the cell surface, PBP play a significant role in the manufacture and regulation of peptidoglycan and cell division. This makes them an ideal target for antibiotics such as the β-lactams, however exactly how these drugs work is still unclear. There is an understanding that they bind irreversibly to the PBP active site preventing the required cross-linking to the peptidoglycan layer; this results in defect in the cell wall, preventing the proper formation of the septum during cell division, which causes the cell to lyse [76].

4.8 Project purpose

STORMForce has the ability to produce high-resolution images that identify specific molecules of interest using fluorescence and high-resolution images and force data is obtained by AFM of these specific molecules. Giving context to the area of interest with regards to the rest of the sample being observed. Using the STORMForce technique on bacterial samples allows the user to observe events that happen at specific times in the cells life cycle. The main focus here being the cell division process, STORMForce is used to identify areas of peptidoglycan inserted into the cell wall and how the structure of old and new material differs. By doing this, a greater understanding is achieved of the main cell wall component of bacteria, which is the main target for antibiotics.

Chapter 5

Materials and methods

5.1 Introduction

This Chapter highlights and explaines the methods used to develop the samples, substrates and imaging techniques used. *E. coli* and *B. subtilis* where the main bacterial species investigated here, which were grown and processed in a controlled manner. In the purpose of keeping the samples close to native conditions and to keep all samples as consistence as possible. To fully understand the different growth stages of the bacterial species used, growth curves were taken until the bacterial where comfortable in stationary phase. Once the growth phases were identified the sample could then be produced. Data aquisistion and processing methods for STORM imaging are outlined, the analysis for relevent data is included in the results chapters.

5.2 Cell culture methods

All bacterial samples where first plated on agar dishes and a single colony was used to inoculate a conical flask of media. The growth media used is depended on the strain and species of bacteria used. Stocks of each strain were kept long term at -80 ℃ and all cultures where grown in duplicate so a back up was always available if failed growth was to occur.

The cells were grown to exponential phase, where a fluorescent tag was added allowing for fluorescent imaging. Azido D-alanine (ADA) is a D amino acid derivative that contains an azide group, which attach to alkyne containing molecules, such as fluorophores, via click chemistry. The ADA tag inserts into the peptide cross-link within the peptidoglycan structure, allowing for fluorescence labelling of the material used.

5.2.1 *Escherichia coli*- media and agar.

The growth media used for *E. coli* is Lysogeny broth (LB). 1 L quantities were made to produce enough *E. coli* sacculi for the experiments. In 1 L of deionised water 10 g of tryptone, 5 g of NaCl and 5 g of yeast extract was added and mixed with a magnetic stirrer until dissolved. To make LB agar 1% of agar powder was added to the volume (250 ml, 2.5 g of Agar powder). Both media and agar were sterilised in an autoclave at 121 ℃ for 20 minutes before use. The agar was poured into petri dishes and left to set; this is done in a lamina flow hood to maintain sterile practice. *E. coli* strain MG1655 stocks were kept long term at -80 ℃ . A bead was removed from the stock and spread onto the agar dish and grown overnight at 37 ℃ . Once visible colonies have developed (typically within 24 hours) the plate was stored at 4 ℃ for a maximum of two weeks. 15 ml of media was transferred into a sterilised universal tube and a colony from the petri dish was selected with a sterile loop and used to inoculate the media. This was left overnight on a rotary shaker set to 250 rpm at 37 ℃ to produce overnight liquid cultures.

5.2.2 *Escherichia coli* growth

The overnight process ensures that the culture has reached stationary phase. A calculated amount of the overnight culture was added to the remaining media to get an optical density (OD) of 0.05. A 600 nm wavelength light was used to measure the optical density of 1 ml of the sample using a spectrophotometer. To produce *E. coli* with completely fluorescent peptidoglycan, at this stage of inoculation 1 ml of ADA at 1 M concentration was added to

the 1 L of media. The inoculated media was the placed on a rotary shaker at 250 rmp at 37 ^{o}C and checked every 30 minutes till the OD showed the solution had reached exponential phase, OD 0.3-0.8. The advantage of growing the samples to exponential phase is that the cells are still at a rapid growth phase. A large proportion of the peptidoglycan will show features that appear in growth and division.

5.2.3 Harvesting Cells for AFM - *Escherichia coli*

Once the cells reached exponential phase, indicated by the optical density, 1 ml of culture was centrifuged at 13,000 rpm for 3 minutes. This forces the cells out of suspension and forms a pellet, the supernatant was discarded and the pellet was resuspended in 1 ml of HPLC grade water and centrifuged again. This was repeated 3 times to wash the cells of the media. 10 µl of the sample was then dried onto the imaging substrate and washed 3 time with 100 µl of HPLC grade water. The sample was imaged in both air and liquid on the AFM. For samples only imaged with the AFM the sample was placed on cleaved mica, if also imaged with a fluorescence microscope a processed glass cover slip was used as the substrate.

5.2.4 Peptidoglycan extraction - *Escherichia coli*

Once the sample was in exponential phase the cells were killed and processed to extract only the cell wall. The culture was chilled on ice and transferred to a 1 L centrifuge bottle and spun down at 10000 rpm for 10 mins and the supernatant was discarded. The remaining pellet was resuspended in minimal PBS (around 5 ml) and transferred to a 15ml falcon tube. 5% boiling SDS was added drop wise (5 ml in total) and boiled for 30 minutes. The solution was then transferred to a 10 ml ultracentrifuge tube and spun down at 400,000 $\times$ g for 15 minutes at room temperature. The pellet is then resuspended in HPLC grade water and the ultracentrifuge process was repeated 4 times. The pellet was the resuspended in sodium phosphate buffer (50 mM, pH 7.3) containing 100 µg/ml chymotrypsin and incu-

bated overnight at 37 ℃ with agitation. The pellet was collected by ultracentrifugation at $400,000 \times g$ for 15 minutes at room temperature and resuspended in 5% SDS (heat SDS if necessary to ensure it's fully dissolved) and boiled for 30 minute. A pellet was again collected via ultracentrifuge and then resuspended in HPLC grade water and repeated 3 times. The final pellet was resuspended in 50 µl of HPLC grade water and stored at 4 ℃ for no more than 3 months.

5.2.5 *Bacillus subtilis* - media and agar.

A common laboratory strain was used named *BS168* which was grown in two types of growth media. The *B. subtilis* samples made were pulsed labelled with ADA and repeated with dipeptide tags to allow for both AFM and fluorescence microscopy. The growth media used for *B. subtilis* is Lysogeny broth (LB) and nutrient broth (NB). Five lots of 250 ml LB were made and one 50 ml volume of NB. NB agar was used to produce plates. Both media and agar were sterilised in an autoclave at 121 ℃ for 20 minutes before use. The agar was poured into petri dishes and left to set, this is done in a lamina flow hood to maintain sterile practice. *B. subtilis* stocks were kept long term at -80 ℃ . A bead was removed from the stock and spread onto the agar dish and grown overnight at 37 ℃ . Once visible colonies have developed (typically within 24 hours) the plate was stored at room temp for a maximum of two weeks. 15 ml of NB media was transferred into a sterilised universal tube and a colony from the petri dish was selected with a sterile loop and used to inoculate the media. This was left overnight on a rotary shaker set to 250 rpm at 37 ℃ to produce overnight liquid cultures.

5.2.6 *Bacillus subtilis* growth

A calculated amount of the overnight culture was added to each of the five 250 ml LB media to get an optical density (OD) of 0.05. The inoculated media was then placed on a rotary shaker at 250 rpm at 37 ℃ and checked every 30 minutes till the OD showed the solution

had reached exponential phase, OD 0.3-0.8. Once exponential phase was reached one was allowed to continue to grow, the remaining four were pulse label using ADA tags in the time intervals of 15 seconds, 2 minutes, 10 minutes and 30 minutes. The ADA tag was added into the media and the cells allowed to continue to grow in a water bath and then immediately placed into an ice ethanol bath to stop growth.

5.2.7 Peptidoglycan extraction- *Bacillus subtilis*

Once the culture from each time pulse was been taken from the water bath and cooled in an ice ethanol bath it was then centrifuged at 15950 × g for 10 minutes to pull the cells out of suspension. The supernatant was then discarded and the resulting pellet was resuspended in 1 ml of PBS, transferred into a 50 ml falcon tube and boiled in a water bath for 10 minutes to kill the bacteria. Once cooled the resuspended solution was added to PBS to increase volume to 15 ml, which was run through a French press at 500 psi and checked under a stereomicroscope with a 100 × oil immersion objective to check degree of breakage. This process was repeated until the desired breakage was achieved. As the septum was the area of interest a high level of breakage was desired to separate each septum from the rest of the sacculus. The solution was then centrifuged at 20000 × g for 3 minutes to pull the material out of solution. The supernatant was discarded and the remaining pellet was resuspended in 1 mL of 5% (w/v) SDS and boiled for 25 minutes. To ensure that the bacteria was completely killed and cleaned from the other cellular components, the centrifuge step and SDS step was repeated and boiled for a further 15 mins. Centrifuging the solution at 20000 × g for 3 minutes then washed out the SDS, the supernatant was then discarded and resuspended in 1 mL of HPLC grade water. This was repeated a further 5 times. The pellet was then resuspended in 0.9 mL Tris-HCl (50 mM, pH7) and 100 µL pronase stock solution then incubated at 60 ℃ for 90 minutes. The material was then centrifuged 2 times for 3 minutes, supernatant discarded and the pellet resuspended in HPLC grade water. After the final centrifuge step the pellet was resuspended in minimal HPLC grade water

(approximately 100 µL) and stored in a -20 ℃ freezer.

5.3 AFM of biological samples

5.3.1 AFM imaging on mica in air to test sample quality

There are a multitude of variables to consider when AFM imaging biological samples, from buffer conditions, probes used, and mode of imaging to substrates used. Initially to test the quality of the samples produced a mica substrate was used. The mica was stuck on a metal stub and scotch tape was used to cleave the top layer off. A 1:100 dilution of the stock material with HPLC grade water was used as a starting point for imaging which would be adjusted for each batch of sample produced. 10 µL of diluted sample was placed onto the mica stub and slowly dried with filtered nitrogen flow. A TESPA V2 probe was used in Tapping Mode^{TM} for imaging in air to test the quality and concentration of the samples. Once the check had been done and the concentration was tailored the sample was moved to a glass substrate.

5.3.2 AFM imaging on a glass substrate

A glass substrate was used for all of the correlative microscopy in the work presented. To ensure the glass was smooth enough for AFM imaging high precision class coverslips were used and cleaned in 1 M KOH in a sonicator for 15 minutes. This removes the top layer of glass, if left any longer the KOH will etch pits into the glass increasing the roughness. For correlative microscopy on separate equipment the glass substrate was stuck onto a plastic correlative grid and this was stuck onto a glass slide. The sample was imagined again in air using a TESPA V2 probe and was also imaged in liquid using a selection of different probes and methods to obtain high-resolution images highlighted in chapter 7. When imaged on integrated equipment the plastic grids where no longer needed and the KOH cleaned cover slip was stuck onto a bespoke sample holder developed for STORMForce imaging. The

sample holder (described as an open sample in chapter 6) allows the glass substrate to be completely emerged in liquid for imaging. To obtain high-resolution images in liquid Bruker Fast scan D probes were used in HPLC grade water.

When imaging in Hyperdirve^{TM} mode a selection of electrolytic salt buffers, such as monovalent salt KCL, were used in attempt to improve resolution [21]. The salt ions are attracted to the tip and the sample, forming a layer around both surfaces. Divalent salts such as MgCL2 can also be used which reduces the double layer thickness measured by a factor of two [21]. The addition of the salts screens the charge between the sample and tip the reducing the repulsive forces know as a double layer effect. However this can also reduce the repulsive force between loose fragments of sample and the tip, contaminating the tip and reducing image quality. As the samples used was made up of broken fragments of peptidoglycan, often images of high resolution was taken in HPLC grade water.

5.3.3 Using sample adhesive for AFM imaging

Biological samples are often difficult to image due to their soft and sticky nature. *B. subtilis* sacculi were perticularly difficult to image due to the thick peptiduclycan layer which had the tendency to fill up with liquid and lift off the substrate. There was also a high amount of lateral force applied to the *E. coli* sacculi images which lifted the sample off the substrate, this was reduced when using sample adhesive. As *E. coli* sacculi is only 5-7 nm thick Poly-L-lysine was the adhesive used as only a thin layer is deposited, which does not alter the topography of the sample. Poly-L-lysine is a positively charged amino acid polymer which has a crystalline form, soluble in water. It promotes biological sample adhesion to a solid substrate by enhancing the electrostatic interaction between negatively charged ions of the cell membrane and the substrate. Stock solution is 0.1%, which can be used without dilution. To use, the KOH cleaned coverslip were coated and left to incubate for 30 mins, the slide is then washed with HPLC grade water and dried with filtered nitrogen flow before the sample is placed on the substrate.

For the thicker *B. subtilis* sacculi a stronger adhesive was needed, in the form of Cell-Tak^{TM} , which is a specially formulated protein solution extracted from marine mussel called *Mytilus edulis*. To use, 285 ml of $NaHCO_3$ was added to a KOH cleaned cover slip then 10 µL of Cell-Tak^{TM} and 5 µL of NaOH was added to the droplet and left for 30 minutes for the reaction to occur. The surface of the glass slide was rinsed five times with 500 µL of HPLC water. 100 µL of sample solution was then added and left for another 30 minutes, to ensure the sample was firmly stuck to the substrate. This was washed off with 150 µL of HPLC grade water 5 time to remove any loose material, the sample dish was then filled with 1-2 ml of imaging buffer or HPLC grade water for imaging.

5.4 Fluorescence microscopy of bacteria

For STORMForce imaging it was essential to not only develop a sample that was compatible with both AFM and STORM, but to also not alter the structure of the sample so that the architecture could be observed and the natural appearance of the sample was preserved. The bacterial samples used were tagged with fluorescent molecules via an ADA tag where a fluorophore was incorporated just prior to imaging through a click reaction. Depending on the sample, the material was ADA tagged at different stages of growth for different durations and then the material was processed to retrieve the peptidoglycan, as stated above. Alternatively, some cells were kept whole if intact cells were imaged. To image the material for fluorescence microscopy the sample was placed on the treated glass coverslip as stated above and a Click-iT^{TM} buffer was applied containing the Alexa Fluor 647 nm fluorophore used. ADA tag contain an azido group, the Click-iT^{TM} buffer provides a reaction where the alkyne containing fluorescence dye can attach to the azido group. It was at this stage that a 1:1 mix of 2 mM NHS ester fluorescent dye or 2 mM Vancomycin stains were also used for any epi fluorescence data that was needed. After 30 minutes the sample was washed 5 times with 500 µL of HPLC grade water and refilled with imaging buffer. The imaging buffer is dependent on the type of fluorescence microscopy. For epifluorescence the

sample can be imaged in air, however to keep the sample hydrated to preserve the protein structure imaging in PBS buffer or HPLC grade water was required; PBS was also used for correlative SIM imaging. During the fluorescence imaging process the AFM tip was placed over areas of interest and retracted, this ensured the same area imaged with fluorescence was imaged by the AFM and the position was not lost.

5.4.1 STORM

Depending on the time duration that the samples were tagged with ADA for, epi fluorescence was used prior to STORM imaging to identify areas of interest. This was done using HPLC grade water, which was then swapped out with a specific Glox STORM buffer. Glox STORM buffer contains 50 nM Tris buffer containing 10 mM NaCl at pH 8.0, Mercaptoethylamine (MEA) was dissolved into the 50 mM Tris NaCl to produce 1 M MEA stock. The MEA stock was the diluted 1:100 to 100 mM in 50 mM Tris NaCl for normal working conditions, which was kept cool on ice. The GLOX containing part of the buffer contains Glucose oxidase stock 5 mg/ml, Catalase stock 4 mg/ml and 100 mg glucose. To 100 mg glucose dissolved in 50 mM Tris NaCl, 100 µL glucose oxidase stock (0.5 mg/ ml), 10 µL catalase stock (40 µg/ml) and 100 µL of 100 mM MEA were added. This would last for approximately 2-3 hours before efficiency reduced.

Once the data was acquired a long pipette tip was used to removed the buffer and washed with 500 µL of HPLC grade water 5 times and then filled with 1 ml HPLC grade water for imaging. This was all done whilst the sample was stuck onto the sample stage, in order to avoid movement and loss of the position of interest identified before.

5.4.2 Data acquisition

STORM imaging was taken using a a Hamamatsu ImagEM EM-CCD camera at a frame rate of 31.2 fps. A laser coupled fibre was used and focused on the back plane of an 100 $\times$ 1.42 NA oil immersion objective, mounted on an Nikon Eclipse optical micrscope base. A

filter cube with relevent long-pass dichroic filter was used to match whatever fluorophore and laser wavelength was used. Focus was maintained between image aquisition manually, with the used of fiducial markers. The laser power was adjusted during imaging without saturating the camera and bleaching the sample, but also allowing sufficent power for high quality stochastic blinking. To obtain a STORM image for *E. coli* and *B. subtilis* sacculi, only 10,000 frames were needed.

5.4.3 Data processing

Localisations of events where processed by using the ImageJ/Fiji plug in, ThunderSTORM [77]. Data points were plotted on a 256 $\times$ 256 pixel area histogram, where maximum intensity projections were created. With the used of fiducial markers, drift could be subtracted from the final data. By increasing the threshold of localisations recorded when reconstructing data, noise could also be subtratcted from the data.

Chapter 6

Instrumentation development

The constraints placed on sample preparation by STORM and AFM are different. A key challenge in the development of the STORMForce microscope is the use of a sample preparation protocol compatible with both imaging modalities, combined with a method for locating the same region of the sample in both imaging techniques. AFM images the topography of a sample surface using a sharp probe that is raster scanned over it. Samples are placed on a substrate prior to imaging, and image quality depends strongly on both the sample-surface binding and on the flatness of the substrate, as substrate topography will influence the observed sample topography. STORM is a super resolution light microscopy technique; part of a family of "localisation microscopy" techniques, including Photo-activated Localisation Microscopy (PALM). Localisation microscopy involves the stochastic switching of single-molecule fluorescence signals. Multiple frames are imaged in which light is emitted by a sub-set of molecules that are further apart than the diffraction limit. Each photon of light is fitted to a guassian function in order to determine an estimate of the location of each molecule. These locations are plotted to form an image of the sample.

Here, we use Direct STORM (dSTORM) imaging. This requires optical access to the sample via a coverslip and a specific imaging buffer containing an oxygen scavenging system. By combining AFM and STORM capabilities we are developing an instrument capable of

simultaneously addressing peptidoglycan structure and chemistry (via fluorescence), but also enabling functional imaging of a huge variety of thin biological samples.

The initial step in instrumentation development was to develop a protocol in which a sample could be imaged on the AFM and then moved over to the STORM and the same area could be relocated precisely and imaged. The two images would then be overlaid producing a STORMForce image. This step was essential as the imaging conditions were still ideal for each method of microscopy. Once a correlative method was established it became apparent that there was scope to produce high resolution images on an integrated microscope. STORM components were added to an AFM and a new sample preparation and imaging method was developed to produce STORMForce images, where the sample was not moved between imaging.

Once the equipment was integrated, time was spent optimising imaging conditions to test the capability to produce high resolutions AFM images and good quality STORM images. A number of fluorescence samples where used to test the addition of STORM components and bacteriorhodopsin (purple membrane) was imaged to produce high-resolution AFM images on the integrated equipment. Once imaging techniques were optimised the development of STORMForce was complete and it became a tool to investigate biological material, as discussed in chapter 7 and 8.

6.1 Substrate development

Substrates for STORM and AFM are very different, so a new substrate had to be developed to produce optimal correlative images. The new substrate needed to be near to atomically smooth for AFM imaging and completly transparent to allow for the laser to reach the sample and perform STORM imaging.

6.1.1 STORM substrates

For STORM imagng samples are normally placed on a thin glass coverslip, this allows the laser light and sample signal to pass through the glass effectivly. However the Glox buffer used in STORM imaging is heavily glucose based making the sample sticky, which is not ideal for AFM imaging. Also the sample with buffer is sealed into a glass slide to stop the buffer oxidizing. For correlative imaging on separate machines AFM imaging would have to go first to stop the sample becoming sticky from the buffer used in STORM imaging, this would also remove any risk of the sample moving on the cover-slip if STORM was done first as the glass cover-slip would have to be removed from the slide and thoroughly washed.

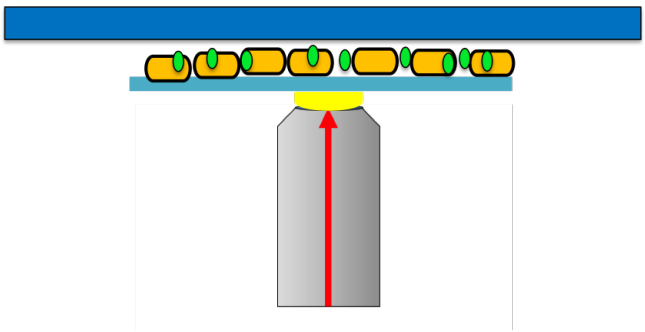

Figure 6.1: A diagram of a traditional STORM sample made up of the sample shown in orange wirh faducila markers in green on a coverslip which is all mounted on a slide. The coverslip is light blue and the glass slide is dark blue.

6.1.2 AFM substrates

AFM substrates are traditionally made out of mica. This is due to its crystalline structure allowing for cleaving of layers exposing an atomically smooth surface. This is to enusre the topography of the sample is uneffected by the substrate. *E. coli* sacculi was used as a test sample as work had been done using this sample previoulsy providing a lot of data as a comparison[13]. The comparison was used to ensure the developed substrate can produce a sample with quality as good as the mica equivalent.

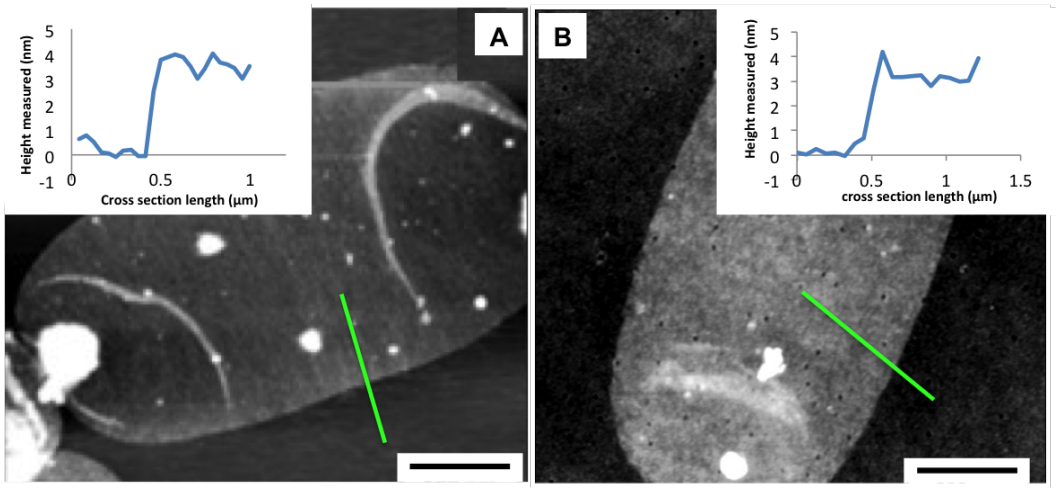

Figure 6.2: A) is the AFM image of intact *E. coli* sacculi imaged on a mica substrate in air using a TESPA cantilever in Tapping Mode^{TM}. B) is the AFM image of intact *E. coli* sacculi imaged on a KOH cleaned high perscison glass coverslip substrate in air using a TESPA cantilever in Tapping Mode^{TM}. The scale bar is 500 nm The height scale shows a height of 8.4 nm for A) and 6.8 nm for B).

6.1.3 STORMForce substrate

High-precision glass coverslips where used as a STORMForce substrate as it is optically compatible for the STORM and a protocol was developed to ensure it was as smooth as possible for the AFM. The glass coverslips where sonicated in 1 molar KOH for 15 minutes to remove the top layer of glass, any longer and the KOH would etch holes into the glass rendering a more rough surface. Once sonicated the substrate was washed thoroughly to remove all KOH from the glass, and then dried using medical grade nitrogen and ready for the sample to be dried onto the substrate. Figure 6.2 A) shows an *E. coli* sacculi imaged on a mica substrate with a height profile showing how the samples topography appears on the substrate. B shows an *E. coli* sacculi imaged on a KOH cleaned glass coverslip with a height profile also showing how the sample sits on the substrate. The height comparisons show that the glass substrate is as smooth as the mica for *E.coli* sacculi imaging, allowing for clear imaging of the sample topography and is therefore sufficient for AFM imaging.

6.1.3.1 Using fiducial markers and correlative grids for STORMForce imaging

As the sample was used for correlative microscopy fiducial markers were used to help to precisely locate the same areas in both techniques. Tetraspecks^{TM} were the fiducial markers used, which are small latex beads that fluoresce in the same 647 nm wavelength as the sample and are 100 nm in height so they can be imaged in the AFM. To initially image in the same larger area of the sample, correlative grids were used. At this stage the only grids available that would not affect both forms of imaging, were printed on small plastic coverslips. As the plastic is both too thick for STORM imaging to be possible as the focal length of the oil objective is very small, and too rough for AFM imaging the sample could not be placed onto it. This was overcome by sticking the plastic coverslip to the underside of the glass coverslip and the plastic side was then mounted onto a glass slide to make the sample easy to transport and more durable. By doing this the grids where visible optically when imaging on the AFM shown in figure 6.3, the sample was then inverted and sealed with STORM buffer on a high precision glass cover slip.

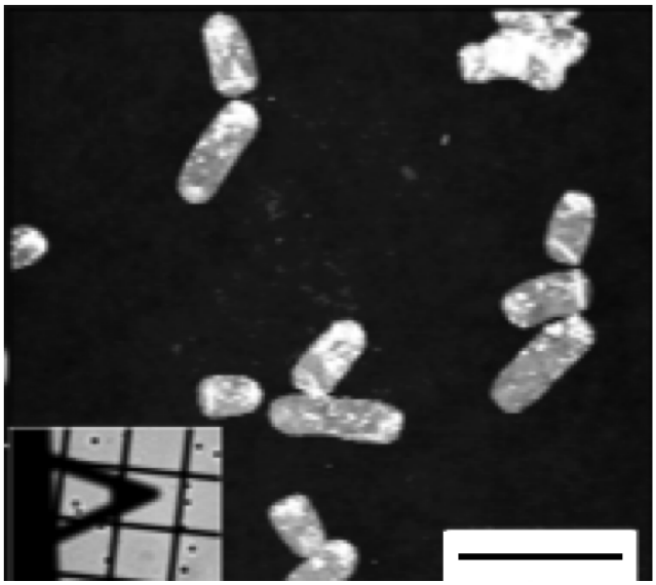

Figure 6.3: An AFM image taken in liquid in contact mode. The correlative grid is visible through the optics to locate areas in the sample. Scale bar is 5 µm and the height scale shows a height of 5.6 nm.

Figure 6.4 A shows the plastic correlative coverslips, B shows a close up of one of the grids where the red line shows that one square in 100 µm, which is also the maximum scan region available on the JPK Nanowizard Bio being used. This means that AFM images taken in this area can be located by the STORM if the same 100 µm area is imaged. C shows the sample setup when AFM imaging and D shows the same setup inverted and sealed onto another glass coverslip for STORM imaging.

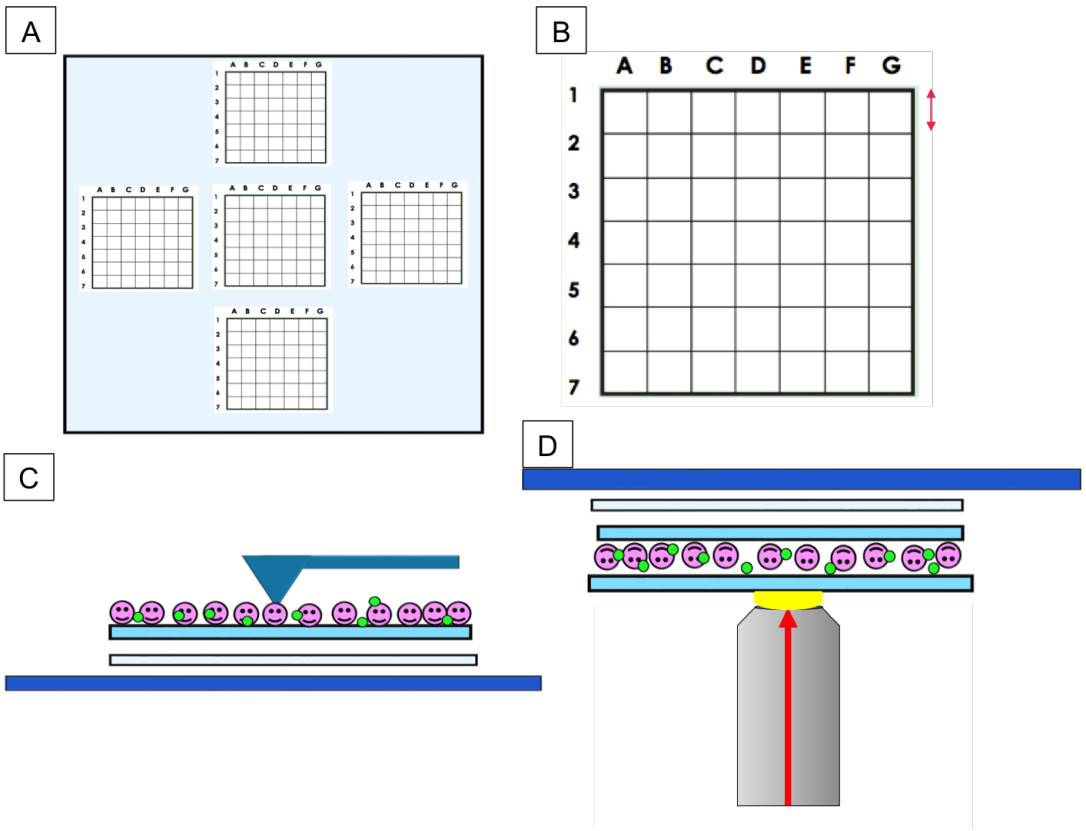

Figure 6.4: A) plastic coverslip with printed grids. B) close up of individual grid, red marker showing one section is 100 µm. C) shows sample arrangement of AFM, first a glass slide, plastic grid coverslip, glass coverslip with pink circles representing sample and green circles representing Tetraspecks^{TM} and AFM tip showing how the sample is imaged. D) shows sample inverted and sealed with another glass coverslip with glox buffer for STORM imaging. An oil objective is in contact with the final glass coverslip.

A small hand held microscope was used to image the grids when on the STORM equipment, this gave a larger field of view and better focus as the focal length of the oil objective

used for STORM is very small. This can be seen in figure 6.5, once the desired area was located the objective is lined up and the laser power was turned up to a minimum 5 mW to ensure the objective is centred before the laser power was increased to 70 mW to acquire a STORM image.

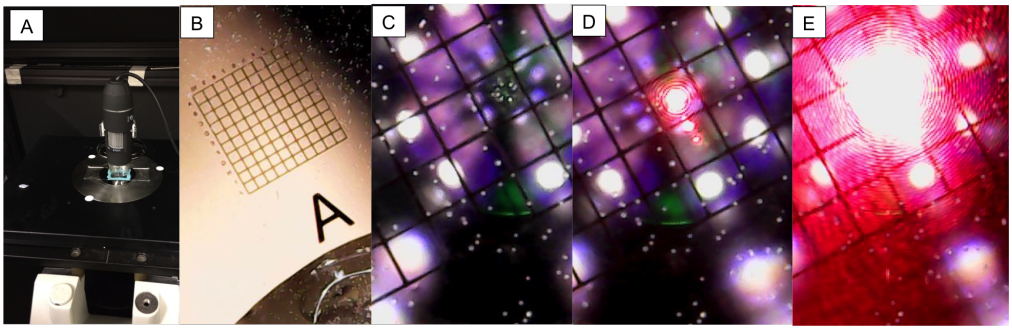

Figure 6.5: A) STORM set up with the addition of a smaller microscope to identify plastic grid co-ordinates. B) Close up of individual grid with additional microscope. C) Alignment of oil objective lens with individual square on grid with bright field illumination. D) Laser power turned up to 5 mW to ensure laser from objective is centred in square. E) Laser turned up to 70 mW to acquire STORM image.

6.1.4 Imaging fiducial markers with the AFM

The Tetraspeck^{TM} fiducial markers used are small latex beads that are 100 nm in diameter so they may not be apparent on a large AFM scan. It is essential to be able to identify the fiducial markers as they were used to give a higher precision overlay for the correlative images. The Tetraspecks^{TM} appear a lot larger in fluorescence microscopy than in AFM where only the true size of 100 nm is visible. Figure 6.6 shows an AFM image of Tetraspeck^{TM}, the latex beads tend to gather together forming large clusters which may make it harder to identify in the AFM.

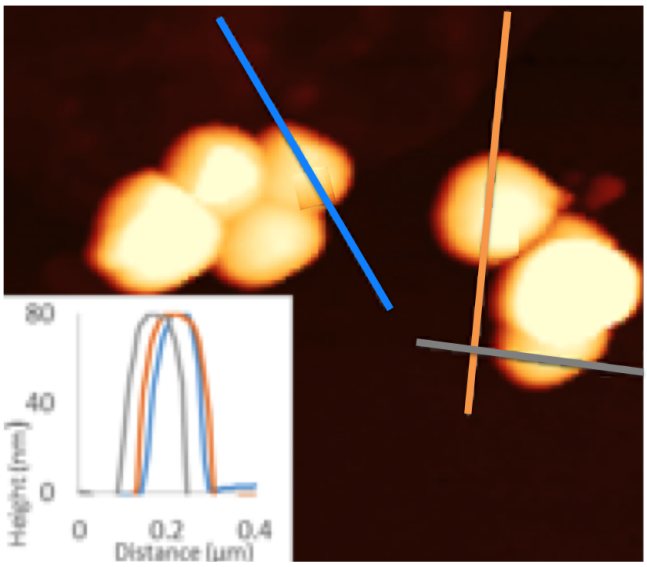

Figure 6.6: An AFM image of Tetraspeck^{TM} showing height profiles. Individual Tetraspecks^{TM} cluster together forming larger structures. The colour scale shows a height of 98.6 nm.

6.2 Correlative images

To obtain a correlative STORMForce image AFM was done first, followed by STORM imaging. This is because the sample needs to be sealed for STORM imaging, unsealing and washing the sample would potentially move the sample. The viscous STORM buffer also leaves a sticky residue even after washing, which is not ideal for AFM imaging of very thin samples. Because of this order of imaging it is impossible to know which cells to focus imaging on in an 100 µm area on the AFM. This resulted in a lot of time being lost AFM imaging material that wasn't visible on the STORM and had insufficient signal for an informative STORM image. The initial idea of STORMForce correlative imaging on separate equipment was to preserve the high quality imaging of each technique. However, it became apparent that this wasn't the case as it was very difficult to obtain both high-resolution AFM and STORM on the same sample. Figure 6.7 shows a STORMForce image obtained from separate equipment. It is apparent that neither the AFM nor STORM is of high quality. This was the catalyst to develope an integrated microscope in hope that less time would

be spent matching and overlaying images and more time spent taking high-resolution AFM knowing a STORM image was obtainable.

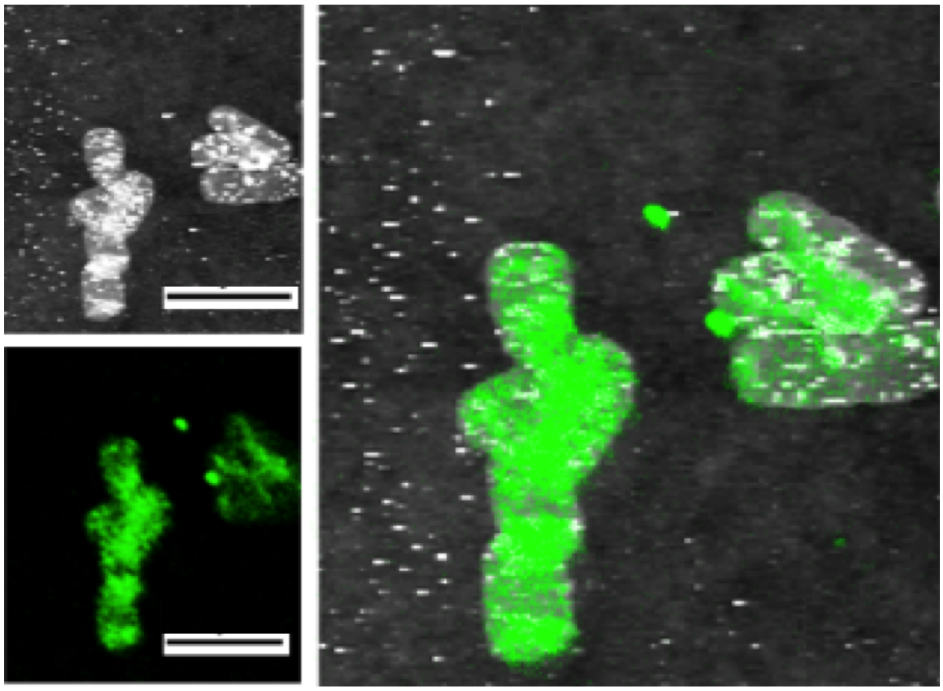

Figure 6.7: A) is the AFM image of intact *E. coli* sacculi imaged in air using a TESPA cantilever in Tapping Mode^{TM}. B) is the STORM image of the same field of view. C) is the STORMForce image where the green indicates where the fluorescence signal is present. The scale bar is 5 µm. The colour scale for A) shows a height of 16.5 nm.

6.2.1 Discussion

STORMForce images were taken on separate equipment to produce and overlay high quality AFM and STORM images. However, as the AFM images were taken 1st, it was not possible to see which areas of sample would produce the best quality STORM images for the high quality AFM images to then be taken. Due to this no high resolution images were obtained and development of an integrated microscope began. Through developing an integrated microscope the sample no longer needed gridded coverslips as the sample did not move and was completely stationary for the imaging process, making it easier to locate the same area of sample for high-resolution imaging.

6.3 Machine integration

The microscope integration was done in a step by step process to identify and reduce noise introduced to the AFM. Integration began by adding an 100 X oil objective with 1.42 NA and a Charge Coupled Device (CCD) Hamamatsu camera on to Nikon Ti Eclipse inverted stereomicroscope base which the AFM sits on top off. A laser-coupled fibre was used instead of open laser as a large optics table with irises was not used to collate the laser beam, saving space and reducing noise to the AFM. An LED coolsnap^{TM} device was also added to allow for epifluorescence imaging. A new sample protocol was developed further to allow STORM in an 'open sample', where the sample is not sealed for STORM imaging. This allows AFM imaging to take place before or after STORM imaging, depending on the sample requirements.

Figure 6.8 shows the equipment set up where a JPK Bio Nanowizard 3 AFM sits on top of a Nikon Eclipse inverted microscope where a Hamamatsu camera was added to a side camera port, a laser coupled fibre was added to the back of the illuminator and an oil objective was added. These three simple additions allowed for STORM imaging. The camera was connected to an independent computer that was not running the AFM. RS Imaging software by Photometrics was used to collect the STORM data and adjust threshold and set an acquisition speed to 31 fps. Images were rendered using ThunderSTORM ImageJ/Fiji plugin [77]. Data points were plotted on a 256 x 256 pixel area histogram. For 2D projections, maximum intensity projections were created.

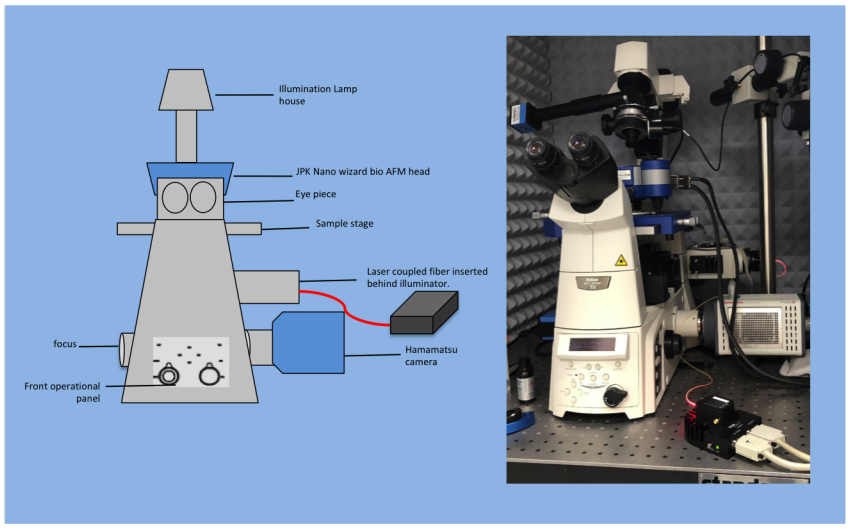

Figure 6.8: STORMForce equipment set up. The diagram showing a JPK Bio Nanowizard 3 sitting on top of a Nikon Eclipse inverted microscope with a laser-coupled fibre inserted through the illuminator to shine through the objective. A Hamamatsu camera was also added.

6.4 Noise control

To ensure equipment added did not reduce image qulaity, during each step of machine intergration the noise added to the AFM was measured. Figures 6.9 and 6.10 show the measurements taken as each compenent was added to the AFM, when imaging in liquid and air. Measurements showed that significant noise was added to the AFM when the Hammamatsu camera used for STORM imaging was running. No AFM images were taken when the camera was in use, so that poor quality AFM images were not produced. Although having both instruments on at different times did not allow for simultaneous images, it does allow for high qulaity STORM and AFM images as well as precision overlaying of the images produced.

Noise measurments where taken in both air and liquid to understand where noise is added in both systems. When comparing figures 6.9 and 6.10 it can be seen that noise added to AFM images was amplified when imaged in liquid, however only by around 10-40 pm which has insignificant effects on image quality. In both cases it is apparent that the

most significant noise is added when the camera is running. To ensure all noise for each component added was mitigated as much as posible, only essential components were left running when AFM imaging. When taking STORM imaging vibrational noise was not an issue as it was only in the picometer range, far less than the resolution achieved by STORM, so all components were left running. When taking AFM images only the inverted microscope base was running. This is to ensure the AFM tip was visible during imaging.

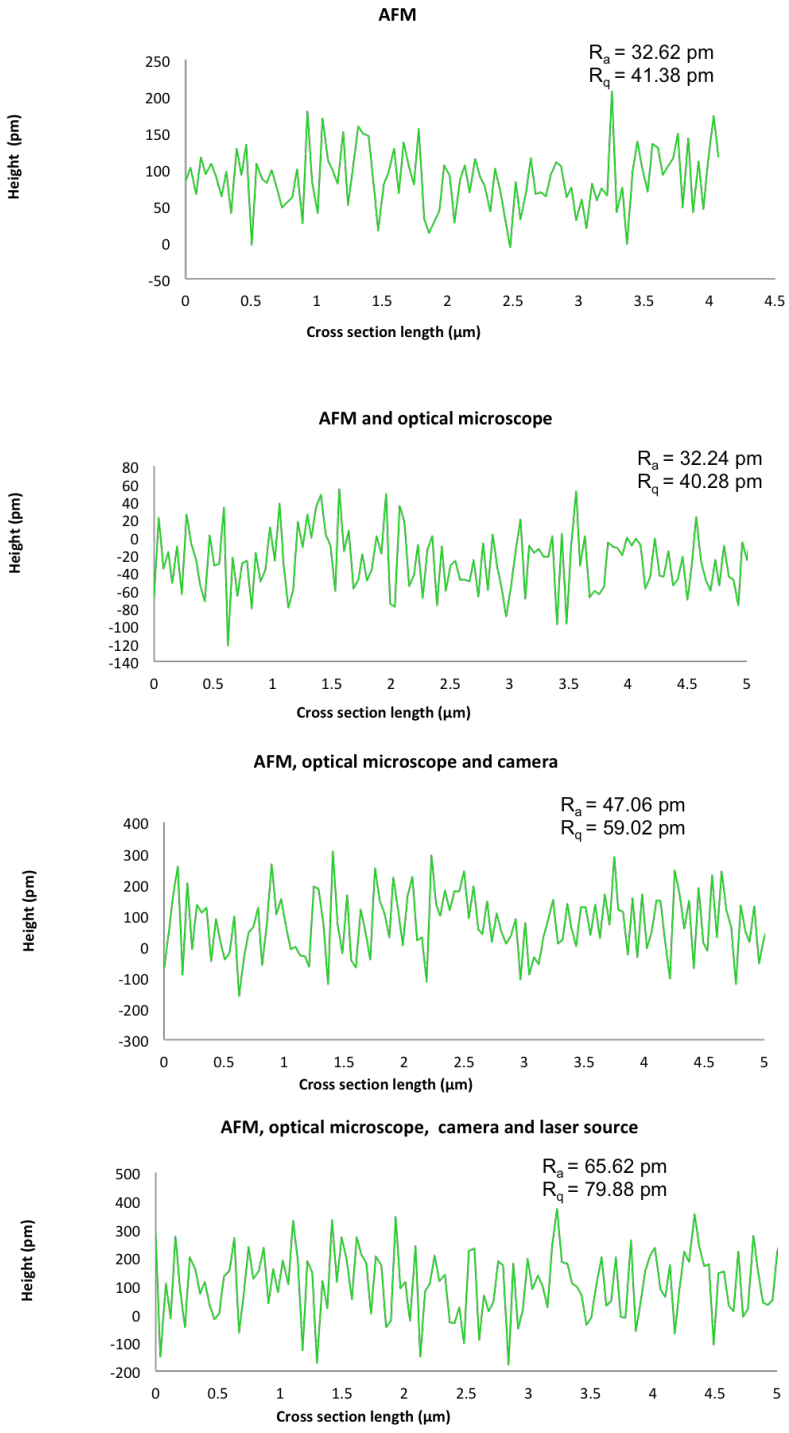

Figure 6.9: Graphs showing how AFM image noise increases as STORM components are added to the system when imaging in air. Most noise is added when the camera used for STORM imaging is running and when the laser source is also running. +-5 pm.

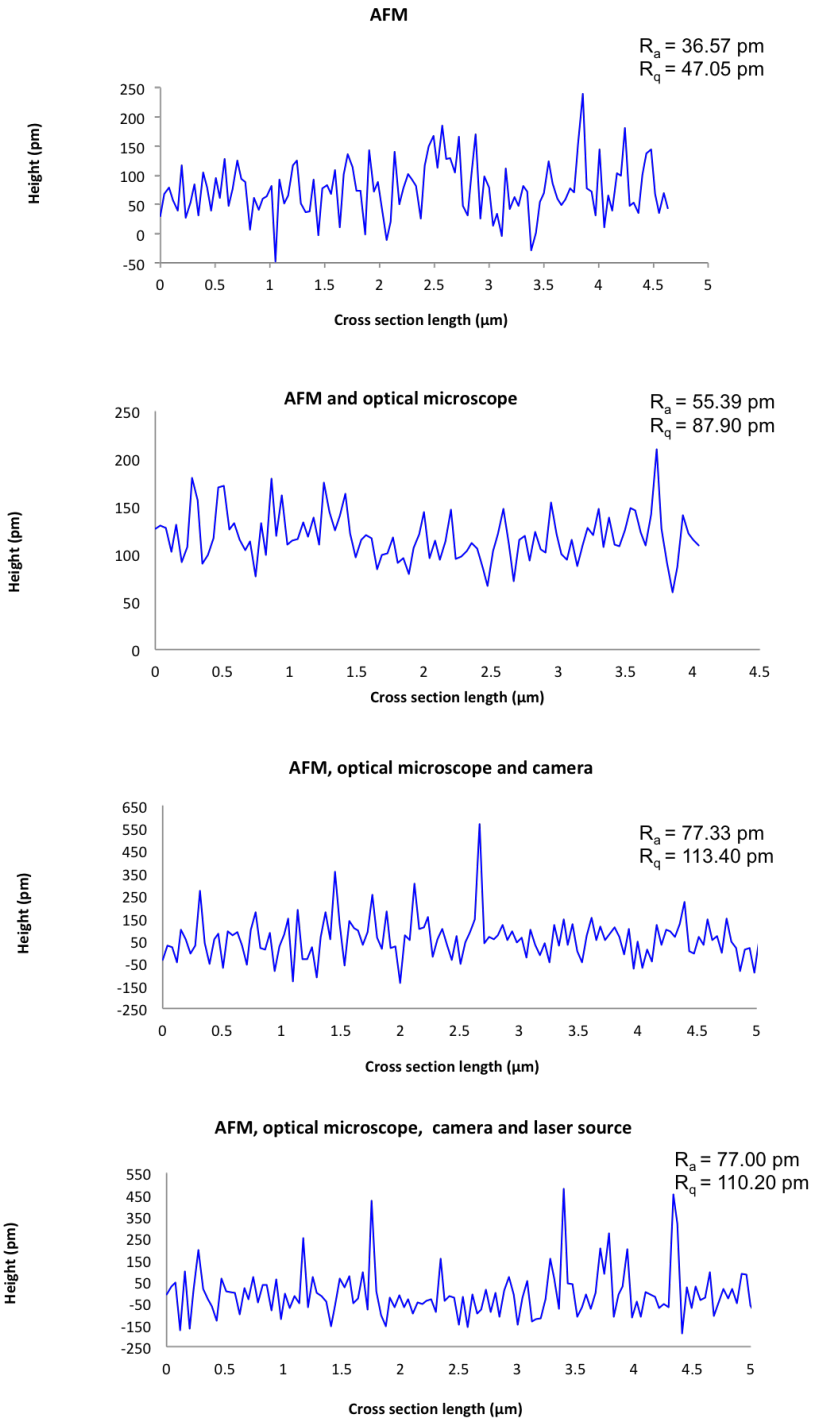

Figure 6.10: Graphs showing how AFM image noise increases as STORM components are added to the system when imaging in liquid. Noise added is amplified when imaging in liquid, however not enough to effect image quality. Substantial noise is added when camera used for STORM imaging is running. +-5 pm.

6.5 Fluorescence imaging addition

6.5.1 LED Epifluorescence

To allow for a variety of imaging techniques the easy addition of an LED Coolsnap^{TM} device can be interchanged with the laser, which is used for STORM. This was also useful for STORMForce imaging as the LEDs were used for epifluorescence imaging to locate samples stained with a dye at a different wavelength than the fluorophore used for STORM imaging. Due to only a small amount of sample being labelled for STORM, if the STORM laser was used to locate areas of suitable imaging concentration the sample would become bleached before the data was acquired. This is highlighted in chapter 8 section 8.2.2. Figure 6.11 shows images of bovine pulmonary artery endothelial (BPAE) cells stained with a combinations of dyes at different wavelengths and images with the LED cool snap. The images are taken with the same Hamamatsu camera and RS imaging software.

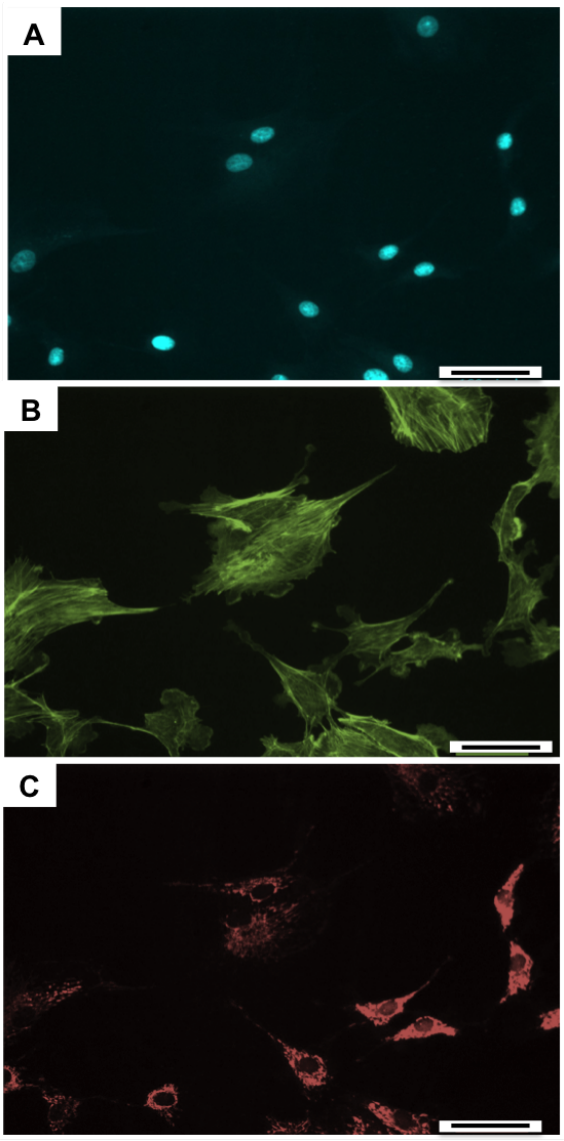

Figure 6.11: Epifluorescence images taken of BPAE cells. A) blue-fluorescent DAPI labelled nucleolus, B) green-fluorescent Alexa Fluor 488 phalloidin stained F-actin and C) red-fluorescent MitoTracker labelled mitochondria. Scale bar 10 µm.

6.5.2 Laser- STORM

Once the laser was added, a protocol was developed for alignment and identifying an area to produce STORM images when the laser power was increase to the maximum 70 mW. Tetraspecks^{TM} where dried onto a KOH cleaned high precision cover-slip, it was then centred onto the sample stage and the laser was turned on to full power. There was a 15 µm diameter field in which laser power was sufficient enough to produce a STORM image as

shown in figure 6.12. Due to only having a small area available for STORM imaging it was essential to identify the desired area with either an epi fluorescence image with the LED coolsnap^{TM} or with the STORM laser on low power. The AFM tip was then placed at the centre of the identified STORMable area, the fluorescence light source and CCD camera were turned off and AFM imaging commenced. In most cases AFM imaging was done before STORM imaging so that the glucose based STORM buffer would not need to be washed out. When STORM is done first the STORM buffer needs to be washed out, which is time-consuming and leaves the sample at risk of being moved during pipette washes, although it is possible and the method used in part of chapter 8.

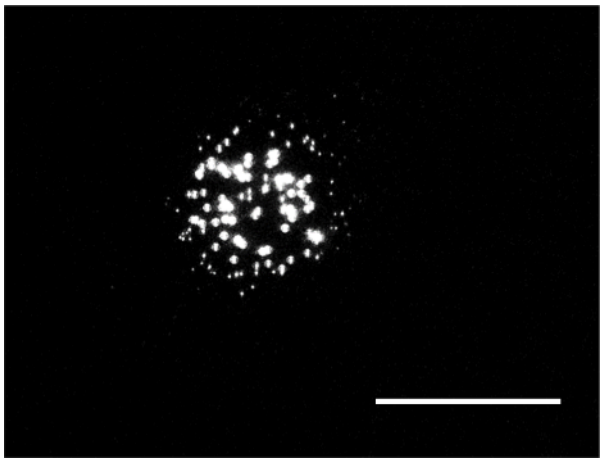

Figure 6.12: Image of signal from tTetraspecks^{TM} as a result of exposure to 647 nm laser. Scale bar 15 µm showing diameter of field with sufficient laser power for STORM imaging.

6.5.3 Sample development for integrated technique

A new sample preperartion method was developed so that the AFM tip could image the topography of the sample, but also STORM imaging could take place without the buffer expiring. A KOH cleaned high precision coverslip was still used however it was not sealed shut. A small 5 cm in diameter Petri dish with a 2 cm square hole cut out of the bottom was used. The cover-slip was stuck on top of the hole and the dish was filled with 2 ml of STORM buffer for STORM imaging. Due to the large volume of buffer used, the sample lasted approximately 2 hours before needing to be fully replaced.

It is essential for the Petri dish to be glued onto the sample stage with an epoxy resin that is easily removed after imaging, to reduce noise and to stop the sample moving through the different imaging techniques. In cases where AFM imaging is done first, the dish was either filled with HPLC grade water if imaged in liquid or left empty if the sample was imaged in air. Prior to AFM imaging the sample was imaged using epifluorescence to find an area of interest, it was then positioned in the centre of the screen and the AFM tip was placed over the area of interest. The CCD camera and fluorescence light source was then turned off to reduced noise and the AFM imaging could commence. In cases where STORM was done first the sample was again imaged with epifluorescence using the 647 nm laser couple fibre at low power to find an area of interest and the AFM tip was positioned above this area and then fully retracted. Then the STORM buffer is added and the laser power was turned up to full power to commence stochastic blinking. Once the STORM data was acquired the buffer was removed with a long pipette tip whilst the sample is still stuck to the sample stage. At this point it was essential to not nudge the sample stage, as the AFM image will not be of the same area. Once the STORM buffer was removed HPLC grade water was added and removed 5 times, to wash the sample of the STORM buffer and then the petri dish was filled with 2 ml of HPLC grade water, the AFM tip was then lowered and engaged onto the sample for imaging.

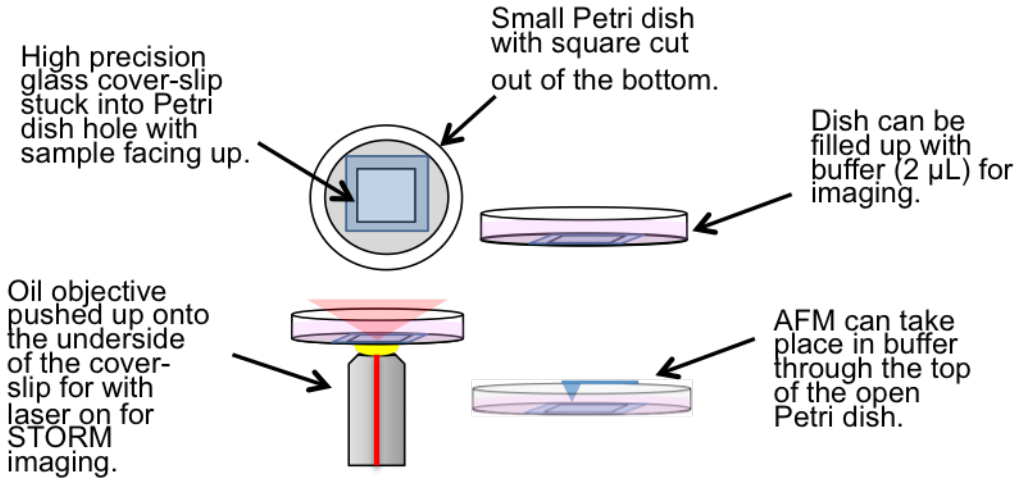

Figure 6.13: Sample holder diagram showing Petri dish 5 cm in diameter with a 2 cm hole cut out in the centre which allows a coverslip to be glued down in the centre allowing for both AFM in liquid and STORM imaging to occur without adjusting sample conditions.

6.5.4 Imaging development

6.5.4.1 AFM

To ensure that imaging was at optimum quality after equipment integration, time was taken to develope AFM imaging techniques on the biological sample bacteriorhodopsin. Bacteriorhodopsin, also known as purple membrane is a photosynthetic protein of the Halobacterium which converts 500-650 nm light (green light) into an electrochemical proton gradient, which is used for ATP production by ATP synthase [**?**]. Purple membrane, was imaged in HPLC grade water using an arrow UHF cantilever to obtain high-resolution images. Hyperdrive mode was used firstly when the sample was placed on mica. Once the size and topography was identified on mica the sample was moved across to the exact same sample setup used for STORM force. Through practice and tailoring imaging parameters the integrated equipment was able to image the trimeric structure of purple membrane.

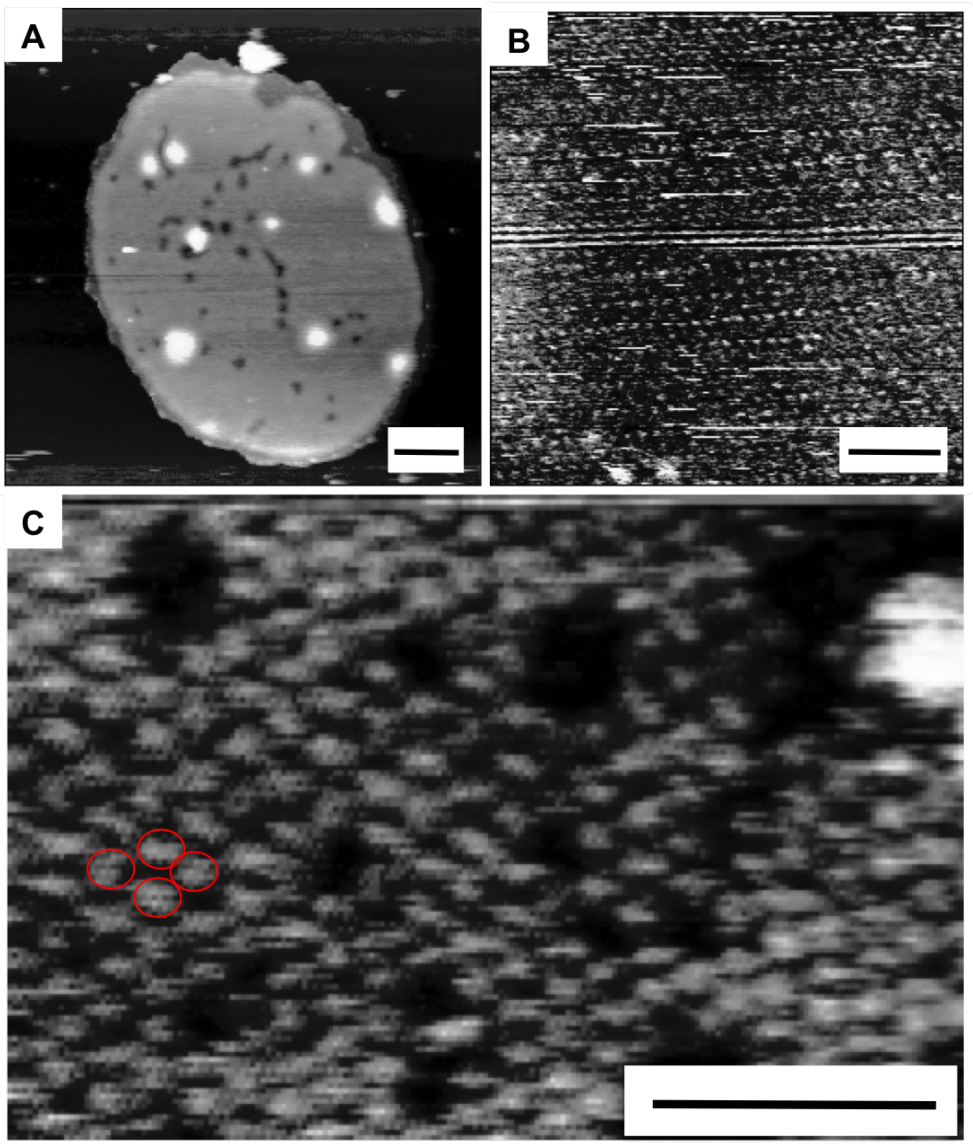

Figure 6.14: High-resolution AFM images of bacteriorhodopsin (purple membrane) imaged using hyperdrive mode in liquid using an Arrow UHF probe. A) an island of arranged purple membrane is visable Scale bar 200 nm. B) an area with minimal defects is imaged at a higher pixel density, scale bar 20 nm. C) a smaller area is imaged to resolve the trimer structure, visible noise in scan which could be reduced by slowing scan speed and decreasing Z range. Scale bar 20 nm. The height scale shows a height of 2 nm.

6.5.4.2 STORM

A key challenge in STORM imaging on the integrated equipment was to produce a sample that was open but where the STORM sample would not expire. As stated previously the open sample was filled with 2 ml of buffer, which would last 2 hours before the buffer

expired, however the buffer would not be optimal for the full 2 hours. During STORM data acquisition the pH of the buffer was checked using pH paper. If the pH dropped too much as it became oxidised the stochastic blinking of the fluorophores would stop. To overcome this 50 mM tris NaCl buffer was added to raise the pH again, allowing for blinking to resume.

Figure 6.15 shows a STORM image of *E. coli* sacculi taken using the open sample. Although there is background fluorescence due to unspecific binding, a high quality STORM image was produced. Individual localisation are visible within the sacculi and features within the sacculi can also be identified such as constrictions of the centre of the sacculi due to the cell division process.

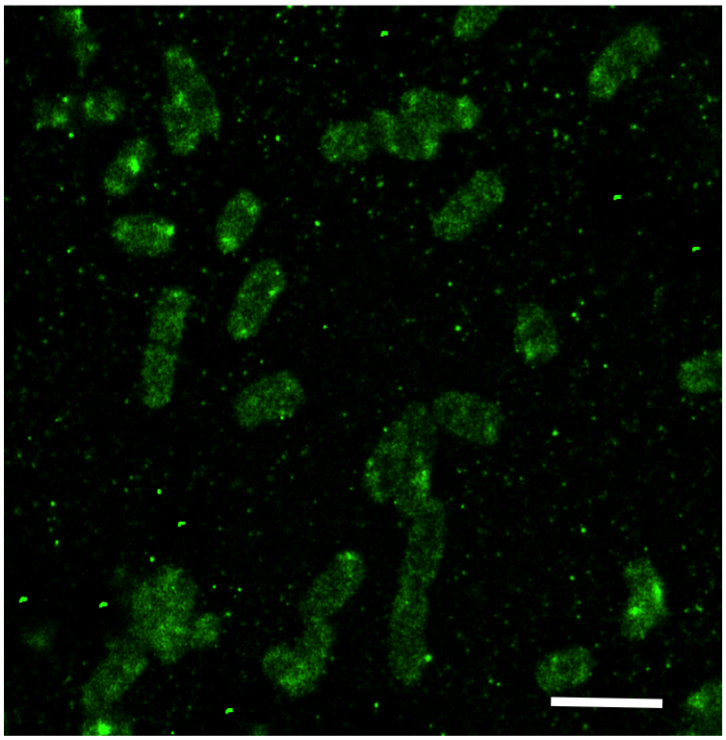

Figure 6.15: STORM image taken of *E. coli* sacculi taken on integrated STORMForce equipment in open sample. Scale bar is 5 µm.

6.6 Conclusion

STORMForce images were first obtained using two separate microscopes. This was done with the intention to preserve the image quality. A substrate that was compatible with both imaging techniques was developed, where plastic correlated cover-slips were attached to the back of the glass substrate were used. This allowed for the same area to be located in both techniques, small latex beads were also used to precisely overlay specific areas in the images taken. In this method AFM imaging had to take place first as the STORM imaging would involve sealing the sample on another glass coverslip. Removing the glass coverslip and washing the sample free of glucose based STORM buffer would potentially move and remove parts of the thin *E. coli* sample from the substrate. As the AFM imaging took place first there was no STORM data to show which sacculi to focus on for high-resolution imaging. Due to this the process, obtaining a high resolution STORMForce image would be very difficult to achieve consistently. A STORMForce image was obtained however both the AFM and STORM were not of good resolution.

The machine integration took place with a new developed open sample, which would make locating samples on the fluorescence and AFM easier, thus allowing for high-resolution imaging of the sample. Noise measurements where taken on the AFM throughout the integration to ensure that the noise added to the equipment was mitigated as much as possible. High-resolution images of purple membrane were taken on the integrated AFM showing that the integration did not have a negative effect on image resolution. By developing an open sample the sample could be imaged with STORM first and then AFM of *vice versa* without the risk of the sample being removed or damaged on the substrate. Epifluorescence was used prior to both STORM and AFM to locate areas of interest, saving time. This was a major improvement compare to imaging on separate instruments.

By imaging on the integrated equipment high resolution STORMForce images are able to be obtained. This can be done in either order and was tested using the biological sample

of *E. coli* sacculi.

Chapter 7

Escherichia coli

7.1 Introduction

E. coli is a Gram negative bacteria, with a peptidoglycan layer that is only a few nanometres thick (see chapter 4). The peptidoglycan is made up of glycan strands, cross-linked by peptides. The peptidoglycan can be purified from bacteria and for each cell a bag-like "sacculus" is extracted. AFM has been a crucial tool for investigating the morphology of these structures [13], but is unable to detect any chemical variations that may be present. This is where STORMForce can be used as it has the ability to investigate the chemical and physical properties of peptidoglycan. One important open research question is that of how the chemical heterogeneity of peptidoglycan within a population of bacteria maps onto the structural variation revealed by AFM. This requires a fluorescent reporter for peptidoglycan chemistry to be attached to the sample. In this study a synthetic amino acid presenting an azido group was used, which is incorporated into the sacculus [78] and linked to a fluorophore using click chemistry (see chapter 5).

E. coli cells reproduce by elongation of the cylindrical part of the cell and contracting in the middle whilst division occurs. The septal ring (Z-ring) is a complex of several proteins coded by the *fts* genes of *E. coli* that forms at the mid-point of the cell. It gives rise to the

septum at cell division. The first of the proteins to be incorporated is FtsZ, which gave rise to the original name of the Z-ring.

It has been propsed that bacterial SPOR domains bind peptidoglycan and target areas where glycan strands lack stem peptides that have been removed by amidase as shown in figure 7.1. Previous work done by Atsushi Yahashiri [18] demonstrates that when *E. coli* with GFP fused SPOR domains are treated with amidase enzymes the removal of stem peptides enhances SPOR domain binding. Whereas treatment with lytic transglycosylase, which removed glycans that lack stem peptides reduce SPOR domain binding. In this work an amiABC mutant was imaged as well as a wild type strain of *E. coli* to investigate the difference in the peptidoglycan structure and glycan strand spacing, with the aim of comparing structure when stem peptides are present to when amidase enzymes have removed them.

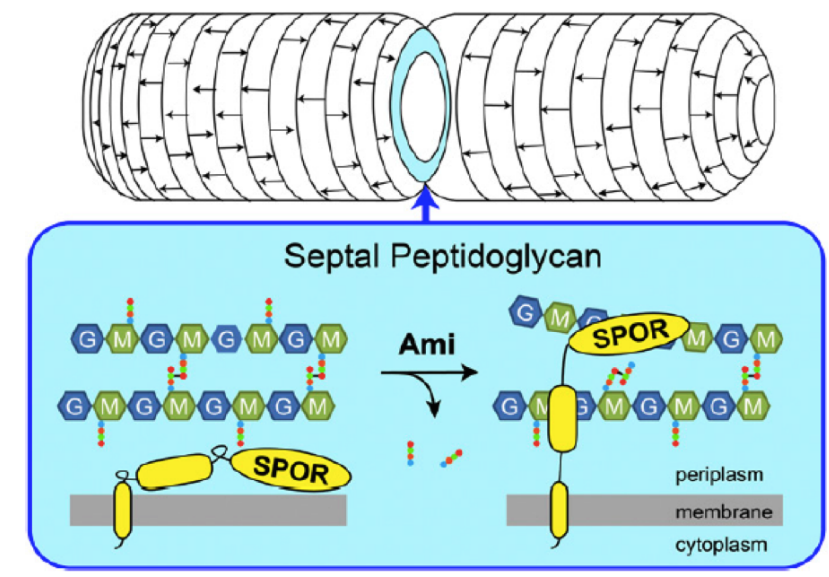

Figure 7.1: Schematics showing where in the cell the amidase enzyme removes the stem peptide and where the SPOR domain then binds to glycan strands with missing peptides, adapted from [18].

The experiments presented in this chapter identify layers of peptidoglycan using fluorescence (STORM), which are overlaid with AFM images. STORMForce images were initially used to map fluorescently tagged material on to high-resolution AFM images to understand the architecture of the material. However, prior to septum formation an area where there

was no fluorescence was identified, but during septum formation the lack of fluorescence is no longer present. Due to this observation the main area of interest became the middle region of the sacculi where division occurs. It is thought this is due to the amidase activity described in figure 7.1 [18]. STORM data was used to identify where the blank strip occurs and at what stage of the cell cycle, and the AFM was used to focus on these areas. Attempts were made to image this area in high resolution, this was done seperately to STORMForce to obtain a higher yield of data. Although optimal resolution on the AFM was not achieved to obtain molecular information of individual glycan strands and peptide cross-links, sufficient resolution was achieved to see structural differences in the material. An analysis was done on the fibres imaged to quantify any structural difference observed in the band area of blank fluorescence and the surrounding area. To confirm amidase enzyme activity is resposible for the blank stripe in the fluorescence images, an amidase mutant was also imaged to further investigate the structure of the peptidoglycan.

7.2 Results

7.2.1 STORMForce imaging of *Escherichia coli*

Purified *E. coli* sacculi were initially imaged via Tapping Mode^{TM} in air using a TESPA cantilever on a KOH cleaned glass cover-slip. Once the sample was purified it was imaged on the AFM first to get a clear picture of its quality and optimal concentration. Once this was done samples were made with a concentration that is compatible with both AFM and STORM. If too concentrated the material becomes overlapped with each other and the material is too close together. This affects the quality of the STORM images, as well as making it unclear as to which areas of the sample are fluorescent. Epifluorescence imaging took place first with the STORM laser at 10% power to find an area with an optimal concentration of single sacculi, as shown in figure 7.2. The laser and STORM camera were then turned off to reduce noise when taking AFM images. Once an AFM image was taken

the same area was then imaged using STORM and an overlay was produced. The cells were labelled for the entire duration of the cell growth (approximately 2 hours for *E. coli* to reach exponential phase.) This resulted primarily in sacculi that have entirely fluorescent peptidoglycan, however some cells have no fluorescence signal. This could be due to those cells having not grown in the two-hour period, therefore the ADA tag was not incorporated into the peptidoglycan.

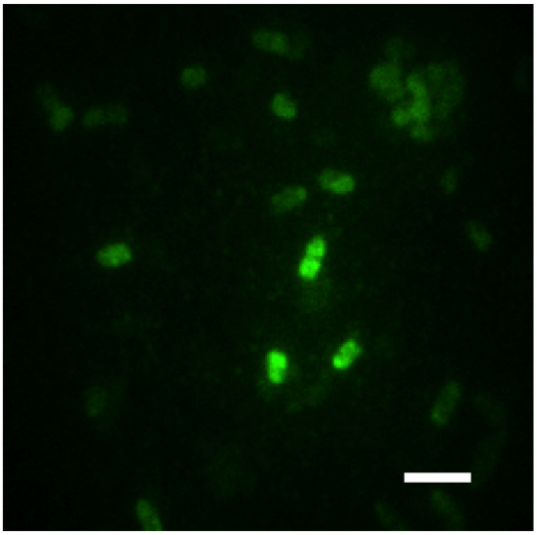

Figure 7.2: Epifluorescence image of *E. coli* sacculi to identify areas of interest for STORM-Force imaging. Scale bar is 5 µm

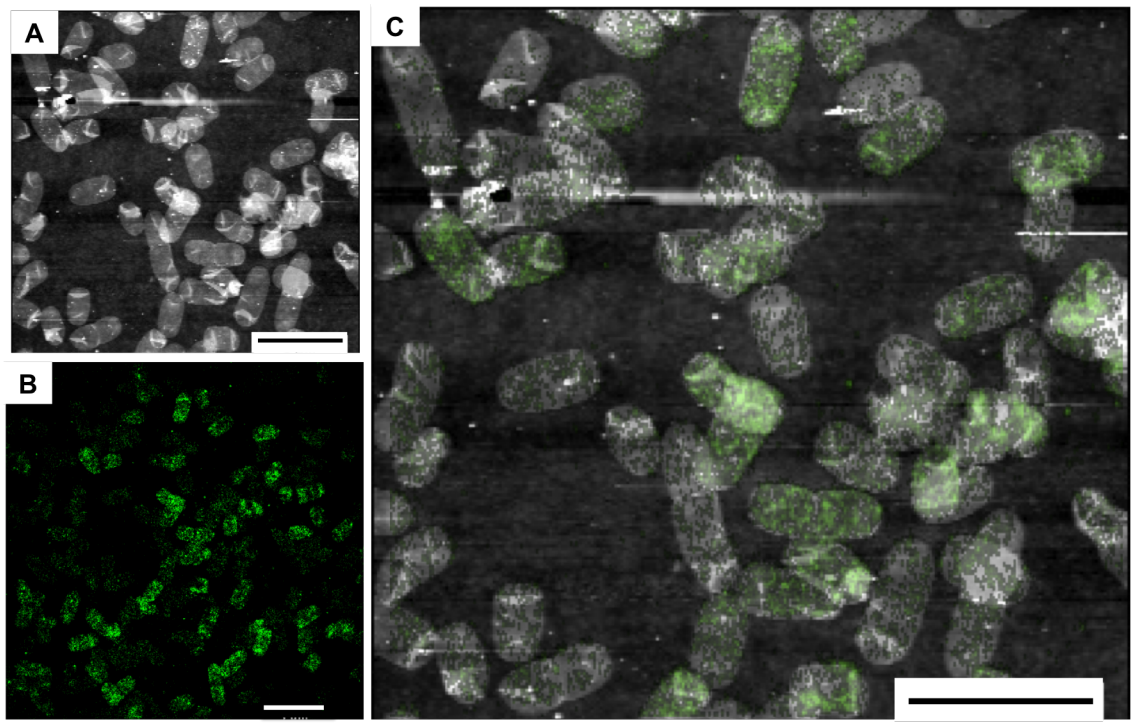

Figure 7.3: A) an AFM image of intact *E. coli* sacculi imaged in air using a TESPA cantilever in Tapping Mode^{TM}. B) a STORM image of the same field of view as in (A). C) STORMForce image where the green indicates where the fluorescence signal is present. The scale bar is 5 µm

In figure 7.3 a STORMForce overlay is shown of *E. coli* sacculi that has been tagged for the entire duration of growth. This results in all of the sacculi fluorescing, although some of the sacculi have less fluorescence than the others, which may be due to some of the bacteria having a reduced amount of growth which most likely occurs naturally.

Through doing large field overlay of *E. coli* sacculi, it became apparent that occasionally there appears to be a blank strip in the fluorescence in the middle of the sacculi prior to septum formation, as shown in figure 7.4 . STORMForce was then used to focus on this area, AFM was optimised by using a variety of different cantilevers, AFM modes and buffers to try and achieve high resolution in the area of reduced fluorescence.

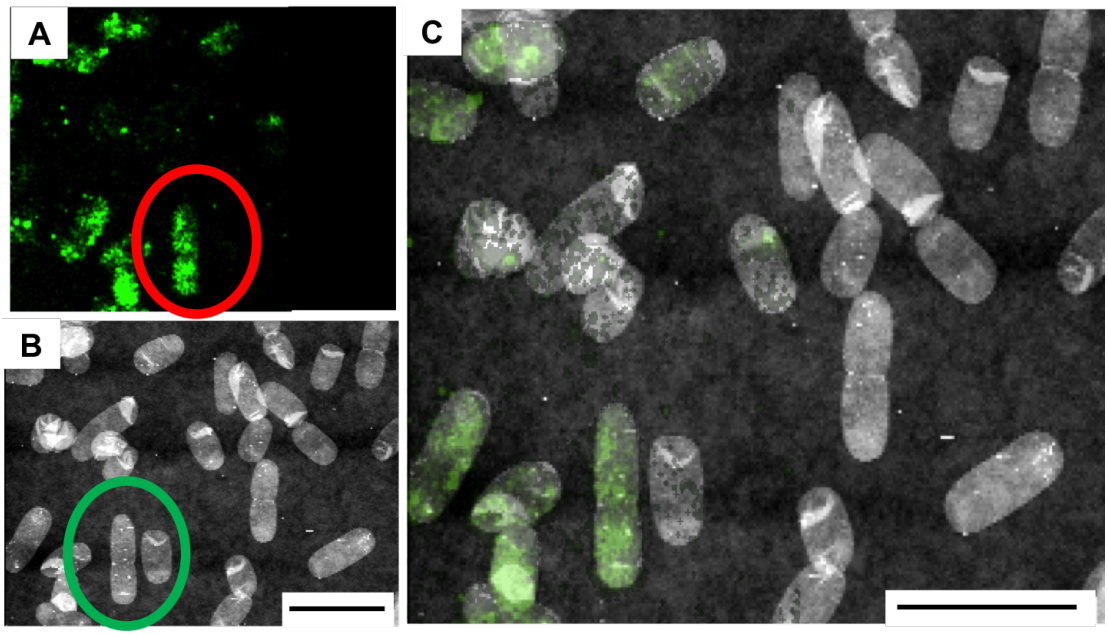

Figure 7.4: STORMForce image of *E. coli* sacculi. A) a STORM image where the red circle highlights a sacculus with a strip of fluorescence missing in the centre. B) an AFM image where the green circle highlights the same sacculus in (A). It can be seen that there is material present in this region and the cell had not yet produced a septum. C) a STORMForce overlay of the two images. Scale bar 5 µm.

7.2.1.1 Background about *E. coli* cell division and amidase enzymes

The blank stripe which appears prior to septum formation at the centre of the sacculi is thought to be caused by the action of amidase enzymes [18]. Amidase are responsible for the removal the stem peptide cross bridge that connect glycan strands. This is also where the ADA tag is incorporated into the peptidoglycan. The blank strip in the fluorescence appears prior to visible septum formation occurs and once a septum begins to form the blank strip is no longer visible. However, it has been shown that when the amidase enzymes are removed in an amiABC amidase mutant strain not only does the blank strip not occur, but the bacteria do not divide and form a septum normally. This suggests that the action of the amidase enzymes that results in the blank stripe is an initial step to septum formation and enables cell division. Figure 7.5 shows STORM images where blank fluorescence stripes are visible and no septum was seen.

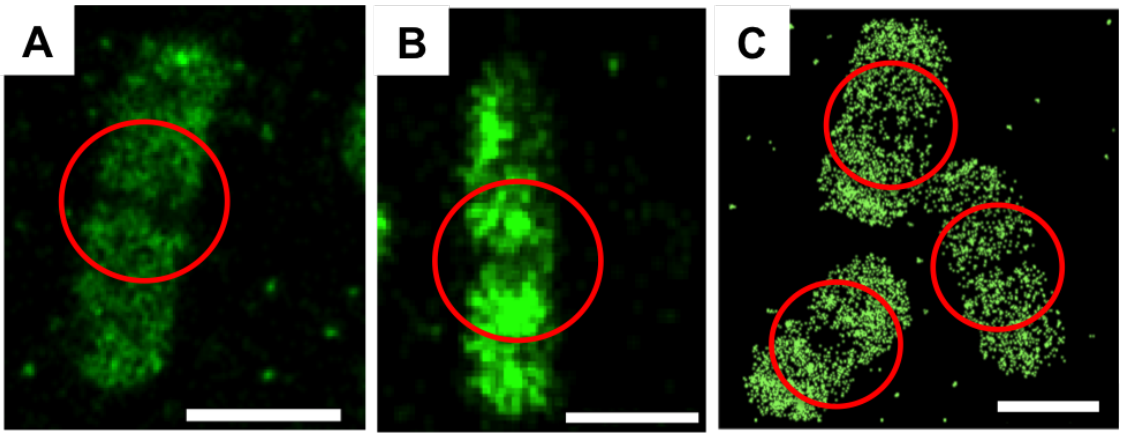

Figure 7.5: STORM images showing *E. coli* sacculi with red circles highlighting the blank strip of missing fluorescence prior to septum formation. Scale bar (A) 2 µm, (B) 2µm and (C) 1µm.

7.2.2 Fluorescence imaging

As previously mentioned, the blank stripe visible in the fluorescence data only appears in sacculi before septum formation. The blank stripe data was analysed, where the width of stripe and length of the cell was recorded with the aim of collecting AFM data of bacteria that match the same profile.

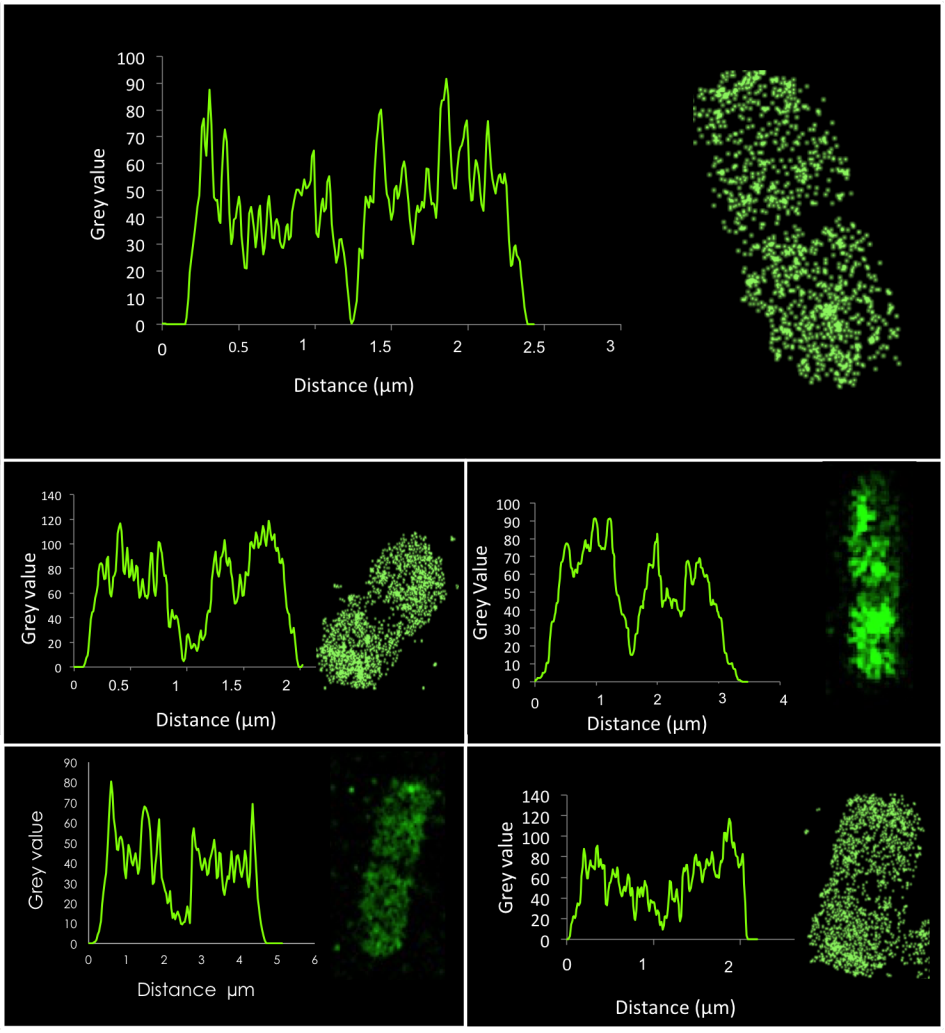

Figure 7.6: STORM images of *E. coli* sacculi with visible blank stripe with intensity graphs to show the sudden loss of signal in the blank strip region. The width of the stripe has been measured.

From figure 7.6 it is clear that the blank stripe is always at the centre of the sacculi and goes across the entire width. The length of bacteria at which the stripe becomes apparent, ranges between 2 µm and 4.5 µm. This indicates that the stripe can also become visible before cell elongation, as an *E. coli* cell in stationary phase is around 2 µm in length and 1 µm in width. This suggests that amidase may remove stem peptide before cell elongation as well as during cell elongation. From the small data set shown, the width of the blank strip ranges between 100 - 800 nm, which is dependent on the length of the sacculi. AFM images were then taken in order to identify structural differences in the peptidoglycan at

the centre of the sacculi compared to the rest.

7.2.3 AFM imaging of *E. coli* sacculi

In order to obtain high-resolution AFM images a number of different cantilevers, imaging modes and sample preparations were investigated. Once a protocol was developed to produce high resolution imaging the middle of the material was targeted.

Samples were imaged in air and liquid to try to improve and increase resolution. When imaging in liquid, a mixture of salt buffers were used, shown in chapter 5.3.2. Using salt allows the tip to get closer to the sample, to enter the short range interactions without being effected by the repulsive regime. As the sample consists of small fragments, using a high salt buffer also contributed to the tip becoming contaminated with the small fragments. The ions from the salts shield out the repulsive interactions between the sample and the tip [28], which also results in fragments of sample contaminating the tip, diminishing image quality (chapter 2).

7.2.3.1 Types of cantilever used

TESPA probes are etched out of silicon and are used for Tapping Mode^{TM} AFM in air and other non-contact modes of AFM. It has an aluminium reflective coating on the backside of the cantilever, increasing the laser signal by 2.5 times. This cantilever was used to test all sample concentrations imaged in air.

Through using a number of different imaging parameters and cantilevers it became apparent that the fine structures in the samples are lost in the drying process. Due to the loss of information, further imaging took place in aqueous conditions.

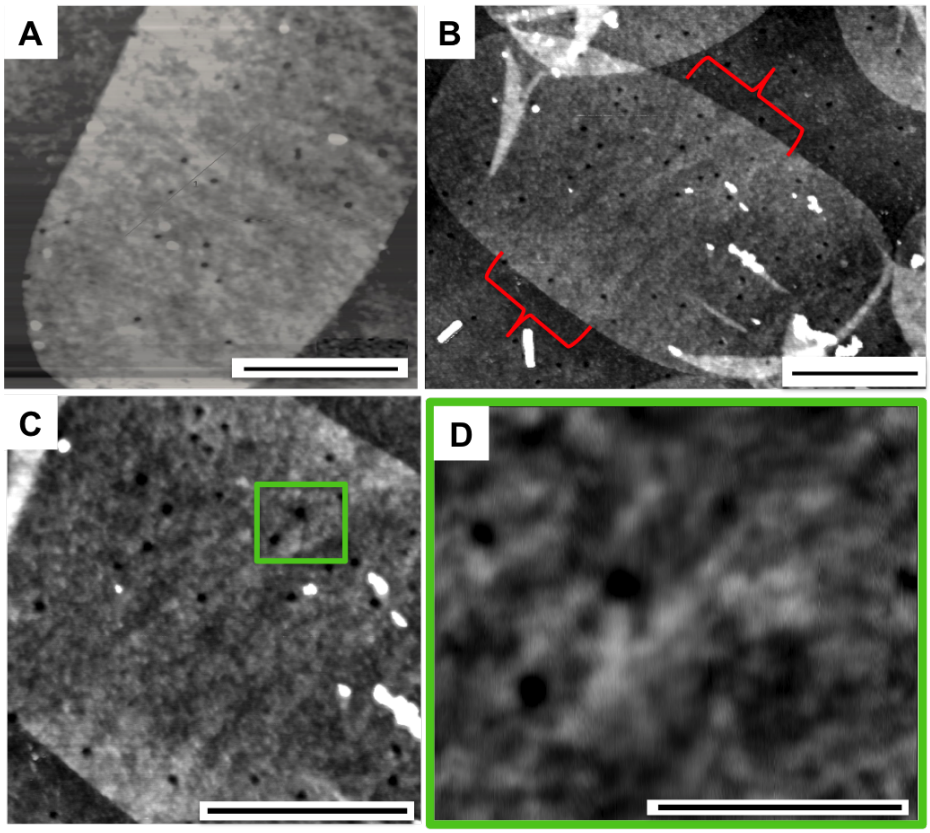

Figure 7.7: AFM image taken of *E. coli* sacculi with a TESPA cantilever using Tapping Mode™ in air. Images A-D decrease in scan area in an attempt to show features present in the middle of the sacculi. A) scale bar 500 nm, height scale 5.3 nm. B) scale bar 500 nm height scale 6.4 nm. C) Scale bar 500 nm, height scale 4.3 nm. D) scale bar 200 nm, height scale 2.2 nm. A banding structure is visible at the centre of the sacculi across the width of the cell, seen in A) and B). C) shows the centre of B) in close up, highlighting the difference in structure at the centre in comparison to the edge. The scan direction is rotated 90° clockwise. D) Image of broad band structure found at the middle of the sacculi C) shown by green box where the scan direction is rotated 90° clockwise.

The AFM images in figure 7.7 are of sacculi dried on a glass substrate imaged with a TESPA cantilever in air. A) and B) show a more ordered banded structure in the middle of the sacculi compared to the disordered material towards each pole. C) a height image of the middle area in more detail. The bands do not appear to be parallel with each other and the band structure has a higher height profile, suggesting the material in these areas is more dense. D) an image of a single band feature where the structure within the band is not resolved, however the data shows the band is wider and higher when compared to the surrounding material. The scan angle was rotated to prevent lateral scan features affecting

the structures seen

To increase image resolution the amplitude set point was increased, however this increased the lateral force applied to the sample causing damage. A softer cantilever, OLTESPA, was used next to try and overcome the issues experienced here.

OLTESPA probes are designed for Tapping Mode^{TM} AFM of soft samples. The backside is coated with aluminium to enhance the cantilever reflectivity but the tip is not, to ensure a sharp tip apex. The tip is situated at the free end of the cantilever on the edge, allowing for accurate positioning over the area of interest and improved correlative overlay.

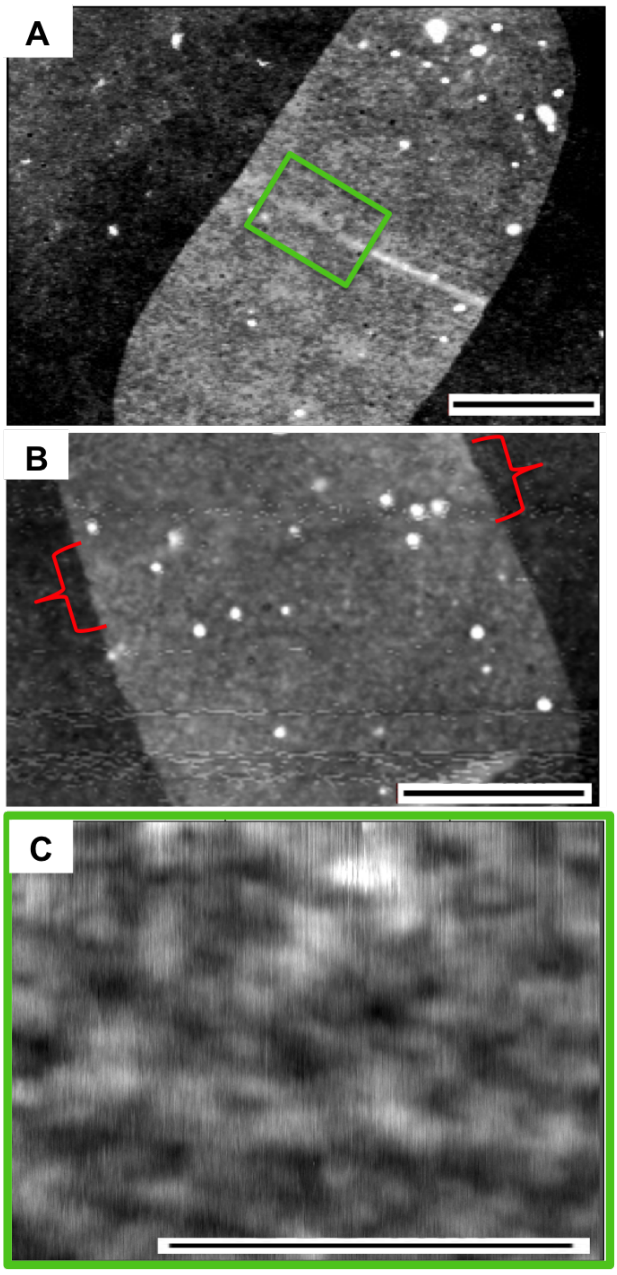

Figure 7.8: A) AFM image taken of *E. coli* sacculi with a OLTESPA cantilever using Tapping Mode™ in air. A) a defined wide high band is visible in the middle of the sacculi. Scale bar 500 nm, height scale 5.2 nm. B) another sacculi imaged from the same sample with less visible band. Scale bar 500 nm, height scale 4.6 nm. C) a close up image of area in A) shown by the green box. The scan direction is rotated 90° anticlockwise. Scale bar 200 nm, height scale 2.7 nm.

The AFM image in figure 7.8 is taken using an OLTESPA cantilever in air using Tapping Mode™. Again a broad high band is visible at the centre of the sacculi shown in A). B) shows a slight hint of a band near the middle of the sacculi however banding is

not resolved throughout the rest of the sacculi. The green box shows the area that has been imaged in higher resolution from A). As before the scan angle was rotated to prevent lateral scan features affecting the structures seen. The band no longer looks as prominent when imaged in C), which could be down to lateral forces applied to the sample and poor tracking of the sample by the tip. The area where the band is present still appears to have more densely packed material, however the structures are not resolved within the band. To try to increase resolution further the samples were imaged in liquid using a different mode of imaging known as Hyper Drive^{TM} mode (chapter 2). Arrow UHF (UHFAuD) probes are an ultra-high frequency probe made out of monolithic silicon, which is highly doped to dissipate static charge. The tip is also situated at the very end of the cantilever allowing for accurate positioning over areas of interest. The cantilever backside is coated in gold enhancing the reflectivity and preventing light from interfering within the cantilever.

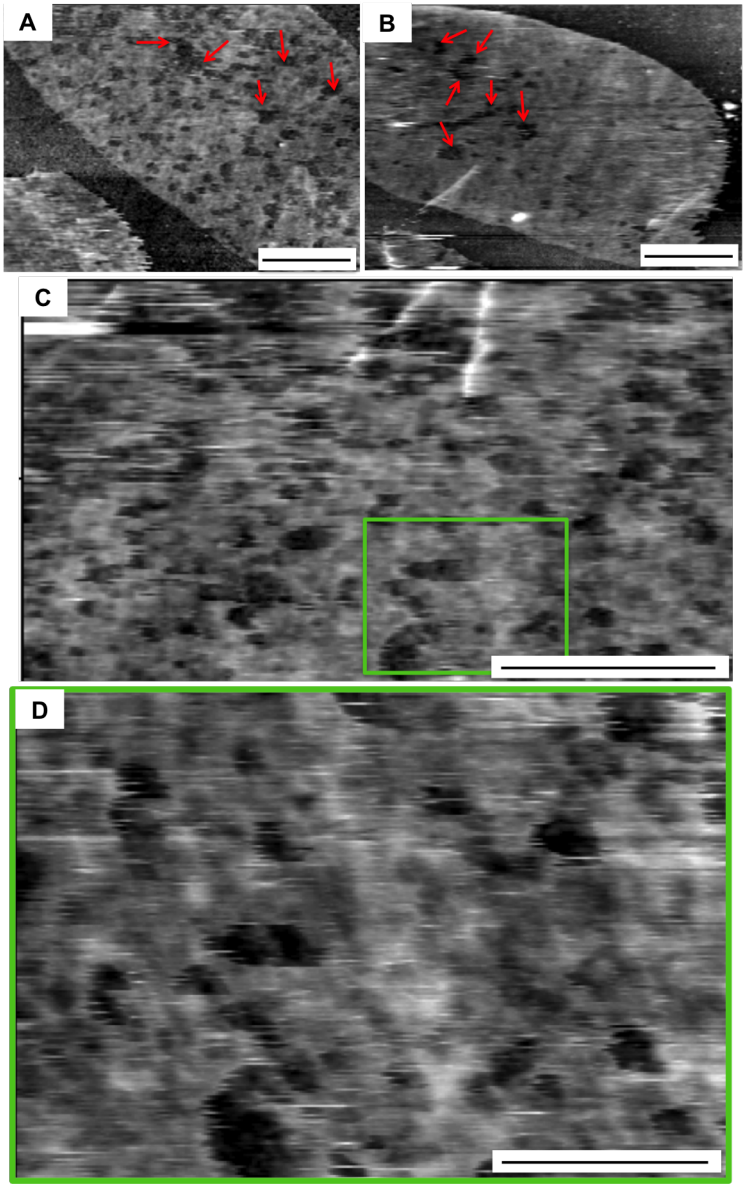

Figure 7.9: AFM images taken of *E. coli* sacculi with an arrow UHF cantilever using Hyper Drive^{TM} mode in liquid. Images A-D decrease in scan size in an attempt to show features present in the middle of the sacculi. A) and B) show the features seen on the sacculi in aqueous conditions using Hyper Drive^{TM} mode. Arrows indicating large holes, which are thought to be due to sample tracking issues. A) scale bar 500 nm, height scale 5.9 nm. B) scale bar 500 nm, height scale 12.3 nm. C) focuses on the middle of the sacculi where the bands are apparent, scale bar 500 nm and height scale 5.9 nm. D) focuses on one band shown in C) scale bar 200 nm, height scale 5.8 nm.

The sample imaged using an UHFAuD probe is shown in 7.9. In A) and B) finer features become apparent around the banding structure visible in the middle of the sacculi. A close up of the middle of the cell was imaged where multiple bands are visible C). The bands do

not sit parallel to each other and are not continuous. The green box indicates which area in C) is focused on in D), where one band is imaged. Hints of a fine structure are visible within the band, but still not resolved. Large holes appear in the material however it is believed this is due to a tracking issue between the tip and the sample as the location of the holes are not consistent between scans.

Biolever mini probes have a two-layered probe structure where the lever is made from silicon nitride and the probe apex being made out of silicon, the backside is coated in gold. They have a high resonance in both air and liquid and are ideal for high-resolution imaging of biological samples. A Biolever probe was used in Hyper Drive^{TM} mode in aqueous conditions. Both salt buffers and HPLC grade water was used but no significant change in resolution was observed between these different buffer conditions.

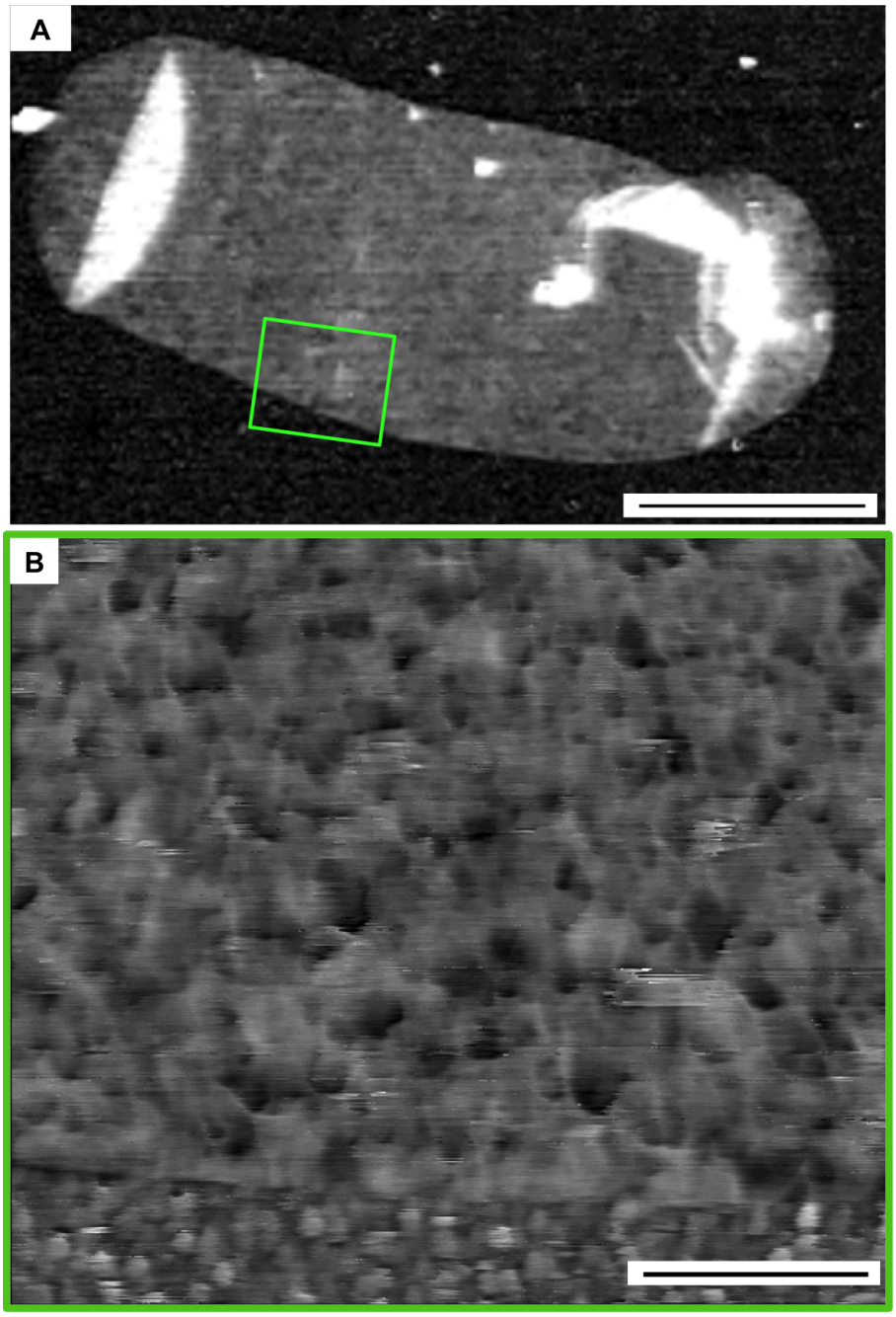

Figure 7.10: *E. coli* sacculus imaged using a Biolever mini cantilever using Hyper Drive™ mode in HPLC grade water. A) is an AFM image showing the height data. Scale bar 1 µm, height scale 21.9 nm. B) is a close up view of the selected area in A indicated by the green box to target the band feature. Scale bar 200 nm, height scale 16.9 nm.

The data taken using a Biolever mini probe shown in 7.10 shows a higher resolution image compared to previous attempts, however the resolution was not achieved in a small scan region at the centre of the sacculi B). The material was imaged in pure water, salt concen-

trations were adjusted to try and image at a higher resolution but unfortunately it was not achieved. The height image shown in B) is of an area where a thick band of material is visible. The material looks more densely packed than the material at the ends seen in A), however individual glycan strands and peptides are not resolved and the gap between the glycans cannot be measured.

Fast scan D probes were used to try to achieve a higher resolution due to the small probe size. Fast scan D probes are designed for optimal performance in liquid at high scan rates. The probe has a high resonant frequency and low spring constant enabling imaging of soft fragile biological samples in native conditions without deforming the sample structure. The tip and probe substrate are made out of silicon and the cantilever is made out of nitride with less than 3 degrees of bend.

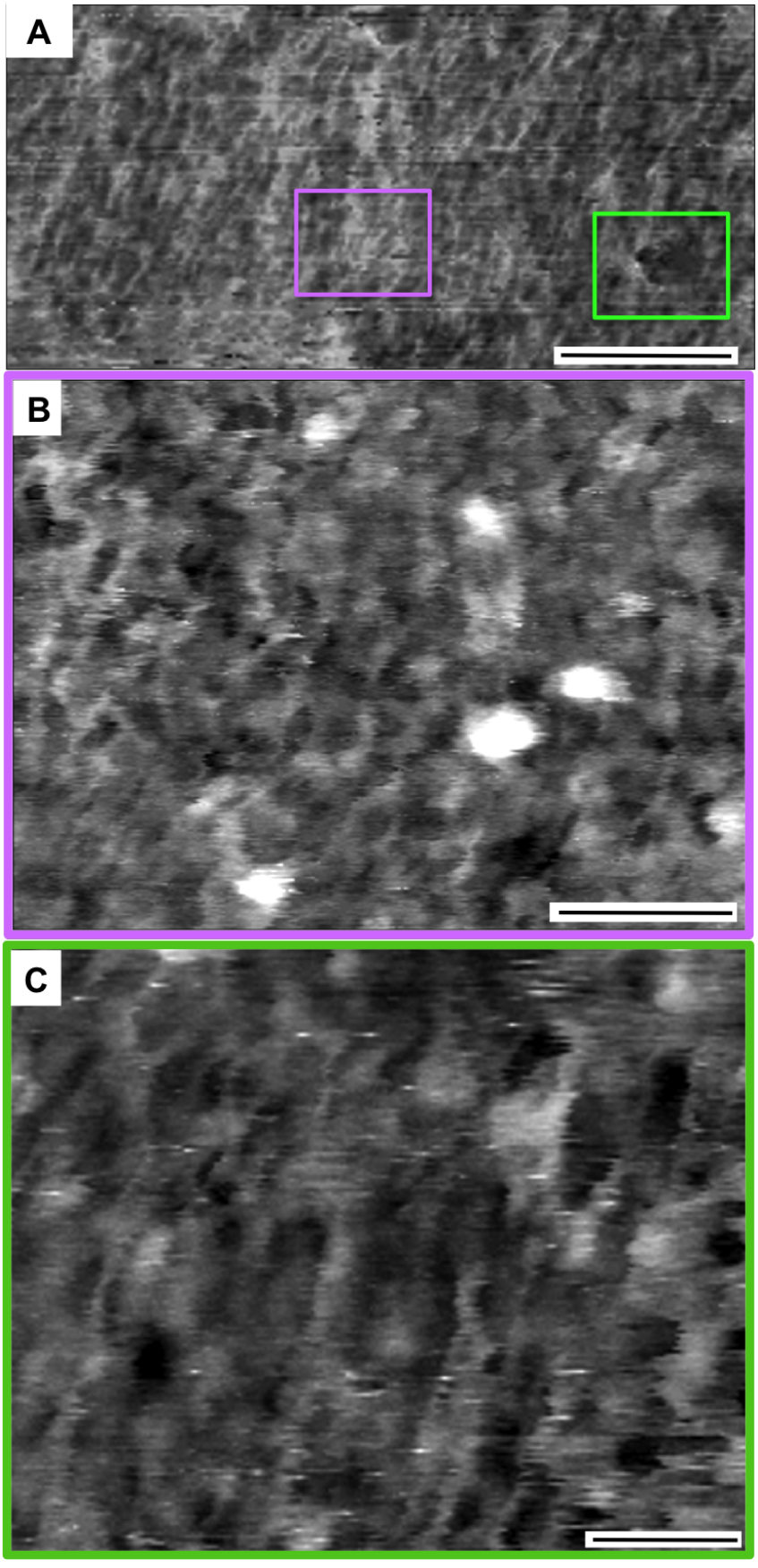
A
B
C

Figure 7.11: AFM image of an *E. coli* sacculi imaged using a fast scan D probe in Hyper Drive^{TM} mode in HPLC grade water. A) image of the rod of the sacculi where a banding structure is visible at the centre. Scale bar 200 nm height is 9.8 nm. B) is a close up image of the purple box in A) focusing on the middle bands. Scale bar 50 nm, height scale 5.2 nm. C) is a close up of the less ordered material near the ends of the sacculi, indicated by the green box in A). Scale bar 50 nm, height scale 4.8 nm.

The fast scan D probe achieved the highest resolution out of the variety of tips used. 7.11 A) shows an AFM image of the sacculi with a high wide band of material amongst thinner strands of material. The image was taken in Hyper Drive ^{TM} mode which is a form of phase modulation, described in chapter 2 section 2.2.3. B) focuses on the banding at the centre seen in A), where the material is dense and fine strands are visible through out the band. C) is a close up of the edge material shown in A) and the material seems to be a lot more spaced out where the strands have larger spaces between them.

7.2.4 Fibre analysis

A fibre analysis of the strand features seen in the AFM images taken using Hyper Drive^{TM} in figure 7.11 was carried out. A small sample size of 22 fibres and spaces between fibres were measured to quantify the visible structural differnces shown in the AFM images. The measurements have an error of 6% of the value given by the equipment calibration. Figure 7.12 A) shows that there is no dramatic difference in fibre width in the band area and the surrounding area of the sacculus. The band area has a mean fibre width of 6.90 nm and the surrounding area 7.38 nm, showing a differnce of 0.48 nm. There is difference of 0.53 nm of the median value, with the band area at 6.87 nm and the surrounding area at 7.40 nm. The range of the values for the band area is 4.94 nm and the surrounding area 3.37 nm, with a differnce of 0.43 nm. This analysis shows that the band area has on average a smaller fibre widths that the surrounding area.

B) shows that there is a more significant difference in the fibre spacing of the strand features in the band area compared to the surrounding area. The band area has a mean fibre spacing of 5.51 nm and the surrounding area 6.72 nm. There is difference of 0.91 nm

of the median value, with the band area at 5.77 nm and the surrounding area at 6.68 nm. The range of the values for the band area is 4.49 nm and the surrounding area 4.18 nm.

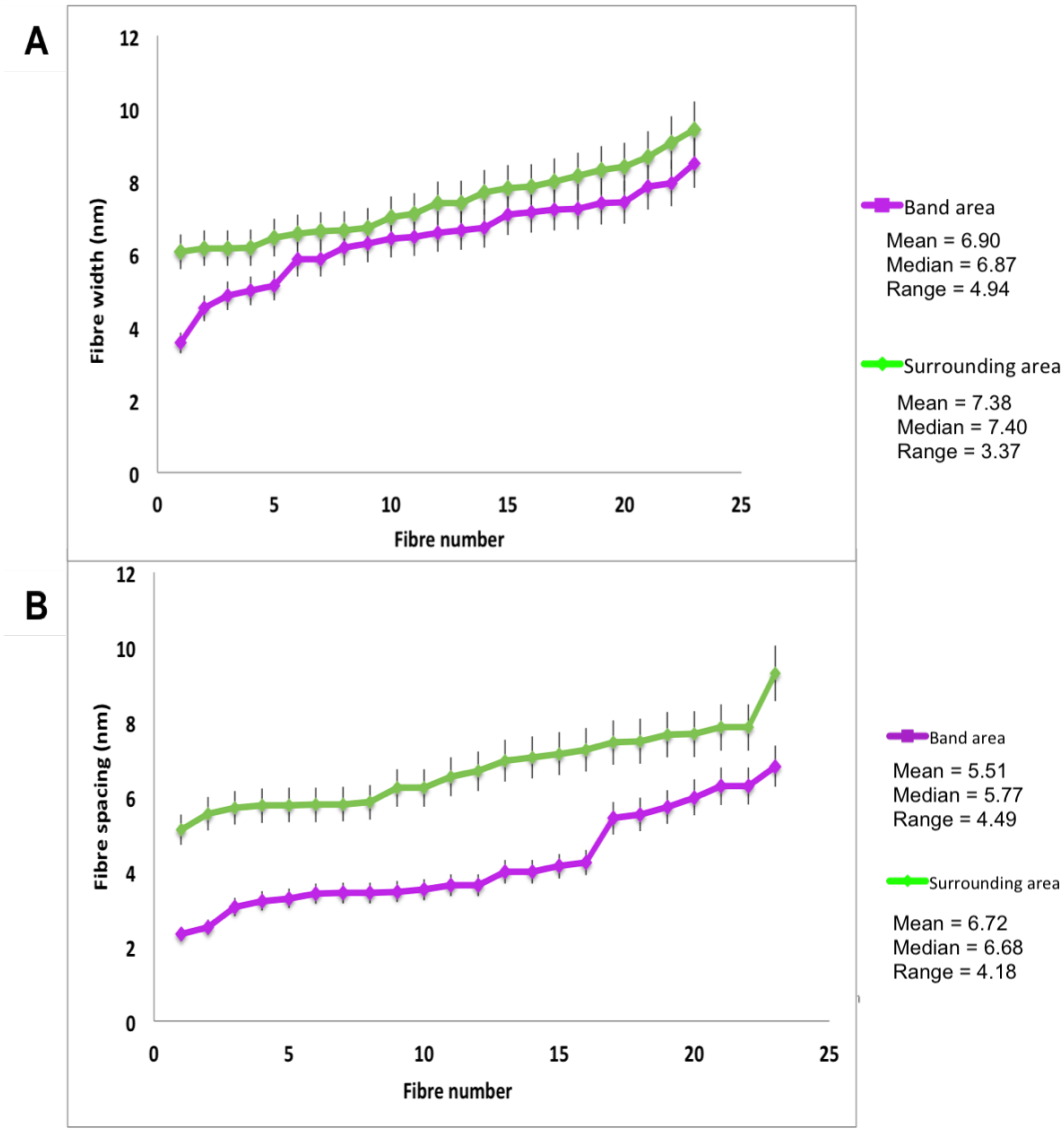

Figure 7.12: Fibre analysis of strand features seen on AFM images taken in Hyper Drive^{TM}. A) shows a comparison of fibre width of strands in the band area of the sacculi and the surrounding area. B) shows the spacing between the fibres in the material in the band area of the sacculi and the surrounding area.

The analysis shows that the most apparent structural difference in the band area compared to the surrounding area, is the spacing between the fibres. The fibre spacing is smaller

in the banding area compared to the surrounding area. This could be due to the absence of the peptide cross-links in the peptidoglycan struture, reuslting in the fibres siting closer together. There is also a larger range in the spacing of the fibres in the band area with the smallest space measuring at 2.32 nm and the largest at 6.81 nm. The could be a result of not all the peptide cross-links removal from amidase activity. It has been reported that glycan strands measure at 1-4 nm in diameter [14], which is significantly smaller than the mean fibre width in the band area at 6.90 nm and in the surrounding area at 7.38 nm. This suggests that the fibres consist of a number glycan strands.

7.3 Discussion

All of the AFM images shown identify a banding structure in the middle of the sacculi with a less ordered and sparsely arranged structure towards the ends of the sacculi. It could be a number of these bands are formed due to the removal of stem peptides, where the free glycan strands being attached to SPOR domains resulting in the glycans sitting closer together forming dense bands. When imaging in air the finer structure present within the bands were not resolved at all and instead appeared as high wide bands with no internal structure.

To increase resolution imaging was carried out in aqueous conditions. Through this process salt concentrations were altered in imaging buffers to try to achieve higher resolution via ionic shielding of the charges between the sample and the tip. Using salt did not have a large effect on the resolution achieved as it also increased the instances that fragments of sample contaminated the sample reducing resolution completely. Due to tip contamination imaging was carried out in HPLC grade water, and salt buffers were no longer used. Imaging in liquid produced higher resolution images where it become apparent that the wide high band visible at the middle of the sacculi consisted of a finer structure. The finer structure within the wide band was visible with UHFAuD, Biolever Mini and Fast Scan D probes. It was the smallest probe, the Fast Scan D, which obtained the highest resolution.

When comparing the banding material to the edge material it is apparent the material in the bands consists of fine strand like structures that are tightly packed. The peptides cross-links were not resolved but larger fibre structres were visible. The individual fibres in both scans could be resolved, the fibres and the spaces between the fibres were analysed. The analysis showed that there is a structural difference in the material in the middle and at the edges of the sacculi. The spaces between the fibres were smaller in the band area of the sacculi suggesting peptide cross-links are not present. It is known that glycan strands are 1-4 nm in diameter [**?**] and the average fibre width both in the banding area and in the surroundng area are significantly higher. Suggesting the fibres consist of multiple glycan strands.

7.3.1 Mutant strain lacking amidase enzymes

An amiABC mutant was also imaged on the AFM and STORM to investigate the presence of a blank stripe of fluorescence. The amiABC mutant is a strain of *E. coli* with the gene encoding the amidase enzymes removed. The amidase enzymes are thought to be responsible for the removal of the stem peptides [18]. Removing the amidase should remove the appearance of the blank stripe seen in the fluorescence. As the macro band structure was visible when AFM imaging in air with the wild type, the mutant was also imaged in air.

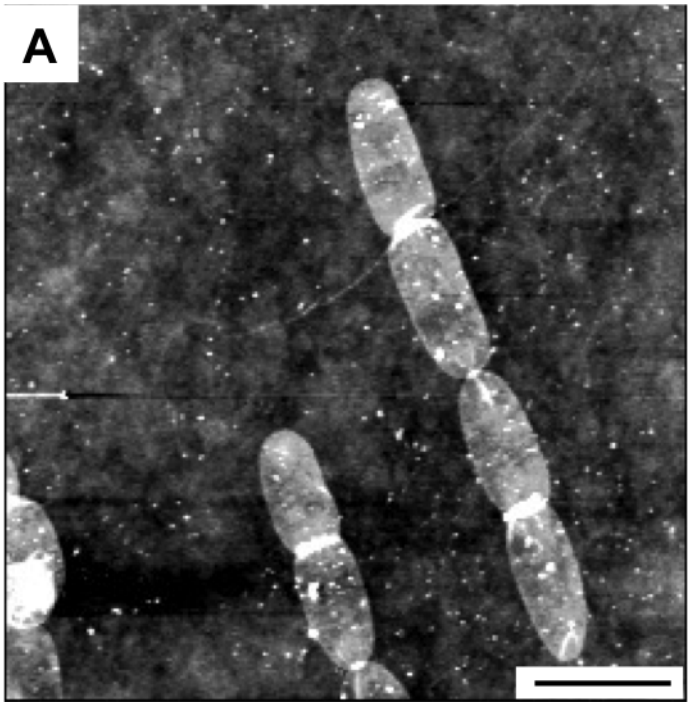

Figure 7.13: AFM images of amiABC mutant taken with an OLTESPA cantilever using Tapping Mode^{TM} in air. A scale bar 2 µm.

The AFM images shown in 7.13 show that the mutant strain do not have any obvious band visible like the images of the wild type strain imaged with the same probe. Also the cells have not separated from each other once the septum was formed. This suggests that the role of the amidase enzyme is not only to remove stem peptides but is also linked to complete cell division.

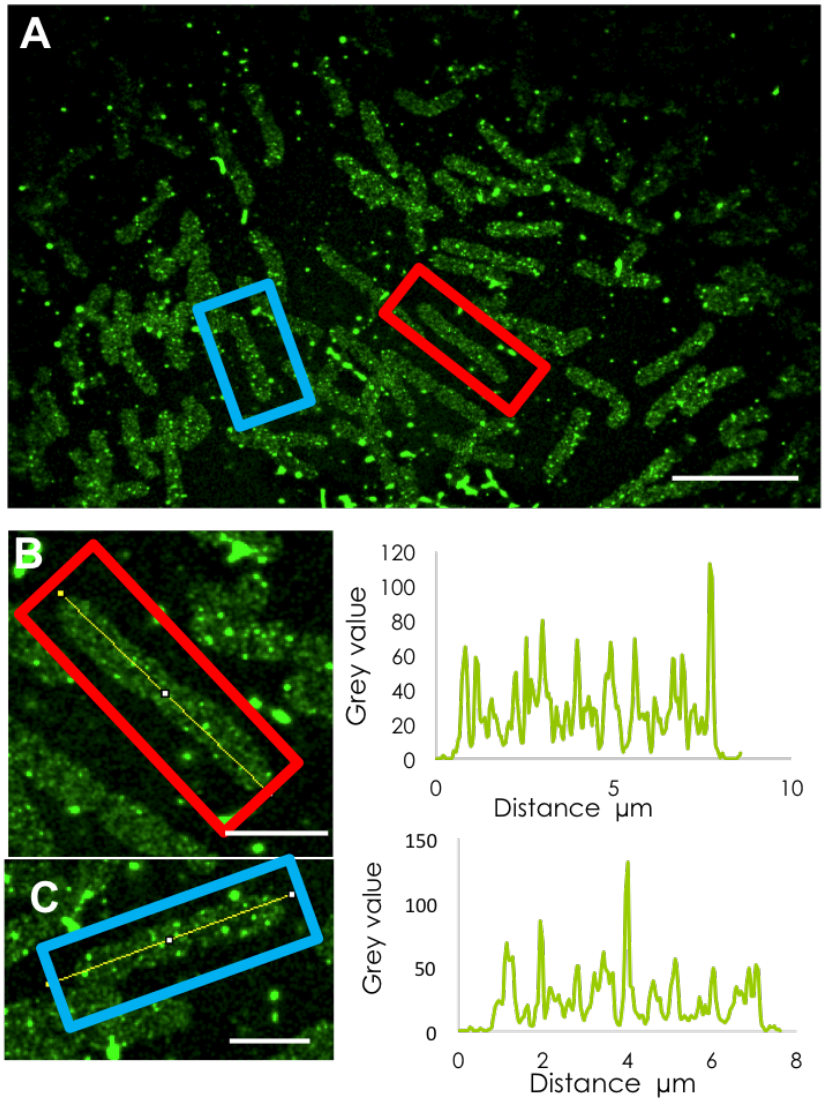

Figure 7.14: STORM images of amiABC mutant showing lack of complete cell separation. Illumination profiles show localisations of fluorescence throughout the sacculi with no apparent band of missing fluorescence. A scale bar 10 µm, B scale bar 2 µm and C scale bar 2 µm.

STORM images of the mutant sacculi shown in 7.14 show much longer cells, again indicating that the lack of amidase enzymes results if over elongated cells that have not separated from each other once the septum has formed. Section B and C show intensity graphs of two cells where the fluorescence occurs in multiple distinct foci spread over the entire sacculi in a homogeneous manner, with no significant thick band of removed fluorescence. The large foci of fluorescence are also visible in areas where sacculi are not present, suggesting contamination and unspecific binding are responsible.

7.4 Conclusion

STORMForce was used to image *E. coli* sacculi to investigate peptidoglycan insertion. During the growth and elongation of the cell STORM data highlighted a blank stripe of fluorescence that occurs at the middle of the sacculi. The strip only occurs in sacculi that have not started to separate and form a septum, once separation and septum formation occurs the blank stripe is no longer visible. Through STORM imaging the band of blank fluorescence was measured, ranging between 100-800 nm. A variety of different AFM methods were used to image the area where blank stripes were typically seen at the centre of the sacculi to try and achieve high-resolution images. FSD probes used in liquid in Hyper Drive^{TM} mode produced images of high resolution where bands of material were visible through the entire body of the sacculi where larger bundles of bands were visible at the centre. Imaging was done in air and aqueous conditions. When imaging in aqueous conditions it could be seen that the wide bands consisted of finer structure consisting of fibres. Individual glycan strands were not able to be resolved therefore the data was unable to determine if stem peptides where missing in these areas or if the glycan strands were closer together due to the removal of stem peptides. It was possible to see the difference between the larger fibre structure of material at the ends of the sacculi compared to the middle.

A fibre analysis showed that the fibre width in the band area are slighly smaller than the surrounding areas. Both groups of fibres are significantly larger than the width of glycan strands, suggesting they are made up of mulitple glycans. The fibre space in the band area is significantly smaller than the surrounding area. This could indicate the lack of peptide cross-links, supporting the amidase enzyme activity resulting in the lack of fluorescence. If the AFM and STORM were correlated the multiple bands seen in 7.11 may have been located to the band where there was a lack of fluorescence in the STORM images.

An amiABC mutant where the amidase enzyme is removed was also imaged. There are no blank stripes visible in the STORM data and the sacculi appear to be a lot longer. The

AFM images show that the cells with missing amidase enzymes do not separate and divide properly, resulting in long cells that remain attached to each other after septum formation. This suggests that amidase enzymes are crucial for healthy cell growth and division.

As molecular resolution was not achieved, it could not be determined if the peptide cross-link in the peptiddoglycan structure was present and connected to the blank stripe in the fluorescence seen by the STORM images. Due to this the decision was made to progess with alternative biological samples to further test the ability of the STORMForce technology. With the main focus of this study being bacteria peptidoglycan and cell division, the Gram positive bacteria *Bacillus subtilis* was investigated.

Chapter 8

Bacillus subtilis

8.1 Introduction

In this chapter I apply the STORMForce technique to gain an improved understanding of *B. subtilis* cell division, septum formation and peptidoglycan insertion. *B. subtilis* is a Gram-positive species with a thick peptidoglycan layer (20-30 nm) compared to *E. coil*, which is a Gram-negative species. The septum forms during different stages in the cell life cycle using different mechanisms (see chapter 4). The rod shaped *B. subtilis* cells reproduce by elongation of the cylindrical part of the main body, followed by septum formation and then complete separation. The MreB machinery is responsible for the insertion of new peptidoglycan along the cylinder of the bacteria, as well as at the septum. Cell elongation occurs through the restricted hydrolysis of old material and the insertion of new peptidoglycan, which is governed by the localisation of MreB. During septum formation the protein FtsZ, which forms the ring structure known as the Z ring, plays a role in localising MreB, which inserts new peptidoglycan into the septum. The Z ring is thought to provide a scaffold for septum formation at the mid point of the cell, laying material down from the outside working its way in a concentric movement inwardly [79]. Once the septum is complete, forming a thick septal disk, the cell divides via hydrolysis cleaving the daughter cells apart. The cell

wall structural dynamics allow for growth and division whilst maintaining the shape and allowing molecules in and out of the cell. The main cell wall structural component for most bacteria is peptidoglycan, made up of glycan strands cross-linked by peptide side chains.

This chapter also identifies the different structures seen in wet and dehydrated septums of *B. subtilis*, leading to a comparison of the internal and external pole structure. Experiments performed were to investigate septum formation and structure in *B. subtilis* with the super resolution technique STORMForce. STORM was used to identify areas of newly inserted peptidoglycan and AFM was used to achieve high-resolution images of newly inserted material, providing contextual information of the surrounding area. This involved the growth of bacteria in ideal conditions and pulse labelling with an ADA tag for fluorescence imaging during the exponential phase of the cell cycle. This was performed for short periods of time, identifying where the newly formed peptidoglycan insertion occurs. The live cells were then processed to produce sacculi where the septum was separated from the inside of the cell, allowing for imaging to take place (see chapter 5).

STORM images were taken to identify where the fluorescently labelled molecules are placed within the material that was shown on the AFM images. The data was taken covering the following time frame; 15 seconds, 2 minutes and 10 minutes, in which the cells where pulse labelled. This was also studied in the main body (rod) of the cell for the same pulse labelled time frames. It has been documented that peptidoglycan is inserted circumferentially along the width of the rod, which is also reflected in this data. To confirm this, an *mreB* mutant was also imaged to compare peptidoglycan insertion.

SIM images were also acquired to ensure the features seen in the STORM data were not due to imaging artefacts and could be reproduced and confirmed using another method of fluorescence imaging. The method developed to image pulse labelled *B. subtilis* sacculi using STORMForce and SIMForce is explained, data is shown and the method used for quantitive analysis discussed.

8.2 Results

8.2.1 AFM imaging of *B. subtilis*

8.2.1.1 Contact mode imaging in liquid

B. subtilis sacculi were initially imaged in contact mode, on freshly KOH cleaned high precision glass coverslips, shown in figure 8.1. This allowed for an observation in the way the material appeared when dried onto a glass substrate and rehydrated in HPLC water for imaging. The images show that the processed sacculi had the tendency to break circumferentially and the septum's separate completely from the rest of the material. However imaging was not very consistent as the material had the tendency to fill up with liquid and lift off the substrate, the lateral force on the sample from the tip in contact mode increased the problem. To overcome this different adhesives were used to initially stick the sample on to the substrate and different modes of imaging were explored.

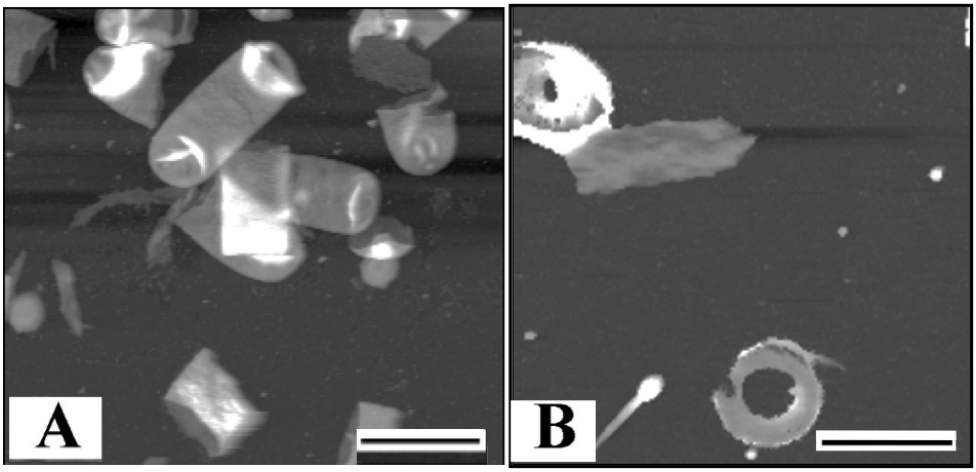

Figure 8.1: AFM height images taken in contact mode of *B. subtilis* sacculi dried and rehydrated for imaging. A) shows how the material tends to break circumferentially, B) shows how the septum separates from the rest of the material. Height scale 228 nm A) scale bar 2 µm B) scale bar 1 µm.

8.2.1.2 QI™ mode imaging in liquid

Quantitive imaging (QI™ mode) was the chosen mode of imaging after exploring Tapping Mode™. QI mode was preferable as the image is taken pixel by pixel, lifting the tip up by a specified amount (300 nm) in between each pixel. This drastically reduced the amount of lateral force applied on the sample by the tip, which reduced the risk of the material lifting from the surface resulting in higher resolution imaging. For this reason all AFM images in liquid are taken using QI mode unless stated otherwise.

To further reduce the risk of material lifting off the substrate, the adhesive Cell Tak™ was used. The surface chemistry of the substrate is altered by the Cell Tak™, allowing the material to firmly adhere to the substrate without the structure of the material being altered. When adhesive agents are used the matter of auto-fluorescence must be considered. As the material was only tagged for short time frames, there was only minimal fluorescence signal; any addition signal from other components would reduce the reliability of the data. Cell Tak™ did not produce any auto fluorescence, unlike poly-l-lysine which does produce small (but significant) amounts of auto-fluorescence.

Previous work [9] showed that dried septum had a spiralled snail shell feature. These features are also present in this work, however the feature is not visible when imaged in liquid. Figure 8.2 shows a wet dry comparison of septums during different stages of formation. The difference in structure is thought to be due to a difference in structure on either side of the septum. When dried, the structures on either side of the septum become imposed on to eachother in a shrink wrapped fashion, giving the snail shell spiral appearance.

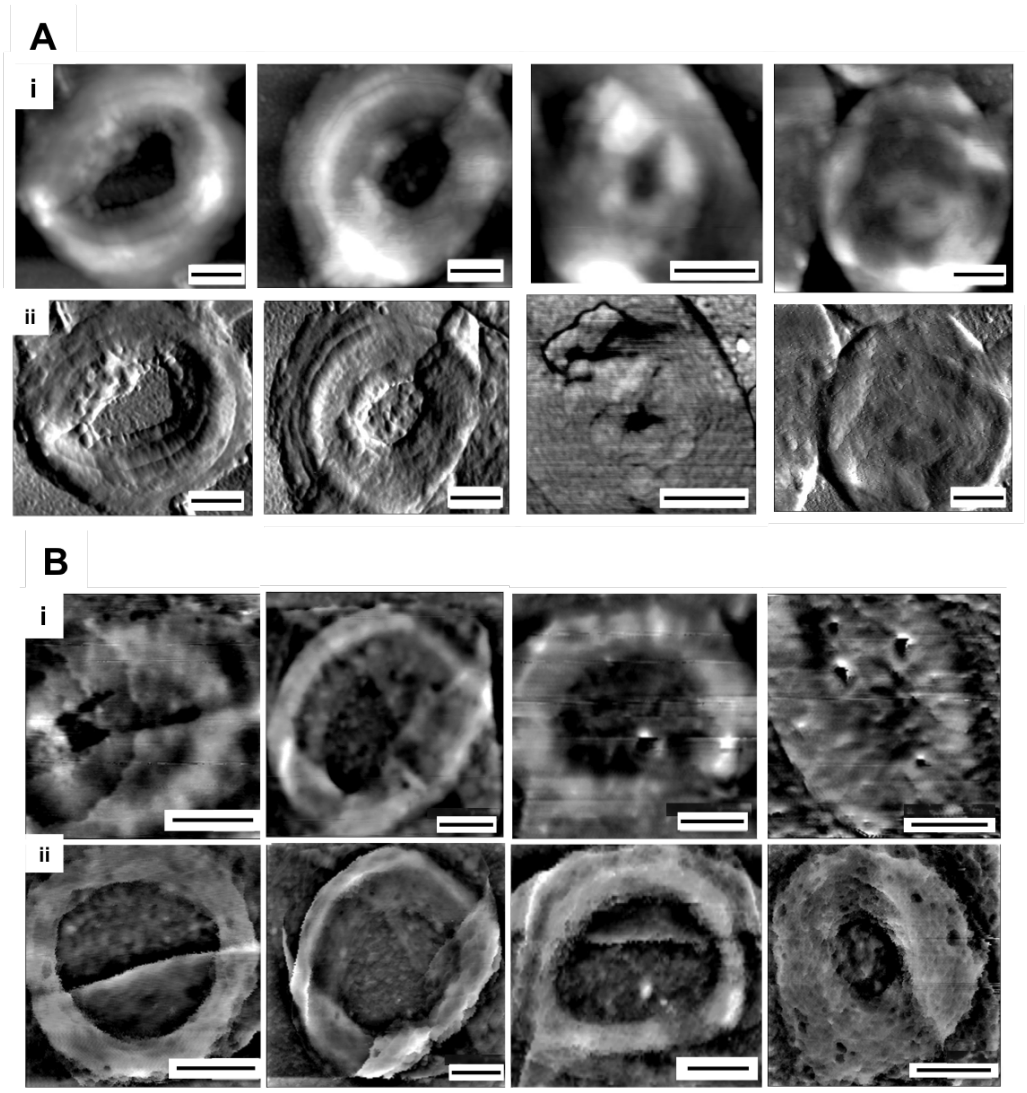

Figure 8.2: AFM QI mode images of *B. subtilis* septum during different stages of formation. The septa were imaged in both wet and dry conditions. Ai and Aii shows dry septum with a snail shell ridged features, i) is the height images and ii)have a pixel difference filter applied to increase visibility of the snale shell features. Height scale 85 nm. Scale bar 200 nm. B) shows a selection of septa during the different stages of formations in wet and dry conditions, where the height images are shown. The dry septa are shown in i) where a similar snail shell feature seen in A) is also visible. The wet images of the exact same septa are shown in ii) where the snail shell ridged features are no longer visible at all, and instead a disordered mesh structure is seen. Height scale 167 nm, scale bar 200 nm.

8.2.1.3 Imaging *B. subtilis* poles and septum

Once a septum is completely formed the cell starts to divide, one septum becomes two poles.

Through imaging *B. subtilis* poles, on both intact sacculi and completely separate poles, it

is clear the structure differs on the inside and the outside of the material. The outside of the pole has a ring structure and the inside has disordered mesh shown in figure 8.3. The schematic depicts which structure is present in the septum within a dividing mother cell, prior to the poles being present of the two daughter cells. The two structures dried on top of eachother results in the spiral, snail shell structure (figure 8.2) seen previously.

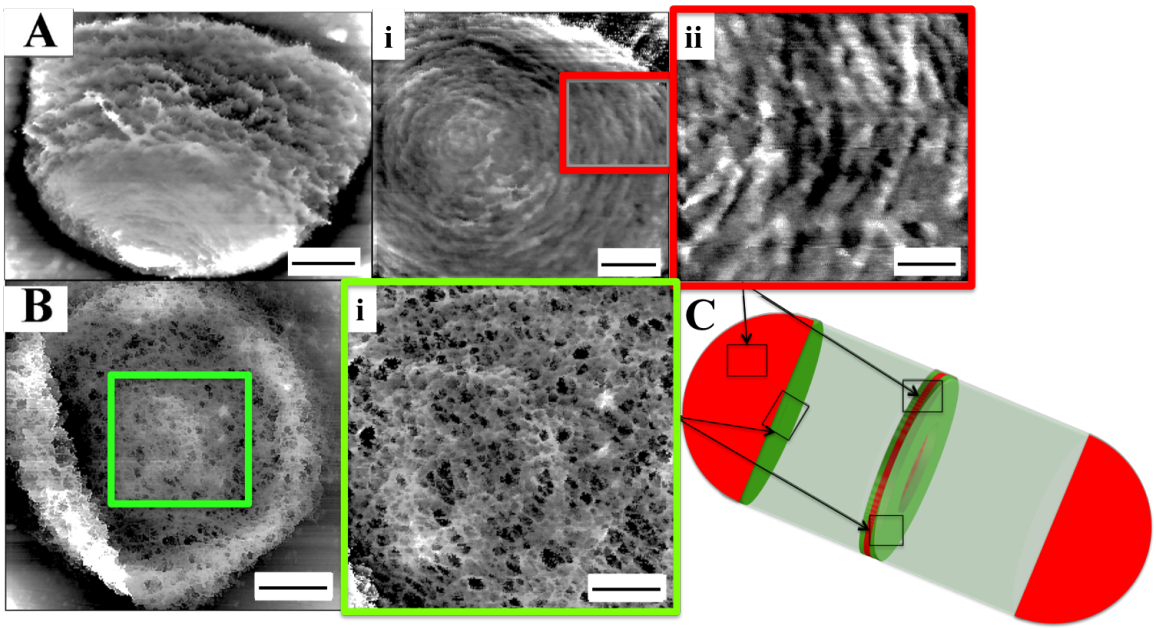

Figure 8.3: AFM QI^{TM} mode height images taken in liquid of the inside and outside of a pole in *B. subtilis*. A) shows the outside of the pole is ordered rings, which is more dense than the rest of the outer material. B) shows a complete pole where i) shows the internal material has a disordered mesh like structure. C) a schematic indicates where these structures would be within a developing cell. A) scale bar 200 nm, Ai) 100 nm, Aii) 50 nm, B) 200 nm, Bi) 100nm

The mesh structure visible in the internal pores can also be seen in septam when imaged with high-resolution AFM seen in figure 8.4. Until the one septum is fully formed and seperates into two poles only the internal structure is visble. Large holes are visible in the septum material measuring up to 50 nm in diameter. Holes of this size are thought to be too large to maintain the turgor pressure of the cell, suggesting that the production of the septum is not complete, despite the holes not being visible near the centre of the septum

where they are incomplete.

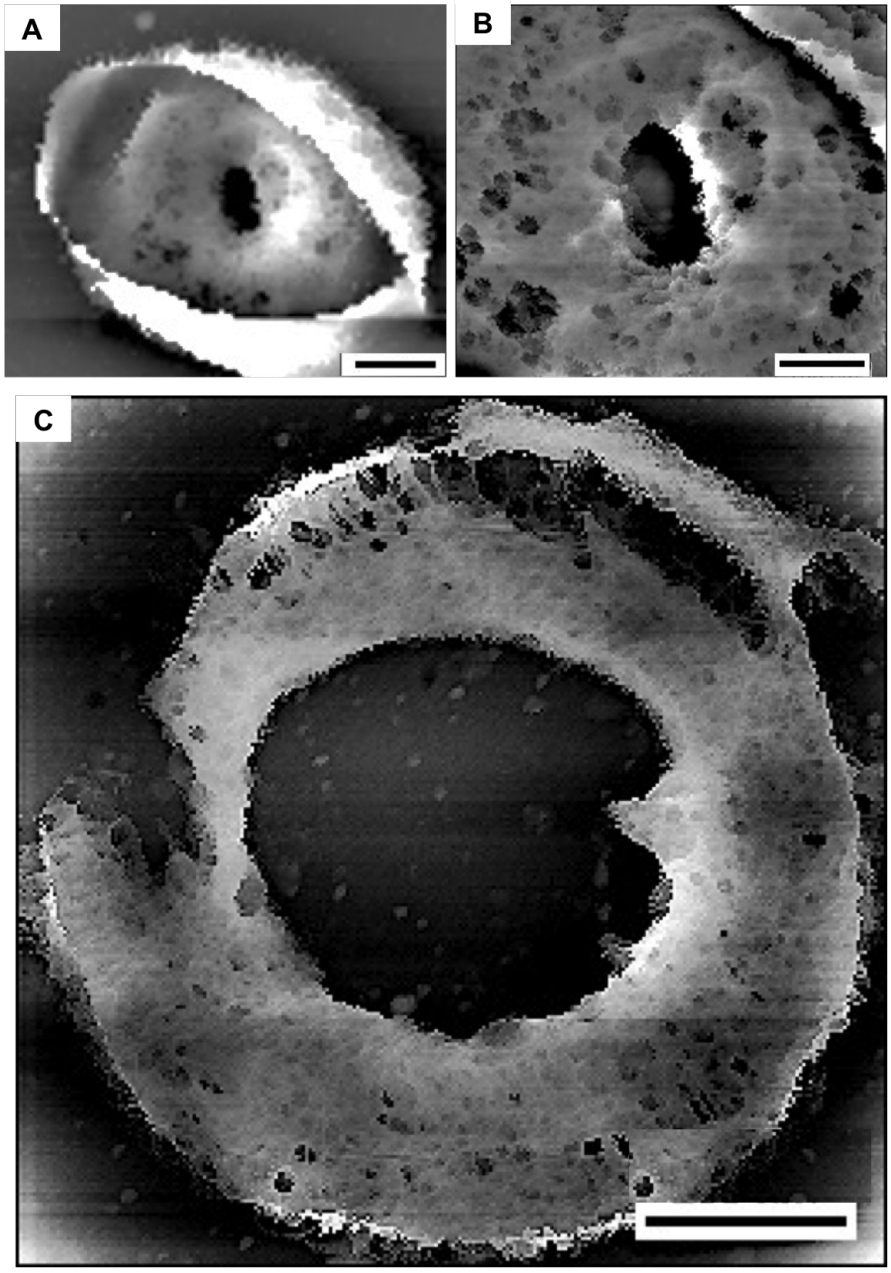

Figure 8.4: AFM QI^{TM} mode height mode images taken in liquid of septa with a visible mesh structure. A) scale bar 200 nm, B) 100 nm and C) 200 nm.

8.2.2 Fluorescence imaging.

8.2.2.1 Epifluorescence images of *B. subtilis* peptidoglycan

Epifluorescence images were taken of the sacculi to check the pulse label was successful. Once confirmed, the material was prepared for STORMForce imaging with some modifications to ensure reliable results. Previously the AFM portion of the technique was done first to obtain a clear field of view of the sample. However, as the 15-second material was only labelled for a short duration the laser used in the AFM would potentially bleach some of the fluorophores as the laser wavelength is in the same spectrum as the laser used for STORM, reducing the signal recorded. To avoid this, STORM imaging occurred before AFM imaging. This resulted in a very lengthy imaging process, as there was no clear insight as to what was being imaged via STORM and it wasn't apparent until the AFM was complete that the field of view could be seen, where the majority of the time there were no septa visible that were intact and lying individually flat on the substrate. To overcome this, the material was stained using NHS ester (at wavelength 488 nm to ensure no cross over in wave length with the 647 nm fluorophores used in the pulse labelled areas). NHS ester labels peptide and amine containing material, resulting in the entire peptidoglycan become fluorescently labelled allowing for easy sample identification. Epifluorescence images were taken using an LED light source to identify areas of interest, once identified STORM data was acquired and then the AFM imaging took place.

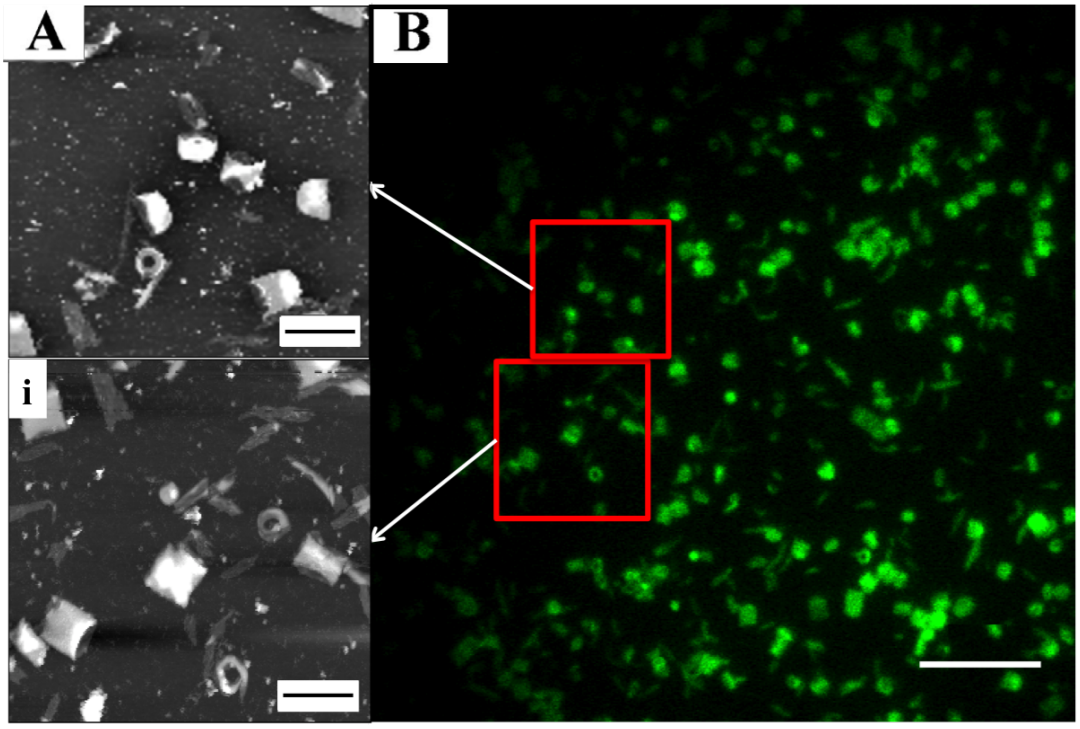

Figure 8.5: B) Epifluorescence image (NHS ester 488 nm) shows 15 second pulse labelled material present on the substrate. Areas of interest identified to allow for STORM and AFM imaging. A) Areas imaged with AFM indicated. Height scale 265 nm, scale bar A) i) 2 µm B) 5 µm.

8.2.2.2 STORMForce imaging of septum

Once an area of interest was identified it was centred in the field of view (where the 15 µm area with sufficient laser power was located), the LED was turned off. The 647 nm 70 mW laser coupled fibre was turned on to maximum power and STORM data was acquired for 5000 frames at 30 fpm. This was repeated 3 times, if the sample started to bleach the pH of the buffer was checked with pH paper and if too acid (not ideal conditions due to oxidation of the buffer as a result of being exposed to air) Tris NaCl buffer was added to raise the pH allowing blinking of the fluorophores to continue. The laser was then turned off and the GLOX buffer used for STORM imaging was switched out for HPLC grade water, the buffer was rinsed 3 times to ensure the sample was free of the GLOX buffer as it is not compatible with AFM imaging. The AFM tip was then placed into the same field of view where the STORM imaging took place and the Hamamatsu camera was then turned off to reduce any

vibration, which could affect AFM imaging. Once the tip was left to settle in the liquid for 30 minutes, AFM imaging commenced. Throughout this process the sample was firmly stuck in place on the sample stage to ensure the same area of the sample was being imaged by all imaging techniques.

Initially whilst imaging on the AFM the pixel number is kept low to reduce the time taken to acquire an image. The overall shape and arrangement of the sacculi can still be seen to identify the areas of interest seen on the fluorescence images. When acquiring AFM images the STORM data was reconstructed producing high-resolution images of where newly formed peptidoglycan insertion took place so that the AFM could focus on those regions.

This method of imaging was used to identify peptidoglycan insertion in *B. subtilis* septum formation. Images taken from the 15 seconds pulse labelled sample are shown in figure 8.6. A) shows the STORM image, the fluorescence signal indicates where peptidoglycan was inserted in the last 15 seconds of growth. It has previously been stated that newly inserted peptidoglycan during septum formation only occurs at the leading edge [17]. However the data shows that new localizations are mostly in one area, however localization are still sparsely present through the rest of the septum, indicating that material is not only inserted at the leading edge but throughout the entire septum.

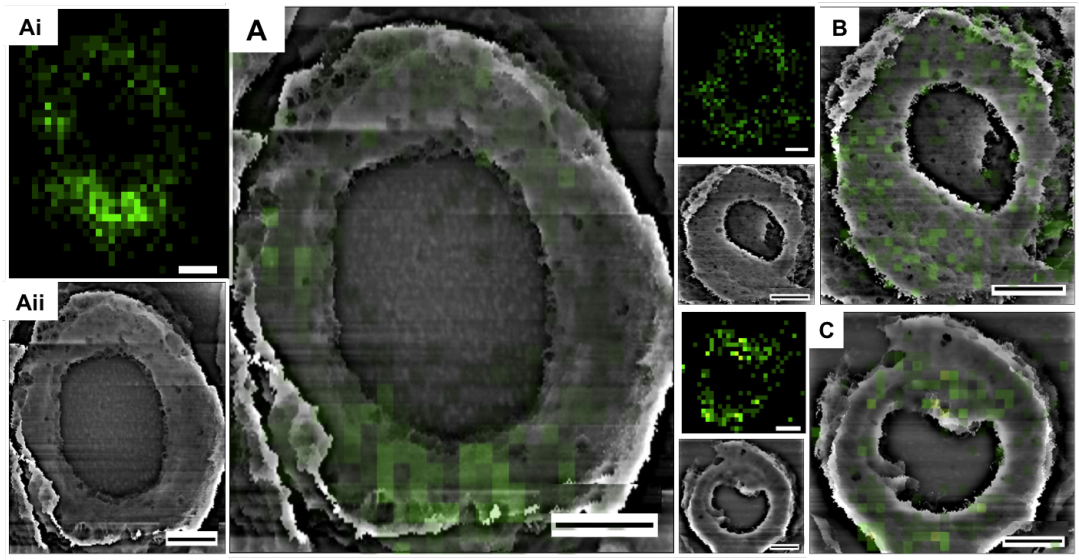

Figure 8.6: STORMForce image of 3 different 15 second pulse labelled *B. subtilis* septum. The STORM image Ai, B, C showing localisation from newly inserted peptidoglycan, the AFM image shows where the localisations lie within the septum. Scale bar 200 nm.

The 2 minute labelled STORMForce data is shown in figure 8.7. There are two main areas with a higher concentration of localisations in the STORM image (A). However there are more localisations around the entire septum, although it is not a completely uniform distribution. There are no localisations in areas with holes, which is shown in the AFM.

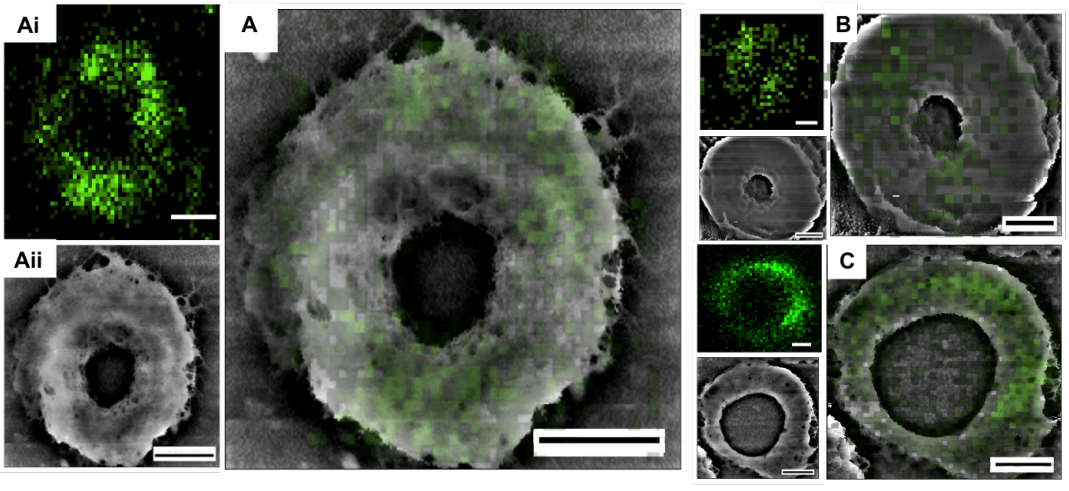

Figure 8.7: STORMForce imagine of 2 minute pulse labelled *B. subtilis* septum. The scale bar is 200 nm

The 10 minute labelled STORMForce data is shown in figure 8.8. The STORM image

shows a more uniform spread of localisation through out the septum. The AFM shows damage to the area of the septum where there are reduced localisations.

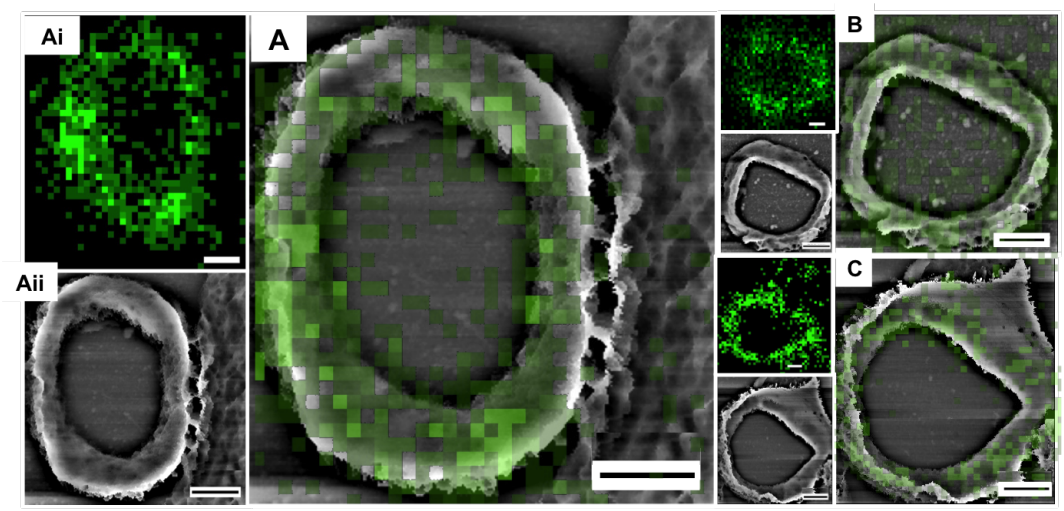

Figure 8.8: STORMForce image of 10 minute pulse labelled *B. subtilis* septum. The scale bar is 200 nm

8.2.3 Analysis of *B. subtilis* septa data

The STORMForce data of pulse labelled septum required quantitive analysis instead of interpretation of qualitative images. This was achieved by using Matlab code that was developed by Dr Robert Turner to originally analysis septum formation in *Staphylococcus aureus*. The code identifies the localisations from STORM data; the user is then able to select specific areas containing septums. The code fits a circle to the septums, registering an origin.The code has successfully been published as a tool of statistically analysing data of this nature [80].

Previous literature suggest that peptidoglycan is only added into the septum at the leading edge at the centre in comet like configurations [17]. The study states that FtsZ filaments treadmill circumferentially around the division ring and drive the motion of peptidoglycan synthesizing enzymes and thus the progressive insertion of peptidoglycan. The newly inserted comet shaped peptidoglycan continues to input around the circumference

until they join making a ring and the process continues until the septum is complete. The original data leading to this model was taken using SIM microscopy where the material was pulse labelled using FDAA tags for 15 seconds, 30 seconds, 5 minutes and 60 minutes [17].

Here the data shown and analysed were taken using STORMForce and also SIM to show the comparison of the same material imaged using two different techniques and an explanation of the discrepancies. In Figure 8.9 section A1 shows the intensity of localisations through the circumference of the septum, where the distance represents the circumference of the septum, for the 15 second labelled material. It shows that there is no uniformity in the circumferential distributions of localisation within the septum. There is one distinctive patch of newly added material, however there are still sparsely distributed localisations through the septum. This supports the AFM images showing large holes in the peptidoglycan around the septum, it is essential that these holes get filled to maintain turgor pressure of the cell, meaning new material must also be added in these areas and not just at the leading edge of the septum as suggested in [17]. Section A2 and A3 represents the localisation distribution through the radius of the septum with a histogram. The localisations are shown to be at the highest intensity at the mid-point from the centre of the septum to the edge. This could be due to the small time frame of 15 seconds; the maximum distance from the centre is 600 nm suggesting that the material labelled is closer to the centre of the septum than at the edge. This histogram also indicates that there are 987 localisations through the septum.

Section B is of the 2 minute labelled material where B1 shows the intensity of localisations through the circumference of the septum. There are two major patches of localisations however there are still localisation found around the rest of the septum, which is also shown in figure 8.7. B2 and B3 show a shift in localisation toward the centre of the septum, indicating that although there are localisations throughout the entire septum the majority of new material is inserted near the centre. The distance from the centre is shown to be around 900 nm, suggesting that more material is added further from the centre of the septum compared to the 15 second material. The number of localisations is also higher at just under 2136

indicating more material has been added during 2 minutes, as expected.

Section C is of the 10 minute material, C1 the intensity of localisations through the circumference of the septum is much more uniform with few areas of slightly less intensity. When referred back to the AFM data the areas of reduced intensity correlate with damaged material. C2 and C3 show a shift in the histogram towards the centre of the septum with an increased distance from the centre of the septum measuring around 900 nm. There is also a sharp increase of number of localisation measuring at around 16980. The data shows that there are no periodic patterns in which new material is added, however it is also not completely random as there are patches of more intense localisations. Material is added at the leading edge, but also elsewhere in the septum to fill in large holes in the material.

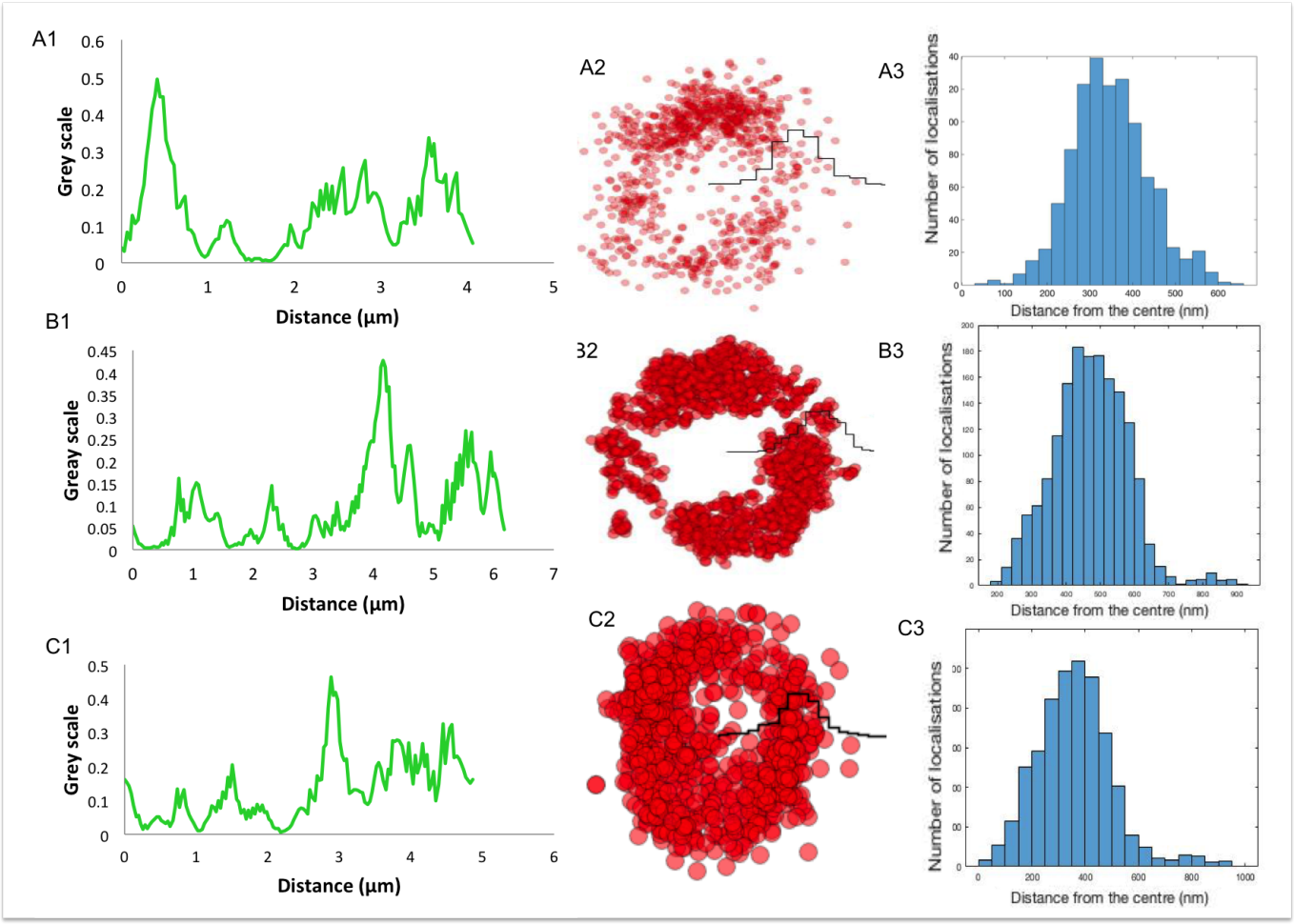

Figure 8.9: Analysis method used for quantifying peptidoglycan insertion in septum's obtained via STORM. Sections A, B and C show comparative analysis for 15 second, 2 minute and 10 minute data. Sections 1 depicts the intensity of localisations throughout the circumference of the septum. Section 2 depicts the distributions of localisations within the septum with a histogram showing the spread of newly added material through the radii of the septum.The size of the circles indicate the intensity of the localisations. Section 3 shows the histogram detailing number of localisations and position of localisations from the centre of the septum.

SIM was also used to image *B. subtilis* sacculi. The difference in intensity can still be observed in the SIM, similar to the STORM. Although individual localisations are not visible in the SIM, patterns formed by peptidoglycan insertion are still identifiable. Figure 8.10 shows SIM images of septa that have been pulse labelled. The 15 second data (A) show patches of localisations with higher intensities, this is also shown by the graph indicating higher pixel values in brighter areas. The newly inserted peptidoglycan forms non-uniform patches within the septum, forming one or two areas of intensity. The 2 minute data (B) although still showing non-uniform intensities within the septum, shows overall more intensity at higher pixel value in the graphs. This indicates more peptidoglycan insertion has taken place within the septum. The 10 minute data (C) shows a more uniform distribution of intensities resulting in complete septums. This indicates that complete septums are formed within 10 minutes, with most of the intensities at the higher pixel level of the graph. Although the patchy insertion pattern is visible in the SIM images, the difference of SIM and STORM data are due to the lower resolution of the SIM not being able to identify the more sparse areas of localisations, which are seen in the STORM. Instead these sparse localisation areas may be represented as another patch where material is inserted with a lower intensity.

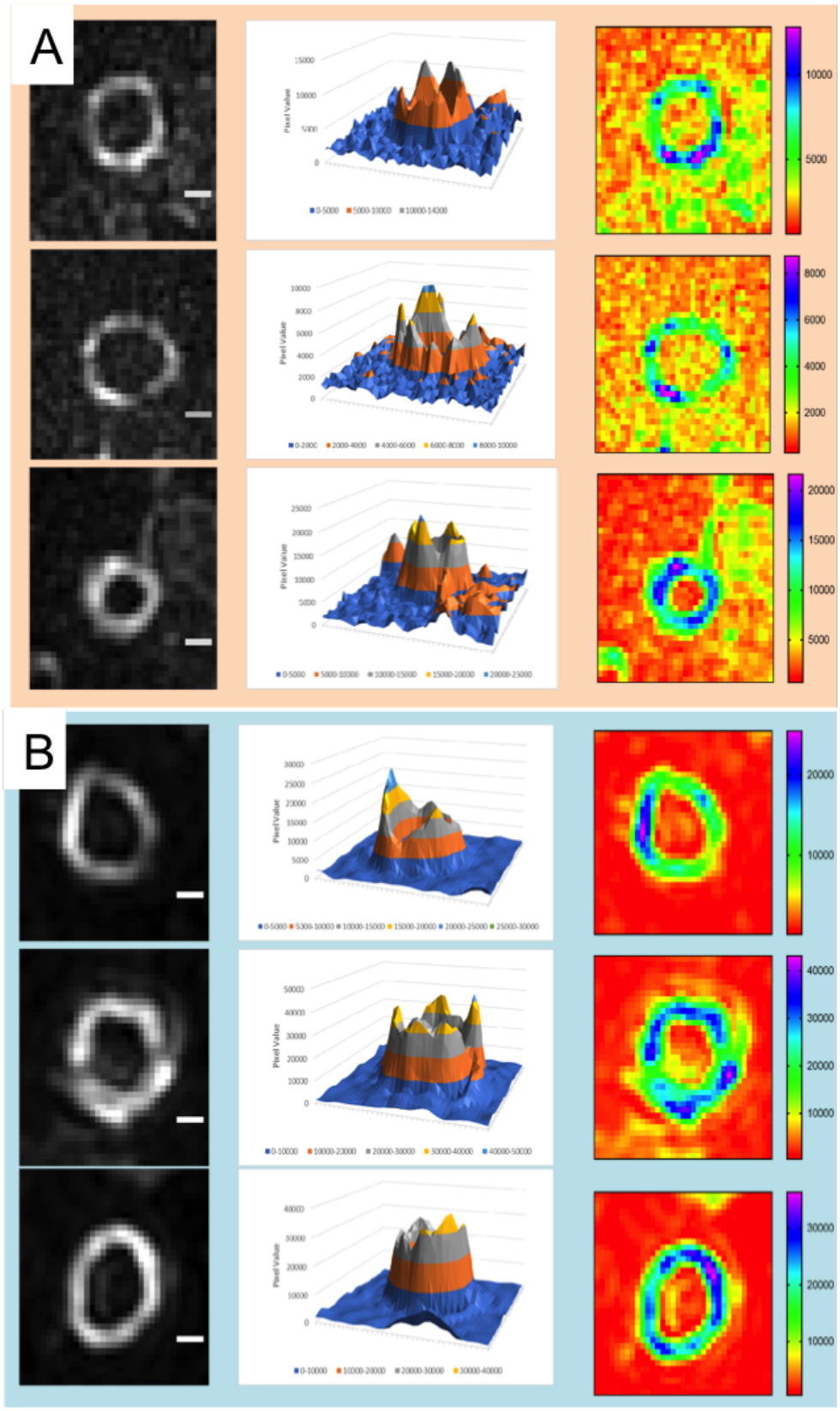
A
B

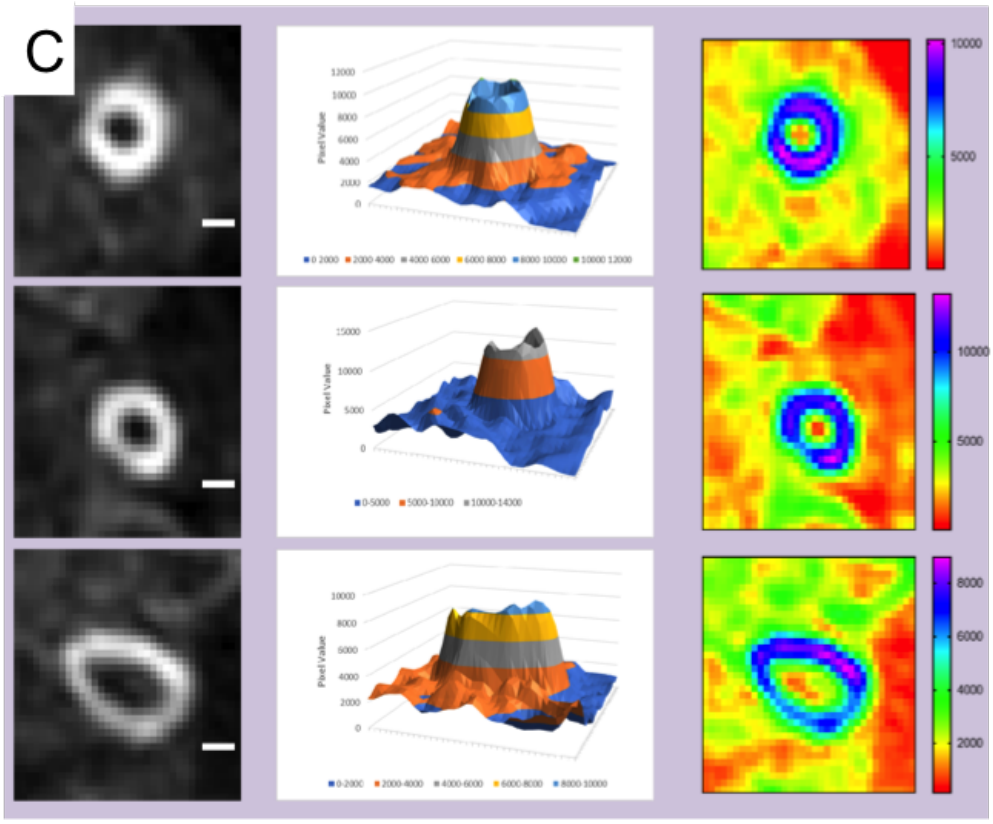

Figure 8.10: SIM data of pulse labelled septum at 15 seconds (A), 2 minutes (B) and 10 minutes (B) with intensity graph analysis. Scale bar is 200 nm.

8.2.4 STORMForce imaging of main body

The sacculi from the main body of the cell were also imaged in STORMForce to identify the way in which peptidoglycan is inserted. As mentioned above the bacterial actin homologue, MreB, maintains the rod shape of *B. subtilis*. It has been shown that MreB localisations appear as concentric rings, which develop circumferentially along the rod shaped bacteria. It has been hypothesized that MreB filaments function as a cytoskeleton which potentially organise PBP2- peptidoglycan biosynthesis complex [68]. This would also result in the insertion of peptidoglycan in the same concentric ringed pattern.

STORMForce data shows the formation of these patterns in 2 minutes pulse labelled *B. subtilis* sacculi. As before the STORM fluorescence indicates where new material has been inserted and the AFM shows where this new material lays within the entire rod body

sacculi. Where the AFM data has a 6% error of the measurements taken from the equipment calibration certificate.

The 2 minute rod data shown in figure 8.11A shows a STORM image with strips along the width of the rod. A thick strip of localizations is visible at the centre of the rod, the AFM image (B) shows a thicker area indicating a partially formed septum in this region. In 2 minutes of pulse labelling most of the peptidoglycan synthesis takes place at the septum. However there is still a lot of peptidoglycan insertion taking place in the main body of the cell, indicating that cell elongation takes place during septum formation.

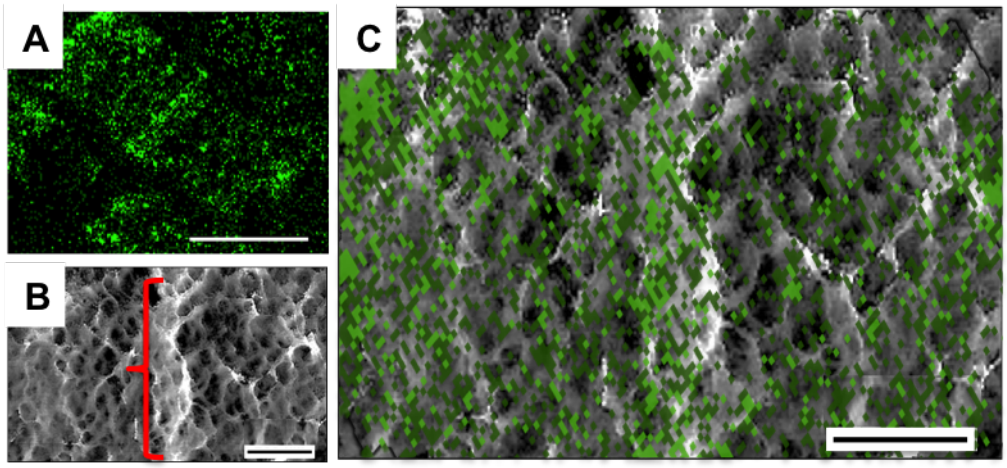

Figure 8.11: STORMForce imagine of an elongating *B. subtilis* sacculi. (A) is a STORM image of sacculi of the rod area of the cell body. A stripe of increased intensity is placed at the centre of the sacculi which correlated to the strip of higher material in (B). The thick line in the centre of the sacculi in the AFM image (B) is the septum indicated by the red bracket, which is shown as a lighter colour and therefore a higher height on the AFM images. (C) is a STORMForce image of where (A) and (B) are correlated. The material was fluorescently-tagged for 2 minutes. The scale bar is 200 nm, height scale 56 nm.

Figure 8.12 shows the AFM (A) and STORM (B) images of a leaflet of material from the rod of the bacteria. A banding structure is visble on the main body of the sacculi, however the mesh structure does dominate. A thick band of material is present at the middle of the sacculi, which correlates with the position of the septum within the cell. The STORM image also shows a striped structure within the sacculi, which indicates where the newly formed peptidoglycan as inserted within the cell wall in a 2 minute time frame. The average

peak distance of the stripes is 180 nm ranging from 210 nm to 160 nm, 6 peaks in a 900 nm length shown in (C). The banding structure of the AFM and the STORM image do not show the same information as eachother. The AFM images shows the topographic structure of the cell wall and all of the material present, where the STORM images shows the material that has been added on the inside of the sacculi (not the outside where the AFM images), in a 2 minute period. Resolution of the techniques may also play a part in the reduction of peaks with the resolution of the AFM much higher than that of the STORM, resulting in broader peaks visible in the STORM images due to less differentiation between multiple peaks and therefor a lower resolution.

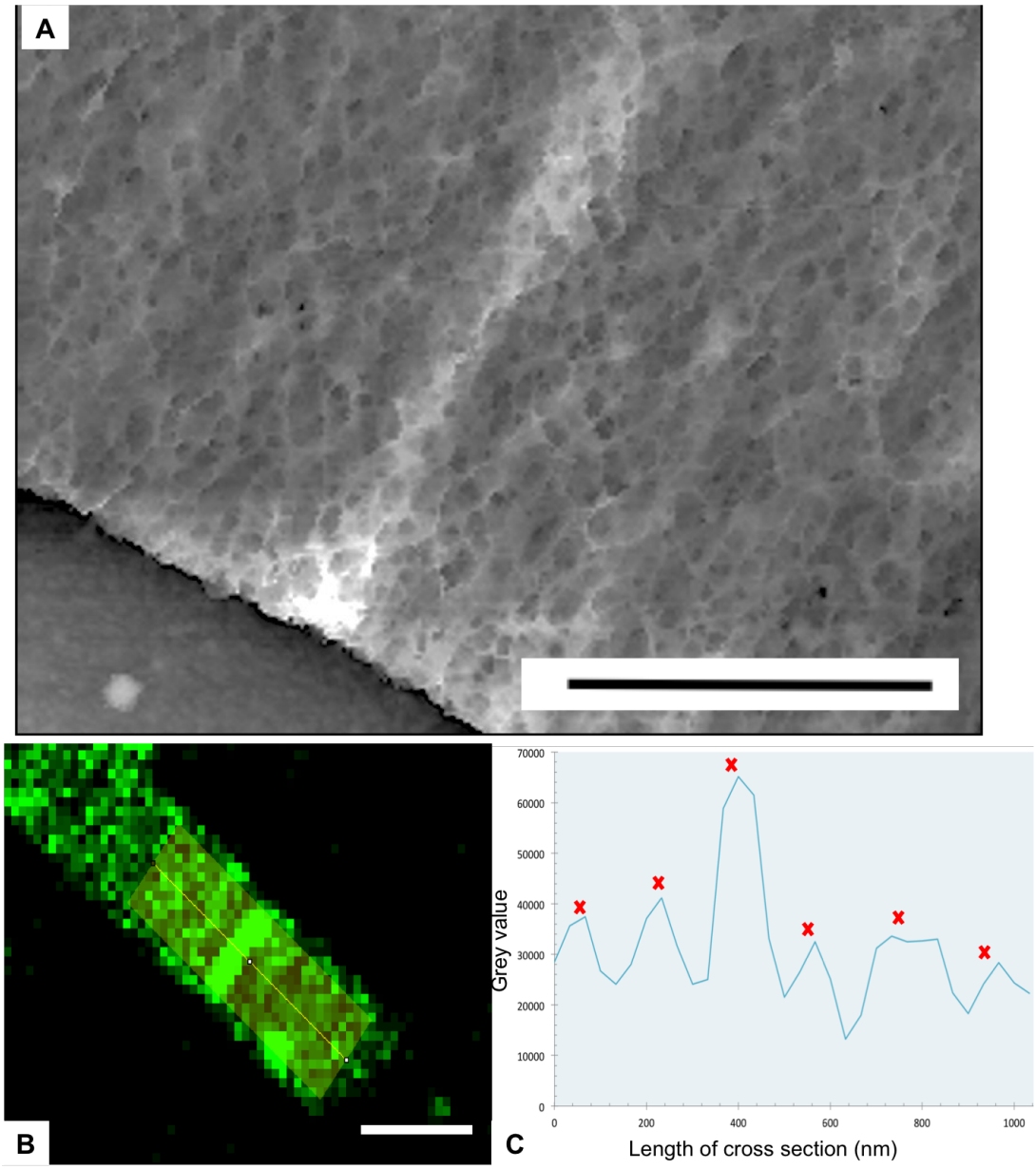

Figure 8.12: A) is an AFM height image of peptidoglycan from a rod (double layer). B) is a STORM image of the same material with C) an average cross-section of illumination. The peaks on the graph indicate areas of higher intensity, the red crosses indicate peaks that correlate to stripes in the material which appear to have periodicity. Scale bar is 500 nm.

The main rod of the sacculi was imaged in both STORM and SIM to ensure the banding features where not an imaging artefact. Figure 8.13 shows 15 second pulse labelled material, where the banding features indicate where material has been added into the cell wall in 15 seconds is visible in both techniques.

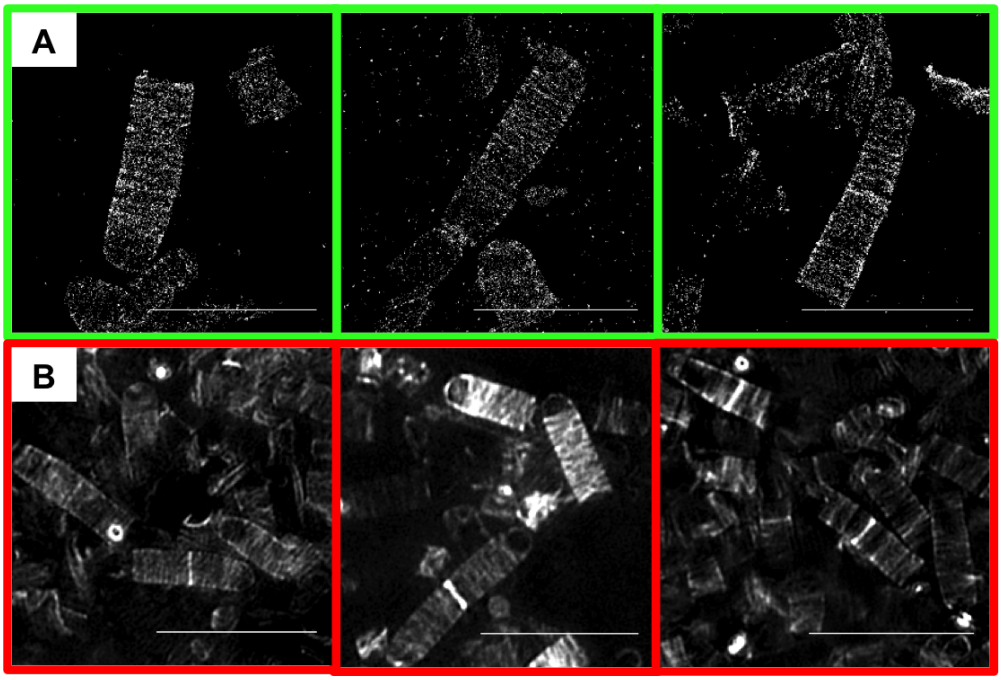

Figure 8.13: A) 3 STORM images of 15 second pulse labelled material, where the banding sturcture is visible along the rod of the material. B) 3 SIM images of 15 second labelled material, where the banding is also visible, although the images have a lower resolution compared to the STORM. Scale bar is 5 µm.

As the time pulses increase the banding structure become less visible. The 2 minute material appears to have a higher periodicity of bands compared to the 15 second material and the 10 minute material is completly fluorescent, with no banding structures visible at all. The loss of banding feature could be due to more material being added into the rod of the cell wall filling in the gaps inbetween the bands and hydrolase activity breaking peptidoglycan bonds, disipating the banding structure to allow for more material to be added via synthesis. It is already known that the internal rope like stucture of the cell wall becomes more rough and disorded forming a mesh like structure on the outside of the cell wall [9][16] making the dissipation of the banding in the fluorescence images in line with expectation.

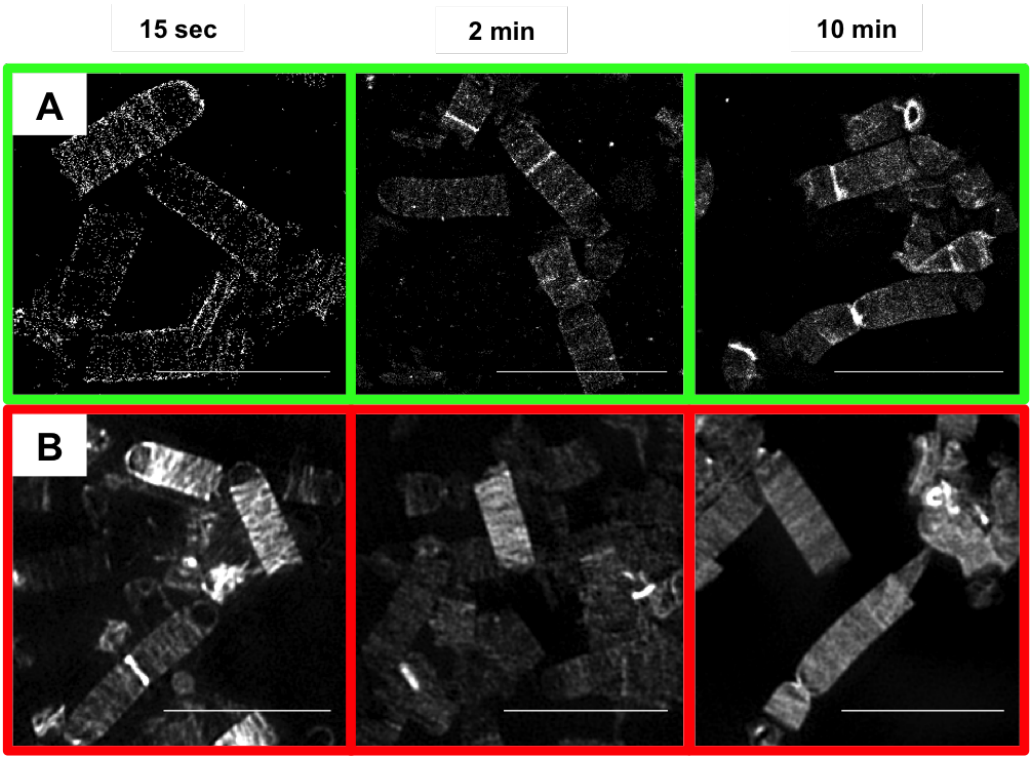

Figure 8.14: A) STORM images showing how the banding features become less apparent as labelling time increases. 15 second material shows the peptidoglycan added in the rod occurs mostly in the banding formation, by 2 minutes the bands are still visible but not as prominent as 15 seconds and by 10 minutes the banding are no longer present and the entire rod is fluorescent. B) SIM images that show the same trend, where again the resolution is lower than the STORM images. Scale bar is 5 µm.

The newly formed material also appears as higher, denser stripes on the AFM images. The material shown in the STORMForce data is made up of two layers of peptidoglycan (leaflet). To truly understand the periodicity of the newly inserted material a single layer of broken peptidoglycan (singlet) was imaged. To increase the yield of fluorescence images and identify singlet's SIM imaging was used as well as STORM. To ensure the same areas were imaged on different equipment glass correlative grids where used shown in figure 8.15.

To further investigate peptidoglycan insertion within the rod of the bacteria glass grids were used so STORM imaging could take place on a more powerful machine (NSTORM) as well as SIM, to detect the weak signal from the 15 seconds samples. The same area was then located and imaged on the AFM.

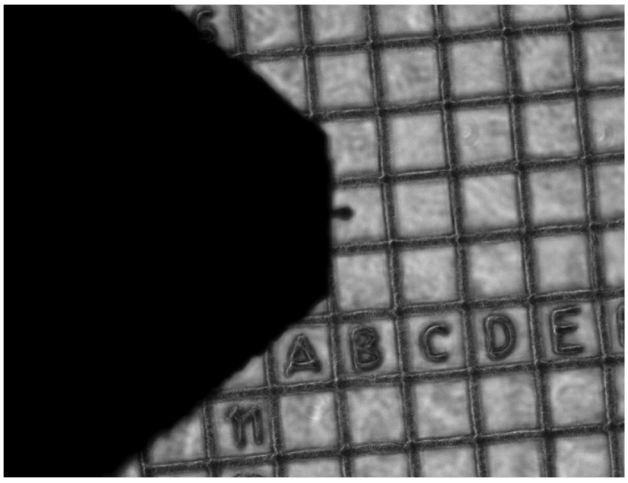

Figure 8.15: Fast scan D cantilever in a square of a glass grid used to correlated SIM and STORM.

8.2.4.1 SIMForce imaging of *B. subtilis* main body

To get a better understanding of the periodicity of the newly inserted material single layered fragments (singlets) of peptidoglycan were imaged. The broken fragments of the material were imaged using SIMforce, due to SIM producing a higher yield of data compared to STORM, although the resolution was compromised. The stripe feature identified on both AFM and STORM are still visible in SIM images, the singlet material was identified first on the SIM using glass grids, shown in figure 8.15, the sample was then imaged in the AFM. At this stage it becomes apparent if the inside or the outside of the material is facing outwards. In Figure 8.16 the outside of the peptidoglycan is facing outwards. The structure still shows the banding which is visible in peptidoglycan from intact sacculi. The external structures is more rough than the internal structure which has a more compact, smoother structure described by [9].

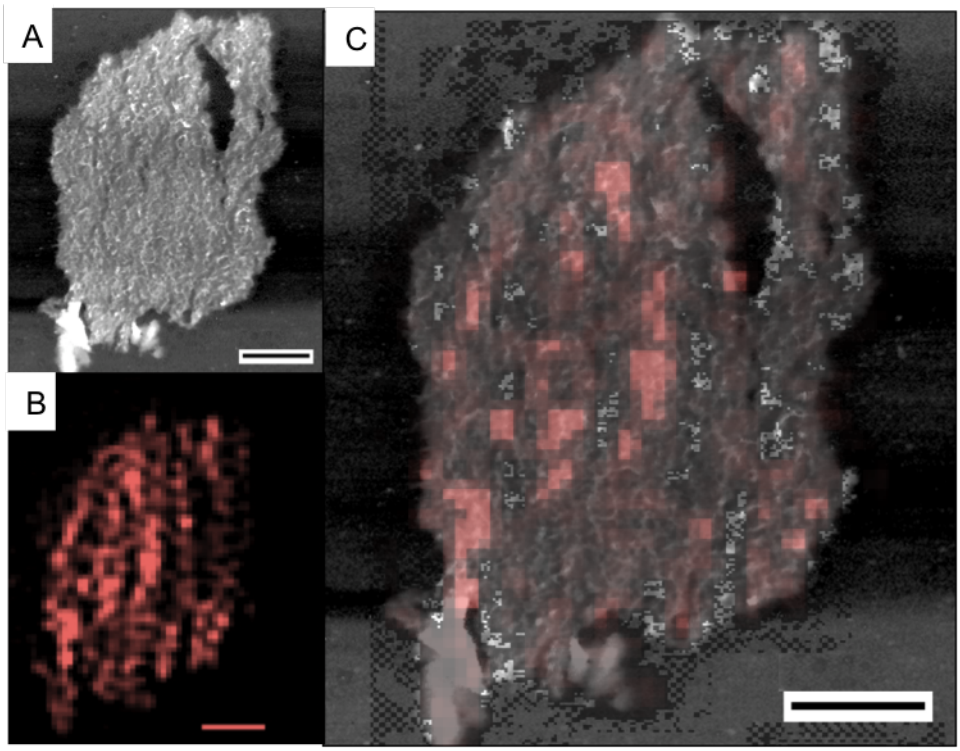

Figure 8.16: SIMForce image of a single layer of peptidoglycan pulse labelled for 15 seconds. A) is an AFM image of a singlet fragment of peptidoglycan with the outside of the cell wall facing up. B) is a SIM image showing material that has been added to the inside of the material (facing down) in a 15 second time frame. C) is a SIMForce image where A and B are overlaid. Scale bar is 500 nm.

Height cross sections and illumination cross sections were taken from the fragment of singlet peptidoglycan. Where the AFM measurments have an error of 6% recorded from the equipment calibrations certificate. The outside of the peptidoglycan is facing outward showing a rough exterior. The banding structure is visible in the height cross section with a strong periodicity. The average spacing between the peaks in the AFM image is 111.5 nm ranging from 127 nm to 97.7 nm with 8 peaks in a 900 nm length. For the SIM image average peak distance is 293.8 nm ranging from 325 nm to 250 nm, 3 peaks in a 900 nm length. Comparing this to figure 8.12 where the STORM images for the double layer material with 6 peaks in a 900 nm length and 3 peaks for the singlet SIM image. With average peak spacing being almost halved with STORM to 180 nm. The data suggests that the bands from both layers are combined together showing and almost doubled frequency of peaks and halved peak spacing for the doubled layered material for both AFM and STORM data. This

highlights the need to image singlets to understand the way new material is added into the cell wall.

New peptidoglycan is assumed to be added on the inside of the cell wall where the material is smoother with a finer structure. To truly correlate the fluorescence with the AFM the inside of the material must be imaged on the AFM.

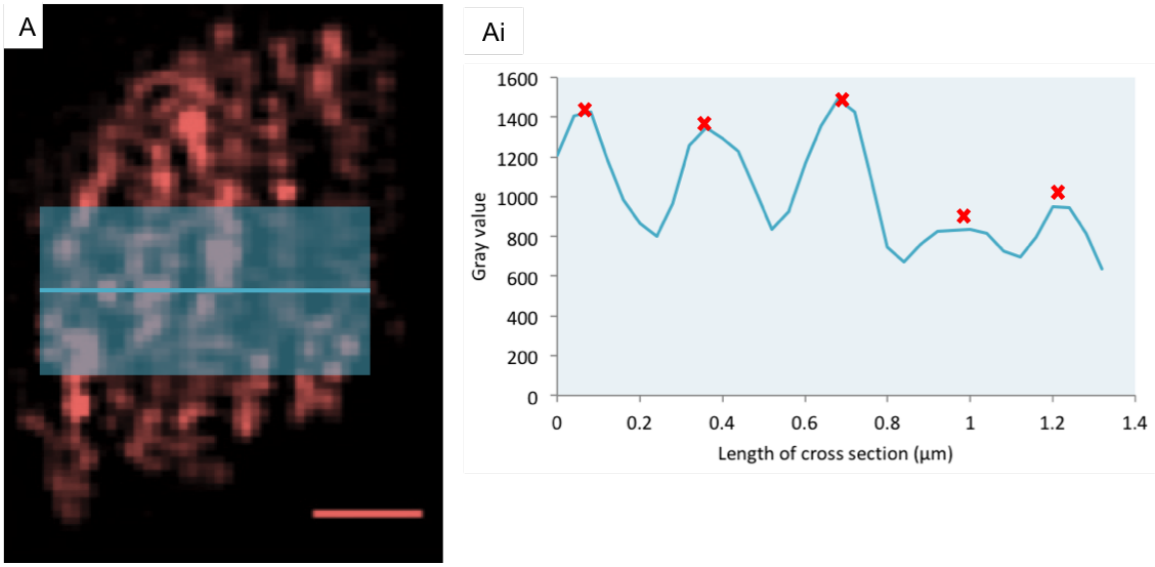

Figure 8.17: A) is a SIM image of the same material with Ai) an average cross section of illumination. The peaks on the graph indicate areas of higher intensity, where the majority of labelled material was added in the 15 second time frame. The peak position was determined by eye. Scale bar is 500 nm.

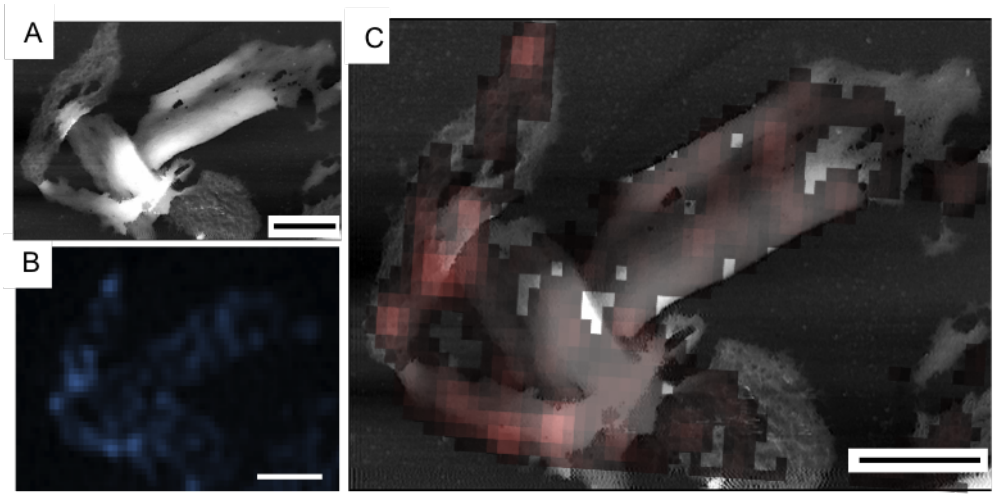

Figure 8.18: Section A) is an AFM image of broken single layer peptidoglycan. Section B) is a SIM images of the same material, however due to the small size of the fragments and the lower resolution of the SIM the banding visible in other SIM images is not visible here. Section C) is the SIMForce image, scale bar is 500 nm.

Shown in figure 8.18 is a SIM force image of singlet material where both inside and outside material is visible. However due to the size of the material the banding feature is not visible on the SIM image. The inside and outside of the material is easily distinguishable by the lack of the rough strips on the inside material, where it is much smoother with a finer structure. Figure 8.19 shows the roughness analysis of the material highlighted. The red broken line on the graphs is a reference marker to where the peaks which correlates to a stripe on the material is assumed to be. This highlights the difference of the inside and ouside material, there are more rough bands visible on the ouside compaired to the inside. The graphs show the measured roughness of the sections highlighted in the AFM image. Graphs a) and b) are of the inside material and graph c is of the outside. The roughness peaks on graph a and b are broader with a lower frequency compared to graph c where there is a higher frequency of peaks which are more narrow. However there is loose material visible on section c in the AFM image that may alter the results. The more broad peaks in a) and b) suggest larger, wider bands of more compact peptidoglycan on the inside of the cell wall compared to looser material on the outside. This also has a strong fit with previous fluorescence images.

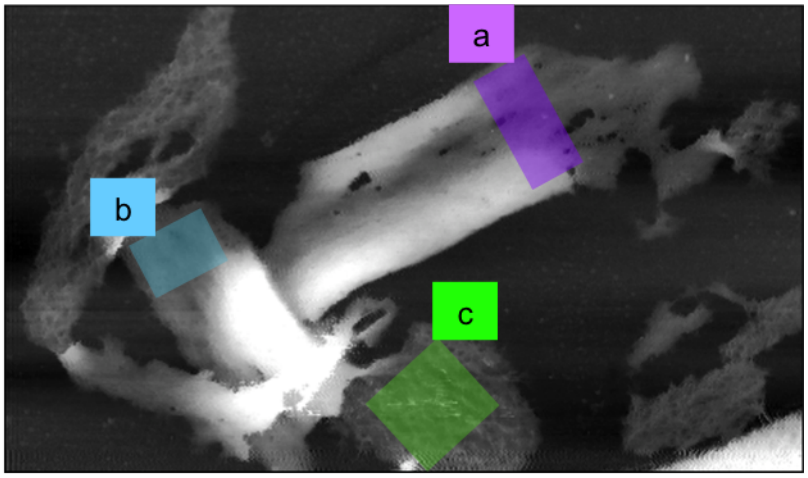
a
b
c

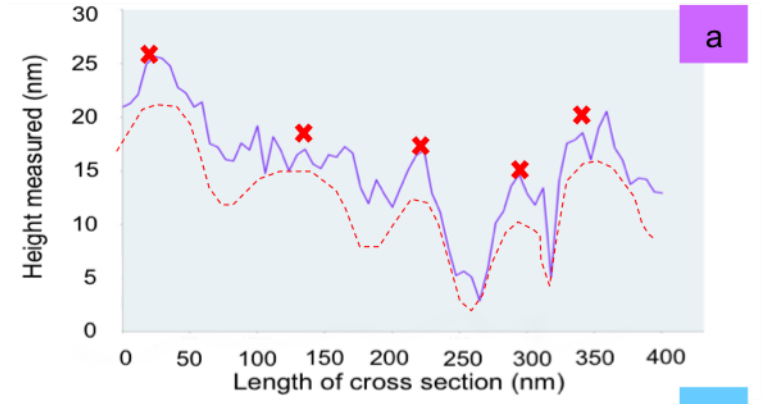
a
Height measured (nm)
30
25
20
15
10
5
0
0 50 100 150 200 250 300 350 400
Length of cross section (nm)

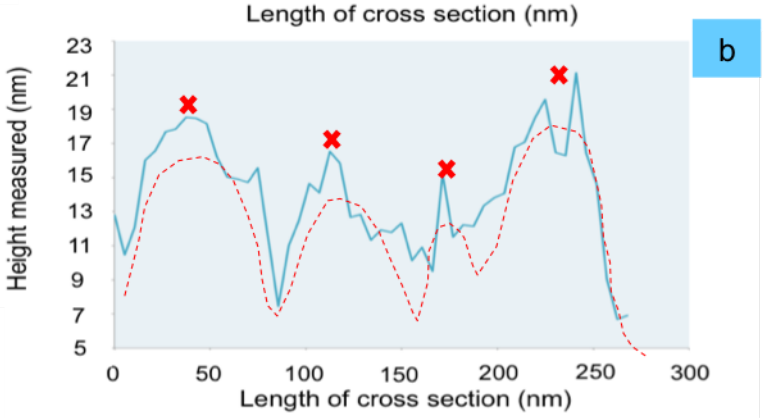
b
Height measured (nm)
23
21
19
17
15
13
11
9
7
5
0 50 100 150 200 250 300
Length of cross section (nm)

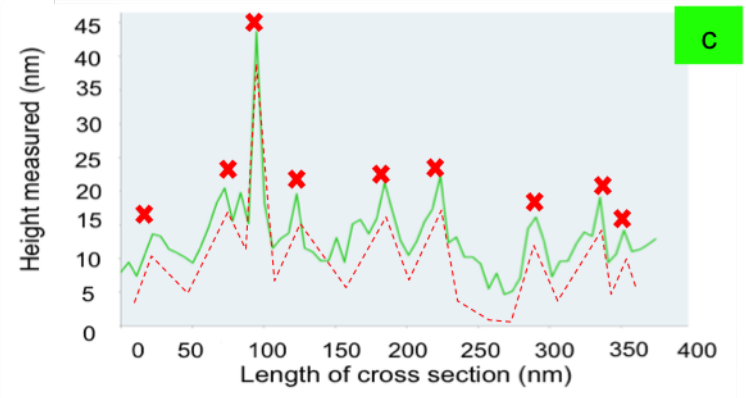
c
Height measured (nm)
45
40
35
30
25
20
15
10
5
0
0 50 100 150 200 250 300 350 400
Length of cross section (nm)

Figure 8.19: The top image shows the 3 fragments of material investigated up close. Marker a) and b) the inside of the peptidoglycan and c) shows the outside. The graphs show the height cross section of the material where the red crosses indicate peaks that correlated with stripes in the material and the red broken line shows an assumption of peak position.

Figure 8.20 shows an inside section of 15 second pulse labelled sacculi on a SIM and AFM image. The frequency of the bands in the SIM image is significantly reduced in the single leaflet compared to the double leaflet. This agrees with the observations in figure 8.19.

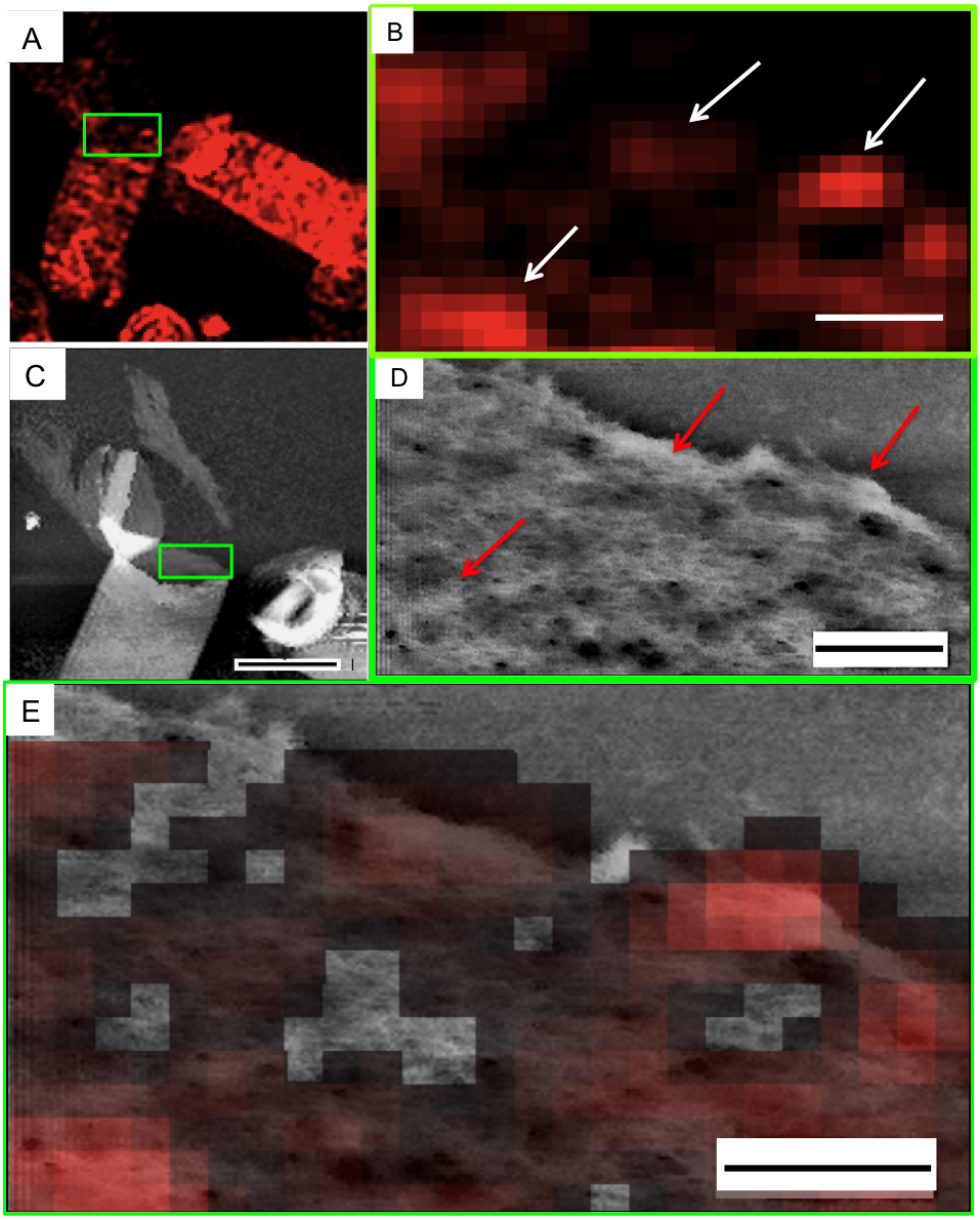

Figure 8.20: A) SIM image of 15 second pulse labelled sacculi where the green box highlights an area of single layer of material (singlet). B) zoomed in view of same singlet area highlighted in A) where white arrows indicate areas of high intensity. C) AFM image showing same field of view as seen in A), with singlet area highlighted in the green box. D) Zoomed in singlet area shown in the green box, where red arrows show areas od dense material. The AFM images clarifies that the material is only one layer thick and that the inside of the material is facing up. Scale bar 1 µm. D) High-resolution height image of highlighted area, showing a dense mesh like structure with visible more dense areas in a banded structure. Scale bar 100 nm. E) shows a SIMForce image where the SIM data is overlaid onto the AFM data, showing where the newly inserted peptidoglycan was placed. The areas of high fluorescence material shown in B) overlay with the areas of dense material shown in D). Scale bar 100 nm.

8.2.4.2 SIMForce imaging of MreB mutant

The mutant used has deletions of MreB Mbl MreBH and rsgI, which are versions of mreB that *B. subtilis* has which maintain the rod shape of the bacteria and are thought to organise peptidoglycan synthesis [81]. Without them the cells no longer hold a rod shape as the cells did not undergo elongation and the banding structure in the cell wall is not present. This results in cells that do not break circumferentially but more randomly, producing irregular shaped fragments of sacculi when the cells are broken and peptidoglycan is purified.

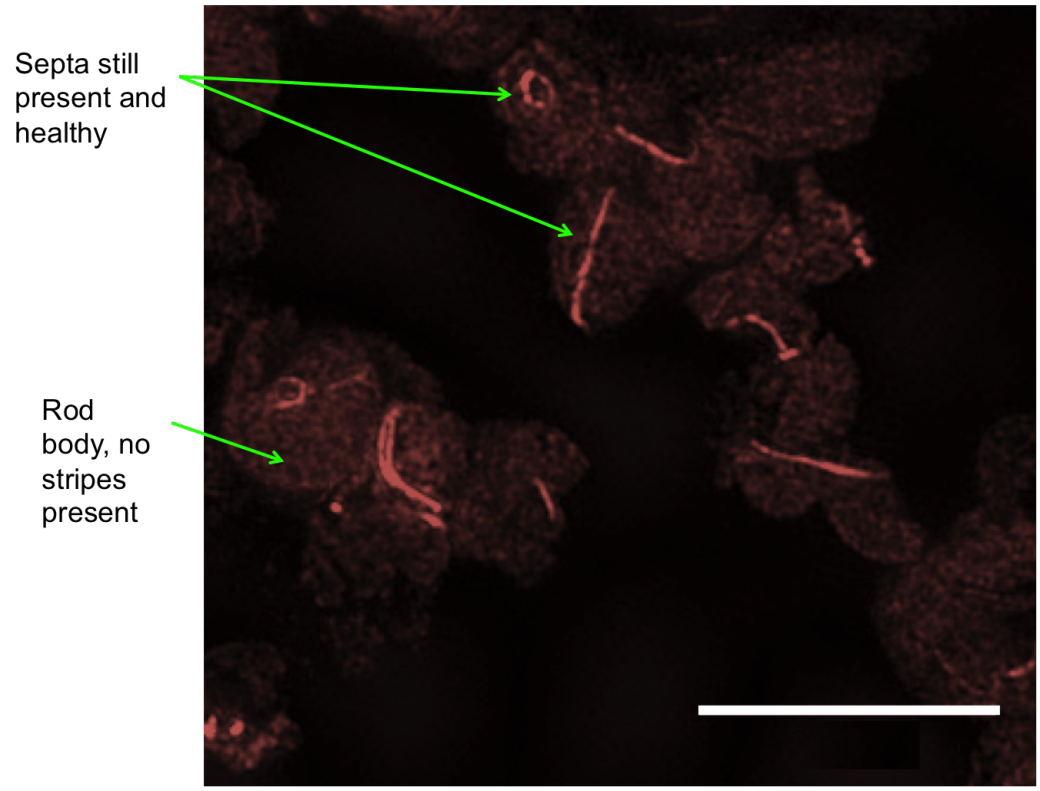

Figure 8.21: A SIM image of *B. subtilis* MreB mutant where the structure is irregular and the rod morphology is no longer visible. Scale bar 5 µm.

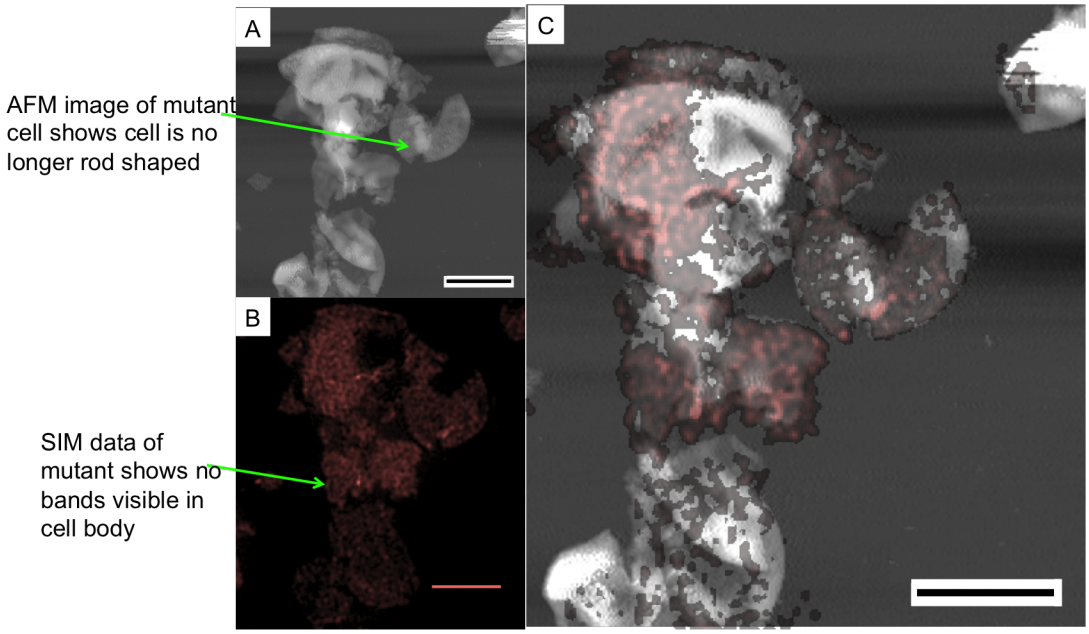

Figure 8.22: A) an AFM height images of MreB mutant, showing irregular spherical shape of sacculi. B) a SIM image of broken sacculi from a *B. subtilis* MreB mutant, no banding or strip formation of newly inserted material is observed. C) SIMForce image. The material was labelled for 15 seconds. Scale bar is 2 µm.

Fragments of peptidoglycan from the mutant are shown in figure 8.23 where a septum is imaged with broken sacculi surrounding it. The green internal section of the septum looks similar to the wild type, however the blue external area looks less ordered and more knobbled compared to the wild type. A height profile of the external material is shown in figure 8.24. The peaks are less periodic compared to the wild type, with peaks clustering together. The average peak distance is 56.5 nm ranging from 65 nm to 15 nm. This is visible in the AFM image as patches of more dense material with higher topography.

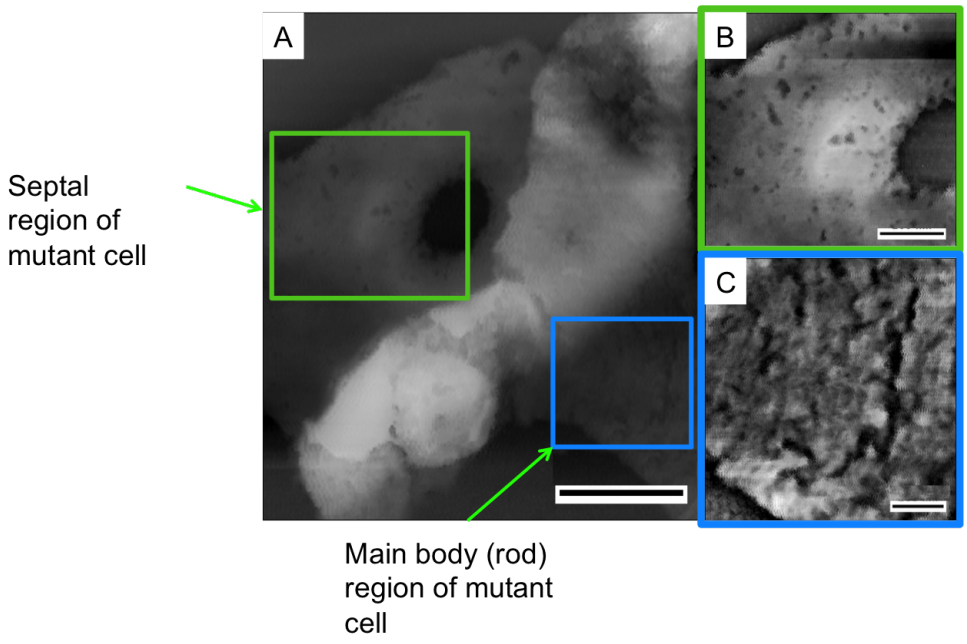

Figure 8.23: A) an AFM height image of MreB mutant showing internal septum and a layer of external sacculi, scale bar 500 nm. B) the green highlighted area focuses on the septum showing no change in septum morphology to the wild type, scale bar 200 nm. C) blue highlighted area shows outer sacculi structure, where no banding morphology is visible, but disordered patches, scale bar is 100 nm.

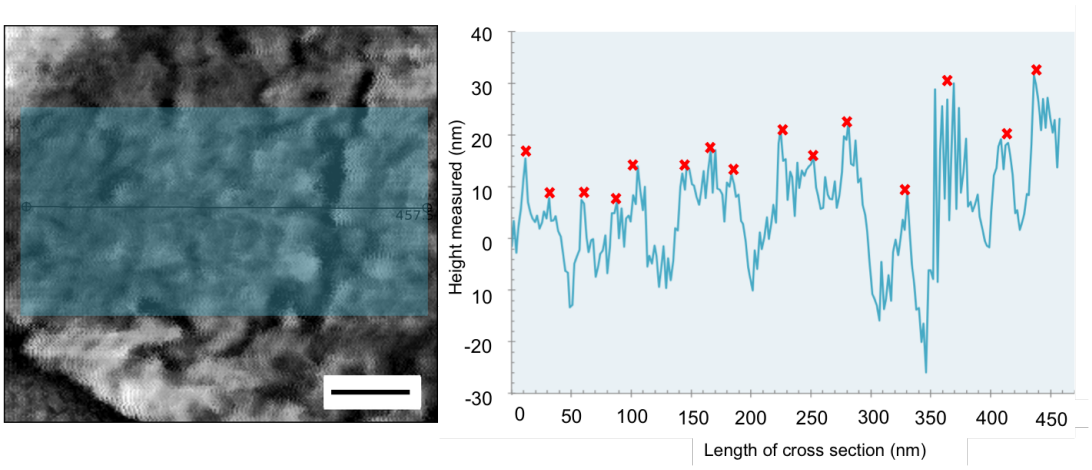

Figure 8.24: AFM image of single layer of sacculi with averaged height cross section. Scale bar is 100 nm.

8.3 Conclusions

Experiments where performed to investigate peptidoglycan insertion in *B. subtilis* during septum formation and along the main body during exponential phase. The cells were grown and pulse labelled for 15 seconds, 2 minutes and 10 minutes during exponential phase with an ADA tag, click chemistry was used to attach an Alexa Fluor fluorophore. The septa were investigated using STORMForce on integrated equipment, where epifluorescence was also used to identify areas of interest where STORMForce imaging focused.

Using the adhesive substance Cell Tak^{TM} on a glass substrate, it was possible to image *B. subtilis* sacculi without the material lifting off the surface during AFM imaging in liquid. Also using QI^{TM} mode during AFM imaging reduces the lateral force applied to the sample by the tip, which resulted in a more stable sample. The Cell Tak^{TM} used did not contribute to any auto fluorescence which would reduced the validity of the fluorescence data when imaging 15 second tagged material.

Peptidoglycan insertion in the septum at 15 seconds occurs mostly in one area at the leading edge of the septum, however new material is also sparsely added in other areas of the septum. When looking at AFM images it became apparent that there were regions not

around the leading edge of the septum where large holes were present, measuring up to 50 nm in diameter. These holes would be too large to maintain turgor pressure of the cell, suggesting that peptidoglycan insertion would also have to occur in these areas as well as the leading edge, prior to cell division. The 2 minutes septum data shows 2 areas where newly formed peptidoglycan is inserted with, again most material being added at the leading edge but also more material being added through out the septum to fill holes in the material. By 10 minutes the entire septum has been labelled. This data shows that, not only does peptidoglycan gets inserted into the leading edge of the septum, facilitating the growth of the septum, but also through out the entire septum. AFM images show large holes, which suggests the machinery must also return to these areas to fill the holes, to allow the material to maintain structural integrity.

Glass grids were used to correlated AFM and STORM images using a higher power STORM microscope (NSTORM) and to correlate AFM and SIM images. SIM was used to produce a higher yield of fluorescence images to identify more areas of interest. Although SIM has a lower resolution, the peptidoglycan insertion pattern visible in the STORM images is still seen. STORMForce and SIM was used on separate equipment to investigate peptidoglycan insertion in the main rod of *B. subtilis* for material tagged for 15 seconds 2 minutes and 10 minutes. Both STORM and SIM images show circumferential banding features in the 15 seconds labelled material, eliminating the question of the bands being a result of imaging artefacts. As the labelling time increased to 2 minutes, the periodicity of the bands increased and by 10 minutes the banding feature is no longer visible as the entire sacculi is labelled. It is already known that the internal structure of the cell wall in *B. subtilis* has a fine smooth mesh structure with dense band like features [9] the external wall has a more open mesh structure without the presence of the dense band features. This could be due to hydrolase activities breaking peptidoglycan bonds, dissipating the banding structure to allow for more material to be added via synthesis. The bands are a secondary feature, the peptidoglycan is inserted circumferentially in the rod area of the cell which, when bundled

together form the band features, which could also suggest the increased periodicity and loss of banding features in the fluorescence images may also be a result of hydrolase activities and peptidoglycan synthesis. However to truly understand peptidoglycan insertions patterns in the main body of the cell, single layers of material (singlets) were imaged. SIMForce was used to investigate peptidoglycan insertion in singlet material and compared to the double-layered material. The frequency of the peaks are halved and the spacing between peaks are almost doubled when comparing the singlet material with double layered material with both AFM and SIM/STORM height cross-sections. This indicates that the features present on both layers are overlaid with each other showing double the number of features present in a single layer of material.

Newly formed peptidoglycan is assumed to be inserted on the inside of the cell. The inside of the broken peptidoglycan was imaged to overlay with what can be seen in the fluorescence. The inside of the material has an entirely different structure, it is smoother and with a broad banding pattern, which is also shown in the fluorescence data. This also supports work done previously [16] [9]. This could suggest that hydrolase activity breaks bonds in the peptidoglycan to facilitate cell elongation, resulting in a different structure of the inside and outside material.

MreB mechanisms are thought to be responsible for the banding structure seen in the main body of the bacterial cell wall. A deleted *mreB, mbl* and *mreBH* mutant was also imaged to see how this changed the structure of the bacteria. The bacterium no longer holds a rod shape, but instead an irregular spherical shape with no banding found in either fluorescence of AFM images. Height cross-section data taken shows that higher regions of material are clustered together giving the appearance of patchy, disordered material. These findings support the pervious work showing that [81] MreB is responsible for cell shape and regular peptidoglycan insertion within the main body of the cell during cell elongation.

The cell wall is a complex and dynamic matrix, where currently little information is available as to how the peptidoglycan is structured throughout the life cycle. By using

the STORMForce technique a greater understanding has been achieved in knowing where newly formed peptidoglycan is inserted within the septum. Where AFM gave context to where peptidoglycan is inserted in the septum and not just the leading edge. STORMForce also highlighted the difference in structure on the internal and external rod area of the cell. Highlighting the banding formation that peptidoglycan insertion occurs in on the inside of the sacculi. Suggesting processes must occur to reorganise the material for a different structure to be present externally.

Chapter 9

Conclusion

A technique to produce correlative STORM AFM (STORMForce) images was developed, allowing for high-resolution topographic images combined with chemical information about the sample. STORM and AFM imaging have previously been combined in [82], [83] to image whole cells. In this study the initial step in developing the STORMForce technique was to correlate images taken on separate AFM and STORM machines. A new sample substrate was developed which is compatible with both AFM and STORM. Images were acquired on individual equipment to preserve the image quality of both techniques. However, there was a low yield of correlated images due to issues with locating the same area of the sample on the different techniques. Instrument integration was then developed to eliminate the location issues experienced when imaging on separate instruments.

STORM components were added to a JPK Bio Nano wizard AFM that allowed for AFM and STORM imaging of the same area of the sample without the sample being moved. During the integration noise measurements were taken to mitigate noise added to the AFM system, which would reduce image quality. The development of an adapted sample holder allowed for images to take place without the sample being moved at all between each imaging technique. The sample holder consisted of a small Petri dish with a hole cut out of the bottom, where a glass coverslip containing the sample was placed on top. This allowed

for the oil objective used to have access to the bottom of the glass coverslip and the petri dish to be filled with buffers for STORM imaging. The sample holder was glued to the AFM sample stage so it did not move when the buffers were rinsed out using a long pipette tip. The AFM tip was used as a fiducial marker to relocate the same area seen in the fluorescence images. Imaging protocols were tailored for each technique on the STORM force instruments to optimise image quality. An increased amount of STORM buffer was used to compensate for the buffer oxidising reducing effective blinking. pH paper was used to monitor the pH of the buffer, once it began to oxidised and pH dropped. To increase the pH Tris NaCl was added. Increasing the pH allowed for blinking to continue for a long enough time to acquire high resolution STORM images. Imaging Bacteriorhodopsin under a number of different conditions, tailoring imaging conditions to the sample, optimised AFM imaging. Optimising AFM imaging also involved using a number of different cantilevers, imaging modes and buffers. Through doing this the unit cell structure of Bacteriorhodopsin was imaged on the STORMForce instruments. By taking noise measurements during the instrumentation integration, noise added when AFM imaging was mitigated. When AFM imaging the only other equipment running was the inverted microscope the AFM is placed on top of, this could also be turned off to further reduces minor noise when obtaining high resolution images.

Once development of the STORMForce was complete the technology was used to investigate a number of biological samples of interest. The cell wall elongation and peptidoglycan architecture of *E. coli* has previously been investigated using AFM and fluorescence in [13]. To further these findings STORMForce imaging was used to give chemical information to the same area of the same sample where high resolution AFM images were taken. An ADA tag was incorporated into the *E. coli* cells throughout the growth process, replacing the peptide cross link within the peptidoglycan structure resulting in the entire peptidoglycan structure being tagged. The cells were then processed leaving only purified intact peptidoglycan sacculi. Sacculi from different stages of growth were imaged and features showing a band with

a lack of fluorescence in the middle of the sacculi were identified. The AFM images from the STORMForce data showed that the areas where the blank stripe was fluorescent in the STORM showed intact material still present in the AFM images. Previous studies showed [18] that during growth and division amidase enzymes remove the peptide cross-link joining the glycan strands together. The peptide cross-link is also where the ADA tag sits resulting in the band of missing fluorescence. STORM data was acquired showing the sacculi where the blank strip was visible. The stripe appears prior to septum formation as no septum or cell constriction is visible at the centre on the sacculi when the stripe is present.

To investigate the lack of peptide cross-link at the centre during this stage of growth, high resolution AFM images were taken in the hope of identifying differences in the distances in glycan strands. The resolution needed to measure glycan spacing was not achieved, although the structural differences between the middle and the area closer to the poles were identified to have some differences. To increase resolution obtained a number of different cantilevers, imaging modes and conditions were tested. When imaging in air using Tapping Mode^{TM} banding formations at the middle of the sacculi were identified however, the structure within the bands could not be resolved. Selections of sharper and softer cantilevers were used in Tapping Mode^{TM} in air to increase image resolution and reduce lateral force on the sample. However, resolution did not improve enough to see the structures in the band area.

Data was then taken in aqueous conditions, a variation of salt buffers at varying concentrations was used to try and obtain higher resolution images. Using salt allows the tip to get closer to the sample where short-range interactions occur. However, the screening of charges also contributes to fragments of sample contaminating the tips, reducing over all resolution and yield of images. For this reason all images taken in aqueous conditions were done so using HPLC grade water. A number of cantilevers and imaging techniques were used to obtain higher resolution. Fast Scan D cantilevers in hyper drive^{TM} gave the highest resolution out of the selection used. Fibre like features were resolved within the

band structure in the middle of the sacculi and at the end of the rod of the sacculi. The fibres in the band were denser compared to the fibre structures in the rest of the sacculi. A measurement analysis shows that the width of the fibres in the band area were slightly smaller with a larger range than the fibres in the surrounding area. Glycan stands have been reported to measure 1-4 nm in diameter, and the fibres imaged are larger than this, suggesting the structures resolved are made up of a number of glycan strands bunched together. The analysis showed the spacing between the fibres was significantly smaller in the band area compared to the surrounding area. The reduced spacing could be due to the lack of peptide cross-link, making the material in the banding area appear denser.

An amiABC mutant strain with removed amidase enzymes was also image. The blank stripe caused by removed peptide cross-links was no longer present in the STORM images. AFM and STORM images also highlighted the mutant cells do not fully separate following septation and stay connected, forming long strings of cells. STORM images also show that the length of cells are a lot longer that the wild type.

Using the STORMForce technology areas of different structures were identified and investigated in the *E. coli* peptidoglycan material. The information gathered gives a better insight into how the peptidoglycan material becomes restructured throughout the life cycle. This information would not have been identified if it was not for the joint information acquired by both STORM, where the lack of fluorescence was observed, and AFM where the architectural structure was imaged.

STORMForce was then used to investigate *B. subtilis* cell division, septum formation and peptidoglycan insertion. Previous work suggests that septa in purified peptidoglycan material form snail shell like spirals when dried on a mica substrate and imaged in air [9]. However work done in this study show that this snail shell appearance occurs as a drying artefact. Through imaging septa and poles it became apparent that there is a differing internal and external structure, where one septum results in two poles. The internal structure is mesh like and the external consists of rings. When septa are dried the two structures

become dried together giving the snail shell appearance.

Studies using SIM in whole cells suggested material is added within the septum in comet like insertion patterns in small time frames. The comets are located at what is believed to be the leading edge of the septum, which join forming ring like formations working inwardly until the septum is complete [18]. STORMForce was used to investigate the septum formation. *B. subtilis* cells were grown to exponential phase and the pulse labelled for three time frames, 15 seconds, 2 minutes and 10 minutes. Peptidoglycan insertion within these time frames was then studied from the STORM data. Through quantitive analysis it was determined that within the 15 second time frame one concentrated area of localisation is identified, however material is also sparsely added throughout the rest of the septum. The 2 minute data shows material added in two concentrated areas, however again material is also added throughout the rest of the septum. By 10 minutes the entire septum is inserted with a fairly uniform distributions of localisations through out the septum. AFM data was taken of the exact same septa in the same areas. The AFM data showed that the concentrated localisations were located at the leading edge of the septum. as well as confirming the condition of the material imaged. The AFM data also identified large 20 nm holes in the material, suggesting mechanisms inserting peptidoglycan would go back and in fill in these areas. This would explain the sparse localisations added throughout the septum away from the leading edge.

SIM data of the pulse labelled septum was also taken to compliment the STORMForce data taken. The SIM data also showed that the 15 second data contains areas of more concentrated intensities, however the individual localisations were not identifiable due to the nature of the imaging technique. Instead it is seen as low intensity areas with a non-uniform distribution. The 2 minute data shows more areas of high intensity, with non-uniform intensities throughout the rest of the septum and the 10 minute data shows the septa have a higher uniform intensities, indicating that the entire septum is complete.

Using the STORMForce technology a greater understanding of septum formation in *B.*

subtilis was achieved. Areas of newly inserted peptidoglycan within the septum in short time frames were identified with the STORM data. Overlaying this information with AFM images not only showed the structure of the newly inserted material, but also the structures of the outer areas of the septum. STORM data showed sparse localisations throughout the outer areas of the septum, which gives an explanation to the structural variations of the septum seen by the AFM. Large 20 nm holes are seen in the outer areas of the septum which are too large to withstand internal turgor pressure from the cell, the sparse localisations around the outer area of the septum suggest that new material is not just inserted at the centre of the septum as it develops, but also to fill these holes. This STORMForce data highlights how septa are formed within the cell and how there is more to be understood about the machinery used in septum formation in the division process.

STORMForce as well as SIMForce was also used to investigate the main body of the bacteria. SIM was used as there is a greater yield of images allowing for more data to be taken. High precision gridded glass coverslips where used to locate the sample in the SIM and AFM allowing for correlative SIMForce imaging. Work done by Hayhurst et al [9] suggested the internal peptidoglycan material has a thick rope like structures consisting of tightly coiled strands, and the external structure is more disordered and mesh like. STORMForce data was taken of the rod at the same pulse labelled time frames to understand the insertion pattern. STORM data showed banding around the width of the body at 15 seconds and 2 minutes, but by 10 minutes the entire sacculi is fluorescent and the bands are no longer visible. SIM data was also taken and showed the same features. Both STORM and SIM data was taken on intact sacculi, which were made up of two layers of peptidoglycan. To gain a true understanding of the periodicity of the banding features a single layer (singlet) of material needed to be imaged. On average, the banding on the singlet of material has around half the frequency of the double layer, as is shown by the SIM data. The fluorescence banding visible in the data is material that has been added to the inside of the sacculi, so to get informative SIMForce images the AFM images must be of the inside of the sacculi. AFM

images of the inside of the sacculi show broad bands of material, which are much smoother and have a finer mesh structure. The bands seen in the SIM images also match with the bands seen in the AFM showing that material is added in these tightly packed regions in both 15 seconds and 2 minutes. As the new material is more tightly packed compared to the older material it is possible that the new material is reordered in the growth process to allow for new material to be added. The addition of new material as the older material becomes reordered allows for cell elongation. Experiments to determine this is discussed in future work.

An MreB mutant was used with deleted MreB, Mbl, MreBH and rsgL. The deleted genes maintain the rod shape of the bacteria and are thought to organise peptidoglycan structure. The fluorescence data showed that all banding features were lost, but peptidoglycan was still added in a random patchy order. SIMForce data showed that the rod shape of the sacculi is also lost and an irregular spherical shape is seen instead. Septa are still seen in both AFM and SIM images suggesting MreB does not affect septum formation.

9.0.1 Future work

Through the development of the STORMForce technique and the use of high precision correlative glass coverslips, the *E. coli* data obtained previously could be taken on an AFM which produces higher resolution images consistently. During developments that occurred when working with *B. subtilis* glass grids where using to take SIM images on separate equipment, the same area was then located on the AFM. Going forward this technique could also be used to get an increased resolution AFM images of *E. coli* by using a Bruker Fast Scan AFM, which consistently produces high-resolution biological AFM images. Using the Bruker Fast Scan, images could be taken of the strand structures within the fibre features observed previously, determining if they are glycan stands. Making it also possible to measure the distances between the stands where it is thought that the peptide cross-links are missing.

To also increase understanding of the banding structure that appears in the rod of the *B. subtilis* sacculi additional fluorescence experiments could be performed. Using multiple dyes and time frames in whole live cells the peptidoglycan insertion could be observed in 15 seconds, a second and third dye could then be used at delayed time points to understand how peptidoglycan is inserted throughout the cell life cycle. As the cells would still be alive the fluorescence added showing the banding features could be tracked as the cell continues to grow and divide. The cell could then be purified to extract the peptidoglycan and specific areas on the inside and the outside of the sacculi would then be imaged to show the change in the labelled material and exactly how the material has changed. Both STORMForce and SIMForce could be used to do this, with the use of correlative glass coverslips. This experiment could then be done in the presence of antibiotics to understand how antibiotics affect the peptidoglycan growth cycle and the peptidoglycan structure. With further developments to image a large variety of biological samples, STORMForce could become a highly advantageous experimental tool in the biophysics world. Allowing the users to gain a greater understanding of the systems under investigations.

Bibliography

[1] JPK Instruments AG, "The NanoWizard ® AFM Handbook," p. 40, 2005.

[2] Z. Yang, A. Sharma, J. Qi, X. Peng, D. Yeop Lee, R. Hu, D. Lin, J. Qu, and J. Seung Kim, "Super-resolution fluorescent materials: An insight into design and bioimaging applications," *Chemical Society reviews*, vol. 45, pp. 4651–4667, 06 2016.

[3] S.-w. Chiu and M. C. Leake, "Functioning Nanomachines Seen in Real-Time in Living Bacteria Using Single-Molecule and Super-Resolution Fluorescence Imaging," *International Journal of Molecular Science*, no. May 2014, 2011.

[4] M. Bates, B. Huang, and X. Zhuang, "Super-resolution microscopy by nanoscale localization of photo-switchable fluorescent probes," *Current Opinion in Chemical Biology*, vol. 12, no. 5, pp. 505–514, 2008.

[5] L. Brown, J. M. Wolf, R. Prados-Rosales, and A. Casadevall, "Through the wall: extracellular vesicles in gram-positive bacteria, mycobacteria and fungi," *Nature reviews Microbiology*, vol. 13, pp. 620 EP –, 09 2015.

[6] I. G. Theodorou, B. F. Leo, M. P. Ryan, and A. E. Porter, "Environmental Science Nano Towards understanding the antibacterial activity of Ag nanoparticles : electron microscopy in the analysis of the materials-biology interface," *Environmental Science Nano*, pp. 312–326, 2015.

[7] W. Vollmer, D. Blanot, and M. A. de Pedro, "Peptidoglycan structure and architecture." *FEMS microbiology reviews*, vol. 32 2, pp. 149–67, 2008.

[8] W. Vollmer and J.-v. Ho, "MINIreviews The Architecture of the Murein (Peptidoglycan) in Gram-Negative Bacteria : Vertical Scaffold or Horizontal Layers," *Journal of Bacteriology*, vol. 186, no. 18, pp. 5978–5987, 2004.

[9] E. J. Hayhurst, L. Kailas, J. K. Hobbs, and S. J. Foster, "Cell wall peptidoglycan architecture in Bacillus subtilis." *Proceedings of the National Academy of Sciences of the United States of America*, vol. 105, no. 38, pp. 14 603–14 608, 2008.

[10] A. Touhami, M. H. Jericho, and T. J. Beveridge, "Atomic force microscopy of cell growth and division in Staphylococcus aureus." *Journal of bacteriology*, vol. 186, no. 11, pp. 3286–95, jun 2004.

[11] D.-j. Scheffers and M. G. Pinho, *Microbiology and Molecular Biology reviews.*

[12] J.-V. Höltje and C. Heidrich, "Enzymology of elongation and constriction of themurein sacculus of escherichia coli," *Biochimie*, vol. 83, no. 1, pp. 103 – 108, 2001.

[13] R. D. Turner, A. F. Hurd, A. Cadby, J. K. Hobbs, and S. J. Foster, "Cell wall elongation mode in gram-negative bacteria is determined by peptidoglycan architecture." *Nature Communications*, vol. 4, pp. 1496–1498, 2013.

[14] R. D. Turner, S. Mesnage, J. K. Hobbs, and S. J. Foster, "Molecular imaging of glycan chains couples cell-wall polysaccharide architecture to bacterial cell morphology," *Nature Communications*, vol. 9, p. 1263, 2018.

[15] E. C. Garner, R. Bernard, W. Wang, X. Zhuang, D. Z. Rudner, and T. Mitchison, "Coupled, Circumferential Motions of the Cell Wall Synthesis Machinery and MreB Filaments in B. subtilis," *Science*, vol. 333, no. July, pp. 222–226, 2011.

[16] R. D. Turner, W. Vollmer, and S. J. Foster, "Different walls for rods and balls: the diversity of peptidoglycan," *Molecular Microbiology*, vol. 91, no. 5, pp. 862–874, 2014.

[17] F. Wu, C. Jukes, Y. Sun, C. Dekker, and S. Holden, "Treadmilling by FtsZ filaments drives peptidoglycan synthesis and bacterial cell division," *Science*, pp. 1–6, 2017.

[18] A. Yahashiri, M. A. Jorgenson, and D. S. Weiss, "Bacterial SPOR domains are recruited to septal peptidoglycan by binding to glycan strands that lack stem peptides," *PNAS*, vol. 112, no. 36, 2015.

[19] M. Asgari, J. Abi-Rafeh, G. N. Hendy, and D. Pasini, "Material anisotropy and elasticity of cortical and trabecular bone in the adult mouse femur via afm indentation," *Journal of the Mechanical Behavior of Biomedical Materials*, vol. 93, pp. 81 – 92, 2019.

[20] "Dynamic Imaging Methods for Scanning Probe Microscopy Submitted for the degree of Doctor of Philosophy . Nicholas William Mullin Department of Physics and Astronomy University of Sheffield September 2009," no. September, 2009.

[21] Y. Gan, "Atomic and subnanometer resolution in ambient conditions by atomic force microscopy," *Surface Science Reports*, vol. 64, no. 3, pp. 99–121, 2009.

[22] G. Binnig and C. F. Quate, "Atomic Force Microscope," *Physical reviews Letters*, vol. 56, no. 9, pp. 930–933, 1986.

[23] M.-h. W. sergei N. Magonov, *Surface analysis with STM and AFM*, John Wiley & Sons, Ed. Technology & engineering, 2008.

[24] F. Moreno-Herrero, J. Colchero, J. Gómez-Herrero, and a. M. Baro, "Atomic force microscopy contact, tapping, and jumping modes for imaging biological samples in liquids," *Physical reviews E - Statistical, Nonlinear, and Soft Matter Physics*, vol. 69, no. 3 1, pp. 1–9, 2004.

[25] J. P. K. I. Ag, "JPK HyperDrive ™ CantileverHolder User Manual," 2012.

[26] A. L. Weisenhorn, B. Drake, C. B. Prater, S. A. C. Gould, P. K. Hansma, F. Ohnesorge, M. Egger, S. Heyn, and H. E. Gaub, "Immobilized proteins in buffer imaged at molecular resolution by atomic force microscopy," vol. 58, no. November, 1990.

[27] R. G. Bailey, R. D. Turner, N. Mullin, N. Clarke, S. J. Foster, and J. K. Hobbs, "Article The Interplay between Cell Wall Mechanical Properties and the Cell Cycle in Staphylococcus aureus," *Biophysj*, vol. 107, no. 11, pp. 2538–2545, 2014.

[28] H.-j. Butt, "electrolyte solutions with an atomic force microscope," *Biophysical journal*, vol. 60, no. December, 1991.

[29] C. B. Keller and C. Bustamante, "Scanning Force Microscopy In Biology," *American Institute of Physics*, vol. 32, no. 1995, 1998.

[30] D. R. Mason, M. V. Jouravlev, and K. S. Kim, "Enhanced resolution beyond the Abbe diffraction limit with wavelength-scale solid immersion lenses." *Optics Letters*, vol. 35, no. 12, pp. 2007–2009, 2010.

[31] E. Abbe, "Beiträge zur theorie des mikroskops und der mikroskopischen wahrnehmung," *Archiv für mikroskopische Anatomie*, vol. 9, no. 1, pp. 413–418, Dec 1873.

[32] M. J. Booth, "Adaptive optics in microscopy," *Phylosophical Transactions of The Royal Society*, no. September, 2007.

[33] J. S. L. H. Schaefer, D. Schuster, "Structured illumination microscopy : artefact analysis and reduction utilizing a parameter optimization approach," *Journal of Microscopy*, vol. 216, no. November, pp. 165–174, 2004.

[34] A. C. Boccara, "Optimization and characterization of a structured illumination microscope," *Optics Express*, vol. 15, no. 24, pp. 1972–1979, 2007.

[35] L. Schermelleh, R. Heintzmann, and H. Leonhardt, "A guide to super-resolution fluorescence microscopy," *The Journal Of Cell Biology*, vol. 190, no. 2, pp. 165–175, 2010.

[36] E. Mudry, K. Belkebir, J. Girard, J. Savatier, E. Le Moal, C. NicoLettersi, M. Allain, and A. Sentenac, "Structured illumination microscopy using unknown speckle patterns," *Nature Photonics*, vol. 6, pp. 312 EP –, 04 2012.

[37] B. Harke, J. V. Chacko, H. Haschke, C. Canale, and A. Diaspro, "A novel nanoscopic tool by combining AFM with STED microscopy," *Optical Nanoscopy*, vol. 1, no. 1, p. 3, 2012.

[38] K. I. Willig, B. Harke, R. Medda, and S. W. Hell, "Sted microscopy with continuous wave beams," *Nature Methods*, vol. 4, pp. 915 EP –, 10 2007.

[39] P. S. Guide, "Snap tag information." *BioLabs*, 2006.

[40] S. Manley, N. Olivier, D. Keller, and P. Go, "Resolution Doubling in 3D-STORM Imaging through Improved Buffers," *PLOS ONE*, vol. 8, no. 7, pp. 1–9, 2013.

[41] J. Xu and Y. Liu, "Stochastic optical reconstruction microscopy (STORM)," *Curr Protoc Cytom*, pp. 1–38, 2018.

[42] N. Olivier, D. Keller, V. S. Rajan, P. Gönczy, and S. Manley, "Simple buffers for 3D STORM microscopy." *Biomedical optics express*, vol. 4, no. 6, pp. 885–99, 2013.

[43] X. Shi, J. Lim, and T. Ha, "Acidification of the oxygen scavenging system in single-molecule fluorescence studies: In situ sensing with a ratiometric dual-emission probe," *Analytical Chemistry*, vol. 82, no. 14, pp. 6132–6138, 2010.

[44] J. Vogelsang, C. Steinhauer, C. Forthmann, I. H. Stein, B. Person-Skegro, T. Cordes, and P. Tinnefeld, "Make them blink: Probes for super-resolution microscopy," *Chemphyschem*, vol. 11, no. 12, pp. 2475–2490, 2010.

[45] Y. Cao, I. D. Parker, G. Yu, C. Zhang, and a. J. Heeger, "Improved quantum efficiency for electroluminescence in semiconducting polymers," *Nature*, vol. 397, no. 6718, pp. 414–417, 1999.

[46] G. Healey and R. Kondepudy, "Radiometric CCD camera calibration and noise estimation," *IEEE Transactions on Pattern Analysis and Machine Intelligence*, vol. 16, no. 3, pp. 267–276, 1994.

[47] D. Dussault, P. Hoess, P. Spie, P. H. Kg, P. O. Box, S. C. Optics, and C. Avenue, "Noise performance comparison of ICCD with CCD and EMCCD cameras," *Infrared systems and photoelectronic technology.*, vol. 5563, pp. 195–204, 2004.

[48] F. Huang, T. M. P. Hartwich, F. E. Rivera-molina, Y. Lin, C. Whitney, J. J. Long, P. D. Uchil, J. R. Myers, M. A. Baird, M. W. Davidson, D. Toomre, and J. Bewersdorf, "Video-rate nanoscopy enabled by sCmos camera-specific single-molecule localization algorithms," *Nature Methods*, vol. 10, no. 7, pp. 653–658, 2014.

[49] L. Hall-Stoodley, J. W. Costerton, and P. Stoodley, "Bacterial biofilms: from the natural environment to infectious diseases," *Nature reviews Microbiology*, vol. 2, no. 2, pp. 95–108, 2004.

[50] L. Daniel, H. Vlamakis, and R. Kolter, "Biofilms," *Cold Spring Harbor Perspectives in Biology*, pp. 1–11, 2010.

[51] J. W. Bartholomew and T. O. D. Mittwer, "The Gram Stain," *Department of Bacteriology, University of Southern California.*, pp. 1–29, 1883.

[52] P. E. Reynolds, "Structure, biochemistry and mechanism of action of glycopeptide antibiotics." *European journal of clinical microbiology & infectious diseases : official publication of the European Society of Clinical Microbiology*, vol. 8, no. 11, pp. 943–950, 1989.

[53] I. T. Paulsen, J. H. Park, P. S. Choi, and M. H. S. Jr, "A family of Gram-negative bacterial outer membrane factors that function in the export of proteins , carbohydrates , drugs and heavy metals from Gram-negative bacteria," *FEMS Microbiology Letters*, vol. 156, 1997.

[54] S. I. Miller, R. K. Ernst, and M. W. Bader, "Lps, tlr4 and infectious disease diversity," *Nature reviews Microbiology*, vol. 3, no. 1, pp. 36–46, 2005.

[55] W. Vollmer, D. Blanot, and M. A. D. Pedro, "Peptidoglycan structure and architecture," *FEMS Microbiology reviews*, vol. 32, no. 2, pp. 149–167, 3 2008.

[56] S. Brown, J. P. S. M. Jr, and Suzanne Walker, "Wall Teichoic Acids of Gram-Positive Bacteria," *Annu review Microbiol*, no. 6, 2014.

[57] M. Haenni, K. Minnig, P. Moreillon, and J. Dubochet, "Granular Layer in the Periplasmic Space of Gram-Positive Bacteria and Fine Structures of Enterococcus gallinarum and Streptococcus gordonii Septa reviewealed by Cryo-Electron Microscopy of Vitreous Sections," vol. 188, no. 18, pp. 6652–6660, 2006.

[58] A. Chakraborty, S. Ghosh, G. Chowdhary, U. Maulik, and S. Chakrabarti, "DBETH : A Database of Bacterial Exotoxins for," *Nucleic Acids Research*, vol. 40, no. November 2011, pp. 615–620, 2012.

[59] K. F. Jarrell, M. Stark, D. B. Nair, and J. P. Chong, "Flagella and pili are both necessary for efficient attachment of Methanococcus maripaludis to surfaces," *FEMS Microbiology Letters*, vol. 319, no. 1, pp. 44–50, 06 2011.

[60] B. R. Parry, I. V. Surovtsev, M. T. Cabeen, C. S. O. Hern, and E. R. Dufresne, "The Bacterial Cytoplasm Has Glass-like Properties and Is Fluidized by Metabolic Activity," *Cell*, vol. 156, no. 1-2, pp. 183–194, 2014.

[61] C. A. Kerfeld, C. Aussignargues, J. Zarzycki, F. Cai, and M. Sutter, "Bacterial microcompartments," *Nature reviews Microbiology*, vol. 16, pp. 277 EP –, 03 2018.

[62] M. P. Williamson, A. Atrih, G. Bacher, and S. J. Foster, "Analysis of Peptidoglycan Structure from Vegetative Cells of," *Society*, vol. 181, no. 13, pp. 3956–3966, 1999.

[63] W. Vollmer, D. Blanot, and M. A. D. Pedro, "Peptidoglycan structure and architecture," *FEMS Microbiology reviews*, vol. 32, pp. 149–167, 2008.

[64] T. MIZUNO, "A Novel Peptidoglycan-Associated Lipoprotein Found in the Cell Envelope of Pseudomonas aeruginosa and Escherichia coli," *The Journal of Biochemistry*, vol. 86, no. 4, pp. 991–1000, 10 1979.

[65] B. A. Dmitriev, F. V. Toukach, O. Holst, E. T. Rietschel, and S. Ehlers, "Tertiary Structure of Staphylococcus aureus Cell Wall Murein †," *Journal of Bacteriology*, vol. 186, no. 21, pp. 7141–7148, 2004.

[66] J. M. Burns, *The University of Sheffield thesis.*

[67] J. M. Monteiro, P. B. Fernandes, F. Vaz, A. R. Pereira, A. C. Tavares, M. T. Ferreira, P. M. Pereira, H. Veiga, E. Kuru, M. VanNieuwenhze, Y. V. Brun, and M. G. Pinho, "Cell shape dynamics during the staphylococcal cell cycle," *Nat. Commun.*, 2015.

[68] R. M. Figge, A. V. Divakaruni, and J. W. Gober, "MreB , the cell shape-determining bacterial actin homologue , co-ordinates cell wall morphogenesis in Caulobacter crescentus," *Nature*, vol. 51, pp. 1321–1332, 2004.

[69] T. Uehara and T. G. Bernhardt, "More than just lysins: peptidoglycan hydrolases tailor the cell wall," *Current Opinion in Microbiology*, vol. 14, no. 6, pp. 698 – 703, 2011.

[70] L. Gan, S. Chen, and G. J. Jensen, "Molecular organization of Gram-negative peptidoglycan," *PNAS*, vol. 105, no. 48, pp. 18 953–18 957, 2008.

[71] C. Heidrich, M. F. Templin, A. Ursinus, M. Merdanovic, H. Schwarz, and M. A. D. Pedro, "Involvement of N -acetylmuramyl- L -alanine amidases in cell separation and antibiotic-induced autolysis of Escherichia coli," vol. 41, pp. 167–178, 2001.

[72] M. Leaver, P. Domínguez-Cuevas, J. M. Coxhead, R. A. Daniel, and J. Errington, "Life without a wall or division machine in bacillus subtilis," *Nature*, vol. 457, pp. 849 EP –, 02 2009.

[73] A. Formstone, "Results mreB is co - transcribed with mreC in an operon," *Molecular Microbiology*, vol. 55, no. 6, 2005.

[74] G. W. Liechti, E. Kuru, E. Hall, A. Kalinda, Y. V. Brun, M. Vannieuwenhze, and A. T. Maurelli, "A new metabolic cell-wall labelling method revieweals peptidoglycan in Chlamydia trachomatis," *Nature*, vol. 506, no. 7489, pp. 507–510, 2014.

[75] A. Fleming, "On the antibacterial action of cultures of a penicllium, with special reference to their use in the isolation of B. Influenza." no. 1923, 1929.

[76] J. M. Ghuysen, "Penicillin-binding proteins. Wall peptidoglycan assembly and resistance to penicillin: Facts, doubts and hopes," *International Journal of Antimicrobial Agents*, vol. 8, no. 1, pp. 45–60, 1997.

[77] G. M. Hagen, P. Kr, J. Borkovec, and M. Ovesny, "ThunderSTORM : a comprehensive ImageJ plug-in for PALM and STORM data analysis and super-resolution imaging ı z," vol. 30, no. 16, pp. 2389–2390, 2014.

[78] E. Kuru, H. V. Hughes, P. J. Brown, E. Hall, S. Tekkam, F. Cava, M. A. D. Pedro, Y. V. Brun, and M. S. Vannieuwenhze, "In Situ Probing of Newly Synthesized Peptidoglycan in Live Bacteria with Fluorescent d -Amino Acids ** Angewandte," pp. 12 519–12 523, 2012.

[79] P. A. Levin and R. Losick, "Characterization of a cell division gene from Bacillus subtilis that is required for vegetative and sporulation septum formation." *Journal of bacteriology*, vol. 176, no. 5, pp. 1451–9, Mar. 1994.

[80] V. A. Lund, K. Wacnik, R. D. Turner, B. E. Cotterell, C. G. Walther, S. J. Fenn, F. Grein, A. J. Wollman, M. C. Leake, N. Olivier, A. Cadby, S. Mesnage, S. Jones, and S. J. Foster, "Molecular coordination of Staphylococcus aureus cell division," *eLife*, vol. 7, p. e32057, feb 2018.

[81] K. Schirner and J. Errington, "The Cell Wall Regulator I Specifically Suppresses the Lethal Phenotype of mbl Mutants in Bacillus subtilis," *Journal of Bacteriology*, vol. 191, no. 5, pp. 1404–1413, 2009.

[82] A. Hermsdörfe, D. J. Madl, and Jun.-Prof. Dr. Winfried Römer, "Combination of high-resolution AFM with super-resolution Stochastic Optical Reconstruction Microscopy (STORM) Introduction," *JPK Technical note*, 2014.

[83] P. D. Odermatt, A. Shivanandan, H. Deschout, R. Jankele, A. P. Nievergelt, L. FeLettersi, M. W. Davidson, A. Radenovic, and G. E. Fantner, "High-Resolution Correlative Microscopy: Bridging the Gap between Single Molecule Localization Microscopy and Atomic Force Microscopy," *Nano Letters*, 2015.